REMARKS

Applicants continue to take exception to the restriction required deleting claims 1-20 from examination. In the instant circumstance, the method is inoperable save for the apparatus of claim 21 *et seq* and the apparatus is not understood nor applied except in the performance of the method of claims 1-20. The stated grounds for rejection of claims 21-41 belie a misunderstanding of the structure and operation of the claimed apparatus and the method which was restricted out.

In the Office Action dated July 19, 2007, claims 21-25, 31-35 and 37-41 were rejected. Claims 26-30 and 36 were objected to. Applicants have reviewed carefully the Office Action and proffer the following remarks.

Claims 21-24, 31-35 and 37-41 have been rejected under 35 USC 103(b) as anticipated by Sun et al., U.S. Patent Number 6,225,653. The elements of the Sun et al. reference are alleged to duplicate those of the claimed invention.

Applicant's invention is an ionization detector which measures the amount (quantity) of electrons with characteristic energies which are produced by an ionization process. The ionization source may be metastable atoms produced during glow discharge in an inert gas. The metastables have a known energy level which ionizes the subject impurities having ionization potentials at or below that level. Alternatively, photoionization using photons of a definite energy (with wavelength in ultraviolet region) are used and the inert gas is not needed because no metastables are required. The wavelength of the photons is selected to ionize impurities only. The important point is that it is the electrons, not ions such as are generated in mass spectrometry, which are being measured. Discrimination is on the basis of energy, not mass.

To make such a measurement, an equipotential space is required as recited in claim 21(b). The location of the equipotential space is shown at the bottom of Figs 1 and 2 and explained in [0045]. Electrons in the equipotential space migrate to cathode 5 by a "random

walk" process and arrive with the initial kinetic energy essentially unchanged. This phenomenon is explained in detail at [0047]. The apparatus is designed and operated to perform the method of claim 1, i.e. electron spectroscopy.

Equipotential space is explained in the attachments, a) Wikipaedie and b), Northwestern Physics Department with an explanation of equipotential lines. It is a region of negligible electric field sufficient to allow free diffusion (random walk) of electrons and, in this invention, is the focus of ionization of impurities. The equipotential space must be sufficient in size that it is greater than the Debye length as described in [0011] and [0047]. Also for the Office's edification, a copy of Kolokolov, et al. Physica Scripta 50, 371 (1994) is attached. Please note page 374, col. 2, lines 1-2 from bottom and page 375, col. 1, lines 1-4.

If an electron is ejected during ionization of an impurity atom by a particle of definite energy (metastable atom, photon, etc.), it gets some kinetic energy and some electric potential energy relative to electrodes of the chamber. Kinetic energy is characteristic to said impurity atom or molecule, it equals the difference between the energy of ionizing particle (metastable atom, photon, etc.) and ionization threshold of the impurity. Total energy of electron is sum of kinetic and potential energy. It is well known from electrostatic laws that if you provide zero (or negligible) electric field in the region, electric potential here is uniform (i.e., equipotential space). Thus, all electrons ejected from one kind of impurity atoms in any point of the equipotential ionization region will get the same total energy. Then they will move randomly through the region. Elsewhere (e.g., with a retarding electric field localized near to one of the electrodes) you can make energy analysis of these electrons and determine a sort of impurity. Thus, providing equipotential space (feature (b) of claim 21) is vitally necessary, if you decide to analyze electron's energy. Sun et al. doesn't teach electron energy analysis and for this reason doesn't anticipate providing of equipotential space at ionization region.

Applicant's claim 21, part (a), requires *inter alia* that "the ionization chamber geometry being chosen in such that a distance from any point inside said ionization chambers to nearest

chamber wall or one of said electrodes *is less than a mean displacement of electrons before they lose the chosen portion of their kinetic energy.*

This limitation is ignored in the analysis of Applicants' claim. Instead, reference is made to col. 4, lines 33-50 of the reference:

> "As discussed above, UV photons from UV lamp 32 ionize volatile gas molecules which are inside ionization chamber 36. An ion detector 48 disposed in ionization chamber 36 and positioned proximal to optical window 34 collects the resulting electrons and ions. Ion detector 48 comprises a pair of electrodes, a bias electrode 50 and a measurement electrode 52."

This is not a detection of electrons with a specific energy, but a simple non-specific ionization detector maximized to low detection limits. No discussion of dimensions in metes and bounds or functionality appears in the cited text.

The same citation (col. 4, lines 33-50 of the reference) is used to invent an equipotential space such as that recited in part (b) of claim 21, not withstanding that a substantial equipotential space inhibits the response time and reduce sensitivity (due to electrons quenching on the wall of the chamber instead of being detecting at (48)) of a PID device measuring gross electrical current. It is another reason for part (b) of claim 21 being not anticipated by Sun et al.

Also Applicants analyze the following explanation offered at page 6, lines 6-11:

> "Applicant is respectfully reminded that, the claim does specifically claim the distance, any distance taught by Sun et al. reads on the claim since kinetic energy lose energy as some work is done to bring body from rest to a particular state of motion. Thus, before being collected at detector (48), the electrons lose energy compared to the energy brought the motion."

It seems like ambiguous mention of energy conservation law and kinetic energy definition only, moreover, detector (48) is defined by the reference as ion detector, not the electron one (see above cited col. 4, lines 33-50 of Sun et al), so it can't support the statement that Applicant's claim 21 (a) is anticipated by Sun. Also regarding this explanation the misunderstanding at the Office is made clear. At paragraphs [0043] through [0047] the random free walk of generated

electrons is described which is quite different from the explanation at page 6 of the Office Action.

Additionally, Applicants provide measurement of electron energies characteristic of a single molecular species and not just total current. The reference, like a dog, responds to a range of odors as well as odorless compounds such as methane, which is the intended use of a PID. Specific impurities are not discriminated in a gross measurement of gasses under analysis by Sun et al.

Claim 25 has been rejected over the combination of Sun with Tooru et al., U.S. Patent Number 5,320,577 which teaches the use of the second derivative as a sensitive way to detect a change in a variable. In Tooru et al's. disclosure, the signal measured is the change in a tungsten oxide detector for air pollution. The concept that a second derivative may be less susceptible to noise is not the point of Applicant's invention. The measurement of electron energy levels is the objective and claim 25 depends from claim 21, which does not "disclose every subject matter as alleged." As has been elucidated above, claim 21 is directed to different subject matter with different physical characteristics. Current detected by Applicant is used to determine peaks vs. energy to obtain $E_i$ values, the peaks being determined using the second derivative to generate a peak from a step-like curve in the first derivative of the raw data according to Eq.9 in paragraph [0052]. The ionization potential $E_i$ is the characteristic which identifies the impurity. The $E_i$ is irrelevant to Sun, demonstrating yet another difference between the reference and Applicants' invention - e.g. the ability to distinguish methane from hydrogen sulfide. As a result, part (d) of Applicant's claim 21 can not be recognized as anticipated by Sun et al.

Claims 26-30 and 36 are indicated to be allowable but no reason has been given. Given the apparent misunderstanding of claims 21 (and apparently claim 31), Applicants cannot know what parts of claim 26 and 36 render them allowable when claims 21 and 31 are not allowed.

In view of the remarks above Applicants submit that the pending claims are now in condition for allowance and request reconsideration and favorable action thereon.

Respectfully submitted,

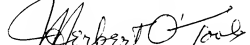

J. Herbert O'Toole
Registration No. 31,404
Attorney for Applicant(s)
NEXSEN PRUET, LLC
P.O. Box 10107
Greenville, SC 29603
Telephone: 864/ 370- 2211
Facsimile: 864/ 282-1177

Attachments:
1- Wikipeadia
2- Northwestern Physics
3- Kolokolov et al. Physica Scripta 50 371 (1994)

# Equipotential



From Wikipedia, the free encyclopedia

**Equipotential** or **isopotential** in mathematics and physics (especially electronics) refers to a region in space where every point in it is at the same potential. This usually refers to a scalar potential, although it can also be applied to vector potentials. Often, equipotential surfaces are used to visualize an (n)-dimensional scalar potential function in (n-1) dimensional space.

Note that an equipotential region might be referred as being 'of equipotential' or simply be called 'an equipotential'.

For scalar potentials, the gradient in an equipotential region is zero, since there is no change in the value of the potential. This is important in physics because the force on a body is often determined by the gradient of that force's potential function.

For example, there is zero electric field in an equipotential region (that is, a region of constant voltage). A charged particle in such a region experiences no electric force. Thus, there is no electric current between two points of equal voltage because there is no force driving the electrons.

Likewise, a ball will not be pulled down by the force of gravity if it is resting on a flat, horizontal surface. This is because points on the surface are at equal gravitational potential.

Interestingly, ignoring local variations in altitude due to geology, the Earth's surface is an equipotential surface in the shape of an oblate spheroid due to its rotation and the Earth's gravity, and this fact allows calculation of its shape. That this is an equipotential may be easily seen, since if it were not so, the oceans and indeed the landmasses (which are subject to motion due to plate tectonics) would move so as to even out the potential.

For more information, see the general article about potential

## See also

- Isopotential map



Categories: Multivariable calculus | Potential | Physics

Northwestern

# EQUIPOTENTIAL LINES

## Electric fields

One way to look at the force between charges is to say that the charge alters the space around it by generating an electric field **E**. Any other charge placed in this field then experiences a Coulomb force. We thus regard the **E** field as transmitting the Coulomb force.

To define the electric field **E** more precisely, consider a small positive test charge $q$ at a given location. As long as everything else stays the same, the Coulomb force exerted on the test charge $q$ is proportional to $q$. Then the force per unit charge, $\mathbf{F}/q$, does not depend on the charge $q$, and therefore can be regarded meaningfully to be the electric field **E** at that point.

In defining the electric field, we specify that the test charge $q$ be small because in practice the test charge $q$ can indirectly affect the field it is being used to measure. If, for example, we bring a test charge near the Van de Graaff generator dome, the Coulomb forces from the test charge redistribute charge on the conducting dome and thereby slightly change the **E** field that the dome produces. But secondary effects of this sort have less and less effect on the proportionality between **F** and $q$ as we make $q$ smaller.

So many phenomena can be explained in terms of the electric field, but not nearly as well in terms of charges simply exerting forces on each other through empty space, that the electric field is regarded as having a real physical existence, rather than being a mere mathematically-defined quantity. For example when a collection of charges in one region of space move, the effect on a test charge at a distant point is not felt instantaneously, but instead is detected with a time delay that corresponds to the changed pattern of electric field values moving through space at the speed of light.

Closely associated with the concept of electric field is the pictorial representation of the field in terms of lines of force. These are imaginary geometric lines constructed so that the direction of the line, as given by the tangent to the line at each point, is always in the direction of the **E** field at that

point, or equivalently, is in the direction of the force that would act on a small positive test charge placed at that point. The electric field and the concept of lines of electric force can be used to map out what forces act on a charge placed in a particular region of space.

Figures 1a and 1b show a region of space around an electric dipole, with the electric field indicated by lines of force. The charges in Fig. 1a are identical but opposite in sign. In Fig. 1b the charges have the same sign. Above each figure is a picture of a region around charges in which grass seed has been sprinkled on a glass plate. The elongated seeds have aligned themselves with the electric field at each location, thus indicating its direction at each point.

A few simple rules govern the behavior of electric field lines. These rules can be applied to deduce some properties of the field for various geometrical distributions of charge:

a) Electric field lines are drawn such that a tangent to the line at a particular point in space gives the direction of the electrical force on a small positive test charge placed at the point.

b) The density of electric field lines indicates the strength of the **E** field in a particular region. The field is stronger where the lines get closer together.

c) Electric field lines start on positive charges and end on negative charges. Sometimes the lines take a long route around and we can only show a portion of the line within a diagram of the kind below. If net charge in the picture is not zero, some lines will not have a charge on which to end. In that case they head out toward infinity, as shown in Figure 1b.

You might think when several charges are present that the electric field lines from two charges could meet at some location, producing crossed lines of force. But imagine placing a charge where the two lines intersect. Charges are never confused about the direction of the force acting on them, so along which line would the force lie? In such a case, the electric fields add vectorially at each point, producing a single net **E** field that lies along one specific line of force, rather than being at the intersection of two lines of force. Thus, it can be seen that none of the lines cross each other. It can also be shown that two field lines never merge to become one.

Under certain circumstances, the rules defining these field lines can be used to deduce some general properties of charges and their forces. For example, a property easily deduced from these rules is that a region of space enclosed by a spherically symmetric distribution of charge has zero electric everywhere within that region (assuming no additional charges produce electric fields

inside). Imagine first a spherically symmetric thin shell of positive charge all at a certain distance from the center. Field lines from the shell would have to be radially outward equally in all directions. If these outward pointing lines continued radially inward beneath the shell, they would have nowhere to end. Hence, the field lines must have ended at the surface charge, and there must be zero field everywhere inside. Next, suppose the spherically symmetric distribution of charge surrounding the uncharged region is not merely a thin shell. We can nevertheless consider the charge distribution to be divided up into many thin layers each at a different radius. Each layer contributes its own field lines that end at that layer, producing none of the field lines in the region enclosed by that layer. Then any point in the region of interest is inside all of the thin layers, where all the field lines have ended. We can conclude that the E field is zero at any point within a region surrounded by the spherical distribution of charge.

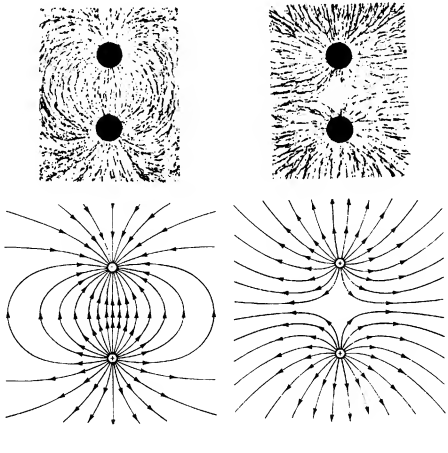

a b

Figure 1 Above: Grass seeds align themselves with the electric field between two charges. Below: The drawing shows the lines of force associated with the electric field between charges. Figure 1a shows a charge pair with negative charge above and positive charge below. Figure 1b shows two positive charges.

In Figs. 1a and 1b it is seen that the density of field lines is greater near the charges because the lines must converge closer together as they approach a particular charge. It can also be shown that the electric field intensity increases near conducting surfaces that are curved to protrude outward, so that they have a positive curvature. Curvature is defined as the inverse of the radius. A flat surface has zero curvature. A needle point has a very small radius and a large positive curvature. The larger the curvature of a conducting surface, the greater the field intensity is near the surface.

The lightning rod is a pointed conductor. An electrified thundercloud above it attracts charge of the opposite sign to the near end of the rod, but repels charge of the same sign to the far end. The far end is grounded, allowing its charge to escape. The rod thereby becomes charged by electric induction. The cloud can similarly induce a charge of sign opposite to is own in the ground beneath it. The strongest field results near the point of the lightning rod, and is intense enough to transfer a net charge onto the airborne molecules, thus ionizing them. This produces a glow discharge, in which net electric charge is carried up on the ionized molecules in the air to neutralize part of the charge at the bottom of the cloud before it can produce a lightning bolt.

The electric field representation is not the only way to map how a charge affects the space around it. An equivalent scheme involves the notion of electric potential. The difference in electric potential between two points A and B is defined as the work per unit charge required to move a small positive test charge from point A to point B against the electric force. For electrostatic forces, it can be shown that this work depends only on the locations of the points A and B and not on the path followed between them in doing the work. Therefore, choosing a convenient point in the region and arbitrarily assigning its electric potential to have some convenient value specifies the electric potential at every other point in the region as the work per unit test charge done to move a test charge between the points. It is usual to choose either some convenient conductor or else the ground as the reference, and to assign it a potential of zero.

This bears some similarity to how the gravitational potential energy was defined. We could have considered the "electric potential energy" of a test charge in analogy with the gravitational potential energy by considering the work, not the work per unit charge, done in moving a test charge between two points. But just as the gravitational potential energy itself cannot be used to characterize the gravitational field because it depends on the test mass used, the electric potential energy similarly depends on the test charge used. But the force and therefore the work to move the test charge from one location to another is proportional to its charge. Thus the work per unit charge, or electric potential difference, is independent of the test charge used as long as the field does not vary in time, so that the electric potential characterizes the electric field itself throughout

the region of space without regard to the magnitude of the test charge used to probe it.

It is convenient to connect points of equal potential with lines in two dimensional problems; or surfaces in the case of three dimensions. These surfaces are referred to as equipotential surfaces, or equipotentials.

If a small test charge is moved so that its direction of motion is always perpendicular to the electric field at each location, then the electric force and the direction of motion at each point are perpendicular. No work is done against the electric force, and the potential at each point traversed is therefore the same. Hence a path traced out by moving in a direction perpendicular to the electric field at each point is an equipotential. Conversely, if the test charge is moved along an equipotential, there is no change in potential and therefore no work done on the charge by the electric field. For non-zero electric field this can happen only if the charge is being moved perpendicular to the field at each point on such a path. Therefore, electric field lines and equipotentials always cross at right angles.

Figure 2 shows a region of space around a group of charges. The electric lines of force are indicated with solid lines and arrows. The electric field can also be indicated by equipotential lines, shown as dashed lines in the figure. The mapping of a region of space with equipotential lines or, in the case of 3-D space, with equipotential surfaces, provides the same degree of information as by mapping out the electric field itself throughout the region.

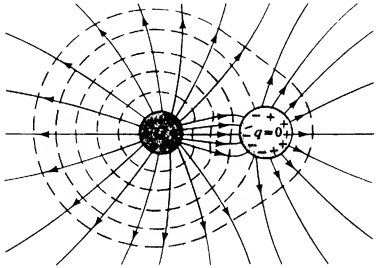


Figure 2 Electric field around a group of charges. Lines of force are shown as solid lines. Equipotential lines are shown as dashed lines.

## Mapping equipotentials between oppositely charged conductors

The equipotential apparatus is shown in Fig. 3. The power supply is a source of potential difference which is measured in Newton-meters per Coulomb. When it is connected to the two conductors, a small amount of charge is deposited on each conductor, producing an electric field and maintaining a potential difference, identical to that of the power supply, between the two conductors. The black paper beneath the conductors is weakly conducting to allow a small current to flow. The digital voltmeter measures the potential difference between the point on the paper where the probe is held and the conductor connected to the other lead of the voltmeter.

Choose the conductor geometry for which you will be mapping the field. Start with a circular conductor on the north terminal post (furthest away from you) and a horizontal bar on the south terminal (nearest you). Mount these conductor pieces on the brass bolts which protrude from the black-coated paper. Secure the conductors with the brass nuts. Tighten down the nuts to ensure good electrical contact between the conductors and the paper. The north banana jack (away from

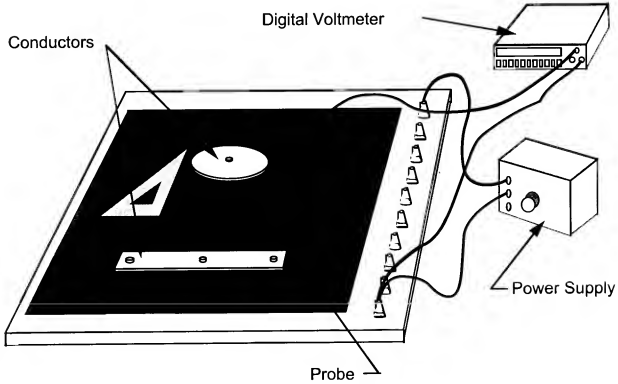


Figure 3 Equipotential Apparatus

you ) is red and the south jack is black. The positive terminal of the power supply is connected to the red banana jack and the negative terminal to the black banana jack, thereby connecting the power supply to the conductors.

The digital voltmeter measures the potential difference between the two input electrodes. The black ground lead of the digital voltmeter (its negative terminal) should be connected to the black negative banana jack on the board. You will use the red (positive) lead of the digital voltmeter as a probe.

## Setting the potential difference

Adjust the power supply to maintain the desired voltage between the two conductors by following these steps. Connect the red lead of the digital voltmeter to the red banana jack on the board. (The black lead was connected to the black banana jack in the previous step.) Adjust the power supply voltage to 6.00 volts, as read on the digital voltmeter. You may have to change the range setting of the voltmeter to get the proper reading. When this adjustment is completed, disconnect the red lead of the digital voltmeter. You are now ready to take data.

## Mapping equipotential lines

Each equipotential line or surface is specified by the same single value of the voltage that all its points have with respect to the conductor. The goal is to locate points at each desired potential in order to trace out the corresponding equipotential line.

Suppose, for example, you want to find an equipotential at 5.00 volts. Place the red probe on the surface of the black paper and move it around until the digital voltmeter reads 5 volts. This point is then at a potential of 5 volts above that of the bar conductor.

To simplify mapping the region, the bar is inscribed with marks at every two centimeters, and we have provided graph paper containing a scale drawing of the apparatus in which we include a scale marked with two centimeter rulings. Use a straight edge as a guide for the probe. Line the straight edge with one of the scribe marks on the bar and slide the probe along the straight edge, maintaining good electrical contact, to find the point where the potential reads 5 volts. Record how far up the straight edge this point is, and mark the point on the scale drawing. Label the point as a 5 volt point. Now, move the straight edge to another scribe mark, similarly find the 5 volt potential point, and mark that point on the scale drawing. Repeat this process until you have a good idea of the shape of the 5 volt equipotential in the region. Draw a line connecting all the 5 volt points to show the 5 volt potential surface.

Now, go after the 4 volt potential using the same technique. Then, do the same for the 3 volt , 2 volt and 1 volt potential surfaces. For each case, draw a smooth curve connecting the points at the given equal potential. The curve is intended to fall along the equipotential between, as well as at, the specific points marked off, so the points should not be connected by straight line segments.

## Finding electric field lines

The result discussed earlier that the electric field is everywhere at right angles to the equipotential surfaces and the fact that electric fields start on positive charges and end on negative charges can now be used to draw the field lines in the region where you have traced the equipotentials. On your drawing, place your pen at a point representing the bar conductor surface and draw a line perpendicular to the bar going toward the nearest equipotential line. As your line approaches the equipotential, be sure that it curves to meet the line at a right angle. Proceed similarly to the next equipotential, and so on until your line ends on the drawing of the round conductor. Keep in mind that each conductor itself is an equipotential. Return to the bar in the graph and construct a new line starting at an appropriate distance (say 2 cm) from the first line. Continue constructing electric field lines to map the entire area on your graph

## Conclusions

The electric field lines and equipotential surfaces that you have mapped should exhibit features consistent with the properties of the Coulomb interaction. You should examine your plot and verify that it shows these features. Here are some suggested questions you might be able to address based on examining and analyzing your data.

Do the electric field lines approach conducting surfaces everywhere at right angles?

Electric fields are more intense near surfaces with larger curvature. Does the electric field intensity increase near the circular electrode as compared to the flat bar electrode, and if so, how?

Is the density of electrical potential lines related to the intensity of the electrical force?

Are there electric fields and equipotentials above the plane of the paper whose equipotential lines were mapped? If so, could we use the probe to map them? How else could they be mapped?

## QUESTIONS

- The following list of questions is intended to help you prepare for this laboratory session. If you have read and understood this write-up, you should be able to answer most of these questions. Some of these questions may be asked in the quiz preceding the lab.
- What are three properties of electric lines of force?
- Why do electric lines of force never cross?
- How do the electric lines of force represent an increasing field intensity?
- How can you prove from properties of electric field lines that a spherical distribution of charge surrounding an uncharged region produces no electric field anywhere within the region?
- In what way are equipotential lines oriented with respect to the electric field lines?
- Are the electric field representation and the equipotential line representation equivalent in terms of how much information they contain about the electric field?
- What are the units of potential difference?
- What are units of electric field?
- Why must the **E** field be perpendicular to the surface of an ideal conductor?

# Interaction Processes With Creation of Fast Electrons in the Low Temperature Plasma

N. B. Kolokolov and A. A. Kudrjavtsev

St. Petersburg University, 1 Uljanovskaja str., St. Petergof, 198904, St. Petersburg, Russia

and

A. B. Blagoev

Sofia University, 5 James Boucher blvd., 1126, Sofia, Bulgaria

*Received November 2, 1993; accepted February 14, 1994*

**Abstract**

The methods and the results of investigations of the reactions in which electrons appear with energies surpassing the average electron distribution's energy in a plasma are considered. Particular attention is paid to the plasma electron spectroscopy method, which combines the advantages of the elementary processes examination in a plasma with the possibilities of conventional electron spectroscopy. Data of the study of chemiionization reactions involving two excited rare gas atoms, Penning ionizations of atoms and molecules by the helium metastable atoms and quenching of excited inert gases and mercury atoms by the electrons are given. The influence of the processes of creating fast electrons on the plasma properties is discussed.

## Introduction

The excited and especially the metastable states of atoms and molecules play substantial roles in the low temperature plasma. Indeed, the density of excited atoms in a plasma can exceed by one order of magnitude the charged particle density and, as a consequence in these cases, the potential energy, stored in the excited states, surpasses many times the kinetic energy of the electron gas. At that, the large chemical activity of the excited states, their effective participation in the ionization, dissociation and excitation processes should be taken into account. We will also point out the role of metastable states in the gases stepwise ionization of particular interest from the point of view of the numerous practical applications and the theoretical description are the interactions between the slow heavy particles in which electrons and ions are formed. They are the so-called chemiionization processes in which one or both colliding partners are excited particles. In order to emphasize their role it is useful to mention the penning lasers, based on creation of population inversion by effective depopulation of the lower lasing level through chemiionization. Besides, the chemiionization could be one of the stages for creation of inversion population on transitions of easily ionized fractions. In particular, the ionization in the powerful high pressure lasers on helium-heavy rare gas mixtures is going on by charge exchange of the helium ions or by chemiionization.

The chemiionization reactions are used as an important stage at the impurity detection in the laser isotope separation.

Many works (see for example [1–5]) have been dedicated to the investigation of the chemiionization reactions. However, up to now the reactions involving two excited particles remain comparatively less studied, while works examining the spectra of the electrons, created in these reactions, simply do not exist, due to the experimental difficulties for conducting such measurements.

If chemiionization reactions are going on in a plasma, it turns out that the ratio between the energy of the appearing electrons and the average energy of the plasma electrons is quite important. At the emerging of hot, fast electrons an unequilibrium is established, which influences substantially the processes of excitation, ionization and recombination, the character of the charged particles diffusion and the temperature of the main group of electrons.

The electron impact quenching is quite important for the variation of the excited states density, especially the metastable density. This process and the chemiionization have common features: participation in reactions with excited particles and delivering of the excitation energy to an electron. It is clear that the study of the quenching processes gives information for the electron impact excitation of atoms and molecules.

In this review the results of investigations of the chemiionization processes and the quenching of excited atoms, which are accompanied by a creation of fast electrons are given. Considerable attention is paid to the least studied problem – chemiionization reaction involving two excited atoms. Different methods for investigations of the processes of forming fast electrons are discussed, including the new method of plasma electron spectroscopy (PLES), based on detection of electron spectra, yielded by the corresponding reactions in a plasma.

## 1. Processes of creating fast electrons and methods for their investigation

From all possible reactions involving excited atoms, as mentioned above, a particular interest represents the processes in which ions and electrons are created by collisions between slow heavy particles (chemiionization (CI) processes),

$$A^* + B^*(B) \Rightarrow A^+ + B + e + \{\varepsilon_p\}, \tag{1.1}$$

$$A^* + B^*(B) \Rightarrow AB^+ + e + \{\varepsilon_A\}, \tag{1.2}$$

or interactions in which the potential energy of the excited states is delivered to the electrons (quenching, second kind

collisions, superelastic collisions).

$$A^* + e \rightleftharpoons A + e + \{\varepsilon_i\}. \tag{1.3}$$

Here, $A^*$ and $B^*$ are different (or similar) excited atoms; $A$ and $B$ are normal atoms; $A^+$ is an atomic ion, while $AB^+$ is a molecular ion; e is an electron acquiring the energy $\varepsilon_e$, $\varepsilon_A$ or $\varepsilon_i$ in the reactions (1.1)–(1.3) exit channels. The processes (1.1) is penning ionization (PI), (1.2) is associative ionization (AI).

The energy of the electrons appearing in the chemiionization processes (1.1) and (1.2) depends on the ratio between the excitation and ionization potentials of the colliding partners. If the total energy of excitation, $E_{1A} + E_{1B}$, of both atoms, $A^*$ and $B^*$, in the reaction entrance channel is much more than the ionization potential of the atom, $E_{A^+}$, or the molecule, $E_{AB^+}$, the fast electrons appear in reactions (1.1) and (1.2) with energy $\varepsilon_{e,A} \approx E_{1A} + E_{1B} - E_{A^+}(E_{AB^+})$. Here, $\varepsilon_{e,A} \gg kT_e$, while $T_e$ is the temperature of the maxwellian part of the electron velocity distribution function in the plasma. For example, this is the case when excited hydrogen, rare gases, halogens, nitrogen or oxygen atoms are involved in chemiionization processes. The reactions (1.1) and (1.2) may go on at nonsymmetric interactions, with participation of normal and excited atoms, if the energy of the excited atom substantially exceeds the partner ionization energy. A distinctive feature of the chemiionization processes is the fact that the ionization and gaining of the kinetic energy (in the first row by the electrons) is implemented at the expense of the internal excitation energy.

Up to now a considerable experimental and theoretical information about the characteristics of the processes (1.1)–(1.3) has been stored (see for example [1–5]).

The ways of influence of the chemiionization upon the low temperature plasma properties have also been cleared out [6]. This influence is multilateral as can be seen from (1.1)–(1.3). Really, the reactions under consideration lead immediately to a destruction of the excited states and appearing of electrons and different types of ions. Therefore, they may cause a change in the charged particles density and, as a consequence, to a change in the determination of the plasma ion composition, the type of ionization and recombination.

Consider the reaction characteristics, the group of the rare gas atoms in which CI always produces fast electrons will be examined most closely.

Since excited atoms take part in the processes (1.1), (1.2) and charged particles with different masses and energies (electrons, atoms and molecular ions) are formed in these reactions, information for the essential characteristics of the ionization can be derived by: (a) – investigating the variations of the excited atom density; (b) – using the method of mass – spectroscopy; (c) – using the method of electron spectroscopy.

Up to now, reactions (1.1), (1.2) in rare gases have been studied mainly in two types of experiments: in afterglow plasma and in merging beams.

The method used to obtain the rate constant for binary interaction of excited atoms in the afterglow plasma consists in calculations and measurements of the corresponding atoms density time dependencies. Such investigations are not widely spread due to the existence of other, more effective channels for a destruction of the excited levels, especially the radiative ones.

By mass-spectroscopy the relative yield of molecular and atomic ions in the interactions of excited atoms He* + He*, Ne* + Ne*, Ar* + Ar* has been studied. Besides, as seen from the review [1], for the common object of investigations – the reaction He* + He*, the discrepancy between the results is more than one order of magnitude. The difficulties of the mass-spectroscopic diagnostic of reactions (1.1), (1.2) are connected with the following circumstances. First of all the interaction chamber (plasma volume) and the ion analyzer are spatially divided. This allows changes in the ion composition of the charged particles at their movement towards the analyzer. Second, atomic and molecular ions may appear in the plasma not only in reactions (1.1), (1.2), but also in other competitive processes, as for example Hornbeck–Molnar reactions, or the conversion of atomic into molecular ions in three-body interactions. On the third place there are definite difficulties in the calibration of the analyzer sensitivity towards different ion species.

The cross-section energy dependence of reactions (1.1), (1.2) in the energy range 0.01–10 eV for the metastable atom pairs He* – He*, He* – Ne*, Ar* – Kr* has been investigated up to now using the merging beam technique [1]. The ion composition of the reactions (1.1)–(1.2) was analyzed there. A weak point in this work is the lack of selection between the different types metastable atoms.

This review shows that at the chemiionization processes examination in the quoted, not so numerous, works, one of the reaction products, namely the fast electrons, have not been used. In this connection it is expedient to compare the methods mentioned above as (a), (b) and (c) from the viewpoint of the information for the interactions, obtained by their application. The following interactions characteristics are of considerable interest: (1) the processes (1.1), (1.2) cross-sections dependence on the colliding particles relative energy; (2) the respective processes rate constants dependence on the colliding particles temperature; (3) the energy spectra of the ions, appearing in reactions (1.1), (1.2); (4) the energy spectra of the electrons, appearing in the same reactions; (5) the angle distribution of these electrons; (6) the energy state of the molecular ion, appearing in reaction (1.2); (7) the potential curves of the particles in the entrance and in the exit channels of reaction (1.1), (1.2); (8) the width of the quasimolecular $A^*B^*$ autoionization term.

The application of method (a) allows to solve the problems "2" or "1" depending on modification of the method. The mass-spectroscopic diagnostics give an opportunity to determine in principle the first and the third characteristics as well as partially the seventh characteristic – the well depth of the quasi molecule potential curve. Only the electron spectroscopy methods allow to find out all listed above characteristics of the interaction. Thus the widest information for the processes (1,1), (1.2) may be obtained, examining the energy spectra of the arising electrons.

It was pointed out that these processes could be investigated in a decay plasma or using beam technique.

The afterglow plasma has definite advantages connected with the comparatively large density of the excited atoms ($10^{10}$–$10^{12}$ cm$^{-3}$), including radiative states. The beam experiments give the opportunity to carry out investigations at fixed energy of the colliding particles but at that completely evident difficulties appear, connected with the creation of two excited atoms beams possessing sufficient

intensity (all the more this could be applied to the atoms in the radiative states).

We shall continue with the reaction (1.3) which has not been discussed in details sofar. Suffice it to say that the examination of this process in the afterglow plasma by its immediate products e.g. – the fast electrons – allows to determine the rate coefficient dependence on the electron temperature, $T_e$, or the energy dependence of the corresponding cross-section.

From the above consideration a conclusion can be drawn for the advisability of the processes (1.1)–(1.3) investigation by a new method, which combines the advantages to examine these elementary reactions in the plasma with the resources of the electron spectroscopy – the method of plasma electron spectroscopy (PLES).

The accomplishment of this task requires an analysis of the relation between the electron energy distribution function in the plasma and the elementary processes (1.1)–(1.3) and, on this ground, a development of experimental methods for determination of their basic characteristics. Let us consider the problems listed above in the given order. Afterwards we shall dwell upon the results obtained in the investigation of the processes (1.1)–(1.3) and the influence of these processes on the plasma properties.

## 2. Electron energy distribution function and plasma electron spectroscopy method

In this section the relation between the spectra of electrons appearing in the reaction (1.1–1.3) and the electron energy distributing function (EEDF) will be examined.

### 2.1 *Kinetic equation for the electrons*

In order to accomplish the task set above, it is necessary to find the electron distribution function from the Boltzman kinetic equation. We shall consider the case $\lambda \ll \Lambda$, where $\lambda$ is the length of the electron free path and $\Lambda$ is the characteristic diffusion length of the plasma volume. For cylindrical geometry with radius $R$, $\Lambda = R/2.4$. Then, at $\nu_a \gg \nu^e$ ($\nu_a$, $\nu^e$ are the frequencies of elastic and inelastic electron–atom interactions) in the EEDF expansion by spherical harmonics we could keep the first two terms only. It is advisable to write down the kinetic equation in variables $r$ and total energy, $\varepsilon$:

$$\varepsilon = \frac{mv^2}{2} + e\phi(r), \tag{2.1}$$

where $e\phi(r)$ is the radial (ambipolar) potential. Then, in a cylindric geometry, the equation for the isotropic part of the EDF could be laid down in the form (see for example [7–9]):

$$\frac{1}{r}\frac{\partial}{\partial r}\left(rvD_r\frac{\partial f_0}{\partial r}\right) + \frac{\partial}{\partial\varepsilon}\left[v\left(D_e\frac{\partial f_0}{\partial\varepsilon} + V_e f_0\right)\right] - \nu_{me}(v)vf_0\Big|_w^{w+E_e} + \nu_{0m}v\left[f_0(\varepsilon, r) - \frac{g_0}{g_m}\frac{N_m(r)}{N_a} f_0(\varepsilon - \varepsilon_1, r)\right] - \beta_m N_m^2 R_m(w)v. \tag{2.2}$$

Here, $D_r = v\lambda/3$ is the coefficient of free electron diffusion, $D_e = D_E + D_a + D_e$, $V_e = V_e + V_a$ are the coefficients of diffusion and dynamic friction in energy space at the expense of the external field (index E), elastic electron–atom (index a) and electron–electron (index e) interactions. In its turn,

$$D_E = 2w^2e^2E^2/(3m\nu_a); \quad D_a = w\,\delta\nu_a T_e; \quad V_a = w\,\delta\nu_a; \tag{2.3}$$

$$D_e = w\nu_e T_e A_0(w), \quad V_e = A_0(w)\nu_e,$$

$$A_0(w) = \begin{cases} 0.385w/T_e, & w/T_e \leqslant 2.6, \\ 1, & w/T_e \geqslant 2.6. \end{cases} \tag{2.4}$$

The approximation $A_0(w)$ [10] enables us to approach the electron–electron interactions in the whole energy region

$$\nu_e = 2\nu_{ee} = 2\pi e^4 N_e \Lambda_k/\sqrt{2m}\, w^{3/2}, \tag{2.6}$$

where $\Lambda$ is the Coulomb logarithm.

$$\nu_{me}(w)f_0(\varepsilon, r)v\Big|_w^{w+E_e} = \nu_{me}(w)f_0(\varepsilon, r)v - \nu_{me}(w + E_e, r) \times f_0(w + E_e, r)\sqrt{v + 2E_e/m}. \tag{2.7}$$

Here, $\nu_{me}$ is the total frequency of stepwise excitation and ionization processes from the level $m$; $E_e$ is the energy threshold of these processes; $N_a$ and $N_m$ are the density of normal and excited atoms; $g_a$ and $g_m$ are the statistic weights of these levels; $\beta_m$ and $R_m$ are the rate constant and the energy spectra of the reactions (1.1), (1.2); $N_e$ is the electron number density; $\nu_{0m}$ is the frequency for excitation of the level $m$ from the ground state; $\varepsilon_1$ is the excitation potential of level $m$.

The first term of eq. (2.2) describes the diffusion departure of electrons to the walls. The second one – the variation of their energy at the expense of the electron–electron and the elastic electron–atom collision as well as the heating in the external electrical field. The first term in the equation right part corresponds to changes in the electron energy in stepwise excitation, the second – to changes in indirect excitation and deexcitation collisions (reaction (1.3) and the inverse one); the third – the appearance of fast electrons in reactions (1.1), (1.2). $R_m(w)$ is the source density for creation of these electrons, normalized by the condition

$$\int_0^\infty R_0(w)\sqrt{w}\,\mathrm{d}w = 1. \tag{2.7}$$

In some cases it is more convenient to rewrite the term corresponding to reaction (1.3) in (2.2), introducing the respective source $R_e(w)$,

$$\frac{g_0}{g_m}\frac{N_m(r)}{N_a} f_0(\varepsilon - w, r)v\nu_{0m}(v) = \beta_e N_m N_e R_e(w)v, \tag{2.8}$$

where $\beta_e$ is the reaction (1.3) rate constant, $R_e$ is its energy spectra, normalized by the condition (2.7).

It is presumed in eq. (2.2), that atoms in one excited state with number $m$ take part in reactions (1.1)–(1.3). In the weakly ionized discharge and currentless plasma this is the metastable state or a block of lower long living resonance and metastable states. Their population is much larger than the population of other excited states and usually is comparable or exceeds the charged particles number density. In the photo plasma this is the resonance level, pumped by the external radiative source, etc. When several excited states, participating in the processes (1.1)–(1.3), should be accounted, the corresponding terms in eq. (2.2) have to be written additively in the form of a sum.

Further, we shall neglect the stepwise processes (if not stated otherwise) at solving of the kinetic equation. Using

the Tomson formula,

$$\nu_{mc} = N_m \frac{\pi e^4 \sqrt{2}}{\sqrt{m} w E_c} \left(1 - \frac{E_c}{w}\right), \tag{2.9}$$

the cross-section for elastic scattering of electrons, $\sigma_c = (10^{-15}–10^{-16}\,\mathrm{cm}^2)$, the typical values of $\delta = (10^{-4}–10^{-5})$ and the Coulomb logarithm, $\lambda_k \simeq 10$, we could get the following estimates:

$$\frac{\nu_{mc}}{\delta\nu_e}\frac{E_c}{w} \simeq 10^6 \frac{N_m}{N_e}; \quad \frac{\nu_{mc}}{\nu_e}\frac{E_c}{w} \simeq \frac{N_m}{N_e}\frac{1}{2\lambda_k} \simeq \frac{N_m}{20N_e} \tag{2.10}$$

It is easily seen from (2.10) that $\nu_e > \nu_{mc}$ up to $N_m/N_e < 20$, which is usually fulfilled in low temperature plasma. For this reason, even at $N_m/N_e > 10^{-6}$, the most typical situation is when stepwise excitation does not compete with the interelectron and elastic electron–atom collisions.

The boundary condition for the EDF on the tube axis is

$$\left.\frac{\partial f_0(\varepsilon, r)}{\partial r}\right|_{r=0} = 0, \tag{2.11}$$

and on the walls,

$$\frac{(\varepsilon - e\phi(R))}{4\varepsilon} f_0(\varepsilon, R) = -\tfrac{1}{3}\lambda \left.\frac{\partial f_0(\varepsilon, r)}{\partial r}\right|_{r=R}, \tag{2.12}$$

where $\phi(R)$ is the potential gap between the axis and the tube wall (the wall potential).

The condition (2.12) could be derived from the particle balance in a thin near wall layer with thickness $\lambda$. The multiplier $e\phi(r)/\varepsilon$ accounts for the reflection of electrons from this layer, which is connected with the existence of near wall potential jump. Its value is usually several $T_e/e$ [9]. At $\varepsilon \gg e\phi(R)$, in the case under consideration here, $\lambda/R \ll 1$, condition (2.12) takes the form:

$$f_0(\varepsilon, R) = 0. \tag{2.13}$$

The distribution function is normalized on the electron density.

It is not difficult to show that the solution of the kinetic equation (2.2) could be represented as a sum:

$$f_0 = f_{0s} + f_{0f}, \tag{2.14}$$

where $f_{0s}$ is the EDF of main group electrons, obtained without taking into account the fast electron sources (solution of the homogeneous equation); $f_{0f}$ is the EDF of fast electrons, born in the CI processes (1.1), (1.2) and in the quenching collisions (1.3). Comparing the radial gradients terms of $f_0$ with the function variations, due to elastic and inelastic interactions, we get that the ratio between them determines the relaxation parameter,

$$K(\varepsilon) = (\nu_e + \delta\nu_e + \nu_{mc} + \nu_{0m})\tau_{df}$$
$$= k_{el} + k_{at} + k_{in} = \frac{\Lambda^2}{\lambda_\varepsilon^2}, \tag{2.15}$$

where $\tau_{df} = \Lambda^2/D_r$ is the time for free diffusion of electrons to the walls,

$$\lambda_\varepsilon = (4D_r/(\nu_e + \delta\nu_e + \nu_{mc} + \nu_{0m}))^{1/2}$$
$$\approx \lambda \sqrt{\frac{\nu_s}{\nu_e + \delta\nu_e + \nu_{mc}\varepsilon_c/\varepsilon + \nu_{0m}}} \tag{2.16}$$

is the energy relaxation length of an electron with energy $\varepsilon$ [7]. Let us make some estimations: at typical values of the cross-section for elastic scattering of electrons on atoms, $\sigma_s \simeq (10^{-15}–10^{-16})\,\mathrm{cm}^2$, $\delta \simeq 10^{-4}–10^{-5}$, $\Lambda \simeq 1\,\mathrm{cm}$ we can get that in the elastic energy region $w < \varepsilon_1$, $\lambda_\varepsilon \gg \Lambda$ at neutral gas pressure, $p \leqslant 10\,\mathrm{Torr}$, and electron density $N_e \leqslant 10^{12}\,\mathrm{cm}^{-3}$.

At $K \gg 1$, which corresponds to the case $\Lambda \gg \lambda_\varepsilon$, when the terms with radial gradient of $f_0$ and the potential $\phi(r)$ could be neglected in the kinetic equation, the electron distribution function can be found in a local approximation. In this case the EDF is determined by the local plasma parameters in every point, while the variable of $f_0$ is the kinetic energy, $w = mv^2/2$.

At $K \leqslant 1$, the terms with gradients of the EDF and the potential $\phi(r)$ became essential. The variables in $f_0$ are $r$ and the total energy, $\varepsilon$ (2.1) [7]. For this reason it is necessary to know the ambipolar potential profile, $\phi(r)$, and the value of the near wall potential jump, $\Phi_k$, in order to find the distribution function. In turn, these quantities are determined by the EDF type. As far as the transverse diffusion of the electrons in the nonlocal case is faster than the variation of their energy in the interactions, the energy distribution function in a given space region is determined not only by the plasma parameters of this region but also by the whole volume. The method for calculation of the EDF in the nonlocal regime has been developed in [7] and was applied for the positive column of the low pressure gas discharge. It was shown there that, accounting for the diffusion of electrons towards the walls, the circumstance of principle became the ratio between the electron energy and the wall potential value, $\phi(R)$. The electrons with energy $\varepsilon < e\phi(R)$ could move across the tube only in the limits from $r = 0$ to $r = r_0(\varepsilon)$, determined by the condition $\varepsilon = e\phi(r_0)$ (Fig. 1). In this way, the electrons with energy $\varepsilon < e\phi(R)$ turn out to be locked in the volume, while those with $\varepsilon > e\phi(R)$ go to the walls in a free diffusion regime. Since the wall potential is $\phi(R) > \varepsilon_1/e$ in the discharge [7], a basic interest constitute the EDF form at $\varepsilon < e\phi(R)$.

A different situation is usually realized in currentless plasma, where, due to the low electron temperature value, the wall potential, (several $T_e/e$) is small. In this case the fast

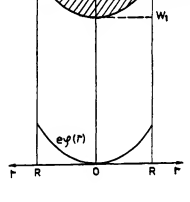


*Fig. 1.*

electrons, born in chemiionization processes and super-elastic collisions, are in a flying regime, e.g. they are moving towards the walls in a free diffusion regime and are neutralized there. Besides, as it was shown in [11], depending on the creation rate of fast electrons, the anomalous potential jump $\Phi_h \simeq \varepsilon_p$, $\varepsilon_1$ could appear and a part of the fast electrons is trapped in the volume. The experiments with controlling of the fast EEDF part, when the large potential jump is created artificially, are of great interest as well. This jump is created by applying a regulated blocking potential on the conducting wall (see Section 7.2).

### 2.2. *Distribution function of the main group of electrons*

In the local approximation, $K \gg 1$, the $f_{0s}$ form had been examined in a number of works (see for example [8] and [9]). For this reason we will shortly review the main results. At $\varepsilon < \varepsilon_1$ the function has the form

$$f_{0s}(w) = C_n \exp\left[-\int_0^w dw/(T(w))\right] + C_1, \tag{2.17}$$

where

$$T(w) = D_e/V_i \tag{2.18}$$

is the characteristic temperature of the electrons with energy $w$; $C_n$ is a normalization constant, which for a Maxwell distribution is

$$C_n(r) = N_e(r)\left(\frac{m}{2\pi T_e}\right)^{3/2}. \tag{2.19}$$

At a diffusion character of the charged particle losses,

$$N_e(r) = N_e(0)\,e^{-[e\phi(r)/T_e]} = J_0\left(\mu_1 \frac{r}{R}\right)N_e(0), \tag{2.20}$$

where $J_0$ is the zero order Bessel function, $\mu_1$ is the function first root, $C_1$ is found by the sewing condition at $w = \varepsilon_1$. In the currentless plasma ($D_E = 0$) $f_{0s}$ is a Maxwellian function with temperature $T_e (\nu_e \ll \delta\nu_a)$ or $T_a (\nu_e \gg \delta\nu_a)$. $f_{0s}$ in a plasma within an external electrical field is also a Maxwellian one when $\nu_e \gg \delta\nu_i$. At $\nu_e \ll \delta\nu_i$, depending on $\nu_e = \nu_e(\varepsilon)$ it is either Druvestain type or some of its analogs. The form of $f_{0s}$ beyond the threshold $\varepsilon > \varepsilon_1$ depends on the parameter $a_1$, which is the ratio between the elastic and inelastic interactions,

$$a_1 = \frac{\nu_{1m}\,T(\varepsilon)}{V_i(\varepsilon)} \simeq \frac{\nu_{1m}(\varepsilon_1 + T(\varepsilon_1))}{(\nu_e(\varepsilon_1) + \delta\nu_a(\varepsilon_1))}\,\frac{T(\varepsilon_1)}{\varepsilon_1}. \tag{2.21}$$

The inelastic processes are not significant at $a_1 \ll 1$ and the function $f_{0s}$ remains in the form (2.17) with $C_1 = 0$. For the intensive excitation from the ground state at $a_1 > 1$ a depletion of the EDF fast part occurs. At the limit $a_1 \gg 1$, "the black wall" approximation is justified in the inelastic processes threshold $f_{0s}(\varepsilon_1) = 0$ [7], so that

$$C_{1(n)} = -C_n \exp\left[-\int_0^{\varepsilon_1} d\varepsilon/(T(\varepsilon))\right].$$

If the condition $K \gg 1$ is not fulfilled, (e.g. when the local approximation is not applicable), an account of the electron diffusion towards the walls is required. We said that the electrons with energy $\varepsilon < e\phi(R)$ turn out to be imprisoned in the potential well. Therefore, the EDF for these energies could be considered independent of $r$ at $K \ll 1$. By integration of the kinetic equation for $f_{0s}$ over $r$ from 0 up to $r_0(\varepsilon)$, taking into account the corresponding boundary condition:

$$\left.\frac{\partial f_0(\varepsilon, r)}{\partial r}\right|_{r=r(\varepsilon)} = 0, \quad \varepsilon = e\phi(r_0), \tag{2.22}$$

we shall get $f_{0s}$ in the form (2.17), with a substitution of $T(\varepsilon)$ by $\overline{T(\varepsilon)} = \overline{D_e/V_i}$. The averaging over $r$ is determined as follows:

$$\overline{X}(\varepsilon) = \frac{2}{R^2}\int_0^{r_0(\varepsilon)} X(\varepsilon - e\phi(r), r) r\, dr. \tag{2.23}$$

As can be seen from (2.17), when $\nu_e > \delta\nu_a$, the EDF is a Maxwellian one too, but now that applies only to energies $\varepsilon < e\phi(R)$. The electrons with energies $\varepsilon > e\phi(R)$ go to the walls in a free diffusion mode. Since during the diffusion time, $\tau_{df}$, one electron succeeds to diffuse in energies altogether to

$$\Delta\varepsilon = \sqrt{4D_i\tau_{df}} \simeq \frac{2\Lambda}{\lambda_i}\,T_e \ll T_e,$$

for the EDF at $\varepsilon \geqslant e\phi(r)$ it is possible to use the "black wall" approximation. Thus, in the non-local forming conditions a depletion of the EDF beyond the wall potential takes place. The EDF nonlocality reveal itself in this since the electrons in every tube point, including the axis region "feel" the character of the near wall electron behavior. This has repercussions on the EDF form in the whole volume. The effect of the EDF depletion beyond the wall potential was observed experimentally in the afterglow plasma in [12].

### 2.3. *Distribution function of the fast electrons*

The case when $T(\varepsilon) \ll \varepsilon_p, \varepsilon_1$ will be discussed below.

In currentless plasma ($D_E = 0$) this is always the case. It usually occurs also in a plasma within an external electric field. In strong fields, at inelastic balance, $T(\varepsilon) \geqslant \varepsilon_p,\ \varepsilon_1$. Under these conditions the EDF is formed by diffusion in energy space in the electric field and by inelastic processes. Then the role of the CI processes (1.1), (1.2) and the super-elastic collisions (1.3) is negligible.

2.3.1. *Nonlocal regime* ($K \leqslant 1$). Let us concentrate on the formation of the EDF fast part, $f_{0f}$, in the currentless plasma under the conditions when the radial diffusion of the fast electrons is significant, $K \leqslant 1$. The opposite case, $K \gg 1$ will be examined further. First, we shall elucidate the qualitative form of the EDF in the considered nonlocal regime. If, in (2.2), we account only for the radial diffusion in the approximate form $f/\tau_{df}$ and the creation of electrons in reactions (1.1), (1.2), then $f_{0f}$ takes the form:

$$f_{0f} = \beta_m N_m^2 R_m(v)\,\tau_{df}. \tag{2.24}$$

For example, the energy distribution is simply copying the source $R_m(v)$ form and exhibits the corresponding maximum with a width of about 1 eV (see below). Accounting for interactions in determination of the function $f_{0f}$ leads to the dilution of the indicated maximum towards bigger and smaller energies, due to diffusion and dynamic friction, respectively, in energy space. For a Maxwellian EDF main body from

(2.8) we get that the source:

$$R_s(w) = 2g_m \nu_{0m}(w)\sqrt{w}\exp\left(-\frac{\varepsilon-\varepsilon_1}{T_e}\right)\Big/\sqrt{\pi}\, g_0\, \beta_e\, N_m\, T_e^{3/2} \tag{2.25}$$

has the form of a narrow peak with a width of about $T_e$ near $\varepsilon_1$. The maximal energy at which electrons appear in collisons of two metastable atoms, $\varepsilon_s \leqslant 2E_m + D_2^+ - E_{ion}$, is usually several eV smaller than $\varepsilon_1$. ($D_2^+$ is the dissociation energy of the molecular ion). Thus, in helium $\varepsilon_1 = 19.8$ eV, $\varepsilon_s \leqslant 15.6$ eV. Since $R_m(w) = 0$ at $w > \varepsilon_s$, while $R_s(w) = 0$ at $w < \varepsilon_1$, the $R_m(\varepsilon)$ and $R_s(\varepsilon)$ spectra could be considered as not overlapping. For this reason, in the cases when it is possible to neglect the processes of direct excitation (reaction, inverse to (1.3)), the terms $R_m$ and $R_s$ enter in (2.2) on equal base. That is why we shall continue the further analyses, using one of them, for example $R_m(w)$.

Following [13], let us find the fundamental solution (the Green's function) of eq. (2.2) with a term $R_m$ in the right part, representing $R_m$ in the form of a $\delta$-function:

$$R_m(w) = \delta(w - \varepsilon_p)/\varepsilon_p^{3/2}. \tag{2.26}$$

Here, $\varepsilon_p$ is the characteristic energy of the fast electrons, born in reaction (1). For instance, $\varepsilon_p \simeq 14.5$ eV for $He(2^3S_1)$ atoms and $\varepsilon_p = 4.5$ eV for $Xe(^3P_2)$ atoms.

The general solution of the kinetic equation, as it is known, is a convolution of the fundamental solution with the real distribution $R_m(w)$. For the problems of the plasma kinetics it is often possible to neglect the fine structure of $R_m(w)$ and $R_s(w)$ spectra. We can represent them in the form of (2.26). From now on, the function $f_{0r}(\varepsilon, r)$ will mean the solution of (2.2) with the right part comprising $R_m(w)$ in the form (2.26). The solution of this equation will be sought in the form of a series:

$$f_0(\varepsilon, r) = \sum_{k>1} f_k(\varepsilon) J_0\left(\mu_k \frac{r}{R}\right), \tag{2.27}$$

where $J_0(x)$ is the Bessel function, which satisfies the boundary condition (2.12). The values of $\mu_k$ are roots of the equation

$$\frac{J_0(\mu_k)}{\mu_k J_1(\mu_k)} = -\frac{\lambda}{R}\frac{\varepsilon}{[\varepsilon - e\phi(R)]}. \tag{2.28}$$

From (2.12, 2.28) it follows that the $\mu_k$ dependence on energy can be neglected for the case when $e\phi(R) \ll \varepsilon_p$, while the $\mu_k$ values are the zero order Bessel function roots.

Let us substitute the series (2.27) into eq. (2.2) and integrate it from 0 to $R$, neglecting the dependence $\nu(r)$ by virtue of the condition $\varepsilon_p \gg |e\phi(r)|$. Since the substantial energy region has the width $\sim T_e$ near $\varepsilon_p$, it is possible to neglect in (2.2) the coefficients dependence on the kinetic energy, taking them at the value $w = \varepsilon_p$. The correctness of this assumption can be easily seen from the final formulas, given below (2.34).

Through a number of transformations, we finally get the following equation for the determination of $f_k(\varepsilon)$, [13],

$$T\frac{\partial^2 f_k}{\partial \varepsilon^2} + \frac{\partial f_k}{\partial \varepsilon} - \frac{f_k}{\varepsilon_p K_k} + I_k n_e^2[\theta(\varepsilon - \varepsilon_p) - \theta(\varepsilon - \varepsilon_p - e\phi(R))] = 0. \tag{2.29}$$

Here

$$T = (T_e\nu_e + T_a\,\delta\nu_a)/(\nu_e + \delta\nu_a). \tag{2.30}$$

Depending on the conditions, in the region $T_a \leqslant T \leqslant T_e$,

$$K_k = (\nu_e + \delta\nu_a)\tau_{dk}; \quad \tau_{dk} = R^2/\mu_k^2 D_r, \tag{2.31}$$

$$I_k = \beta_m \Big/ \left[g(\varepsilon_p)T(\nu_e + \delta\nu_a)\int_0^R J_0^2\left(\mu_k \frac{r}{R}\right) r\,\mathrm{d}r\right], \tag{2.32}$$

$$n_e^2 = N_m^2(r_0) J_0\left(\mu_m \frac{r_0}{R}\right)\frac{r_0}{e\phi'(r_0)}. \tag{2.33}$$

$r_0(\varepsilon)$ is found from the condition $\varepsilon - \varepsilon_p = e\phi(r_0)$, $\theta(x)$ is the Heawyside step function,

$$\phi'(r_0) = \left.\frac{\partial \phi}{\partial r}\right|_{r=r_0} = E_s(r_0)$$

is the radial field.

During the transition from (2.2)–(2.29), when $\nu_e T_e > \delta\nu_a T_a$, we take the first term only in the expansion of $\nu_e(r)$ in series of $r$. This approximation is correct in the axial part of the tube, where $\partial\nu_e(r)/\partial r$ is near zero. However, in the peripheral regions, $\nu_e(r)$ sharply drops and the inequality $\nu_e T_e < \delta\nu_a T_a$ is already observed. Then, it is possible to neglect the term with $\nu_e$, being too small.

The equation (2.29) is solved, using the boundary conditions. Sewing the obtained solutions, as results for $f_k$ [13], we get:

$$\begin{aligned} f_k(\varepsilon) = {} & 2C_1\theta(\varepsilon_p - \varepsilon)\exp\left(-\frac{\varepsilon}{T}\right)\sinh\left(\frac{\lambda_k \varepsilon}{2T}\right) \\ & + [\theta(\varepsilon_p + e\phi(R) - \varepsilon) - \theta(\varepsilon_p - \varepsilon)] \\ & \times \int_{\varepsilon_p}^{\varepsilon} n_e^2(t)\exp\left(-\frac{t-\varepsilon}{2T}\right)\sinh\left(\frac{\lambda_k}{2T}(t-\varepsilon)\right)\mathrm{d}t \\ & + C_2\,\theta(\varepsilon - \varepsilon_p - e\phi(R))\exp\left(-\frac{(\lambda_k+1)\varepsilon}{2T}\right), \end{aligned} \tag{2.34}$$

where

$$\lambda_k = (1 + 4T/\varepsilon_p K_k)^{1/2}, \tag{2.35}$$

$$C_1 = I_{1k}\frac{I_k}{\lambda_k};$$

$$C_2 = 2C_1\exp\left(\frac{\lambda_k(\varepsilon_p + e\phi(R))}{2T_k}\right) - \frac{C_1}{I_{1k}}(I_{1k} - I_{2k}), \tag{2.36}$$

$$\begin{Bmatrix} I_{1k} \\ I_{2k} \end{Bmatrix} = \int_{\varepsilon_p}^{(\varepsilon_p + e\phi(R))} n_e^2(t)\begin{Bmatrix} \exp\left\{-\frac{(\lambda_k - 1)t}{2T}\right\} \\ \exp\left\{\frac{(\lambda_k + 1)t}{2T}\right\} \end{Bmatrix}\mathrm{d}t. \tag{2.37}$$

At $K_k \ll 1$, the terms of the series (2.27) with $f_k(\varepsilon)$ in the form (2.34) rapidly decrease, since the $\mu_k^2$ values create a growing sequence. In this case the first few addends give sufficient accuracy. For the same reason the terms with $m \geqslant 3$ give a negligible contribution in the sum for $\nu_{ek}$.

In the pure nonlocal case, $K \ll 4T_a/\varepsilon_p \ll 1(\lambda_k \gg 1)$, the expression (2.34) acquires clearer form. Here, the fast electrons, created in (1.1) and (1.2), move to the wall practically without changing their energy in collisions. Making a tran-

sition to the limit in (2.34)–(2.37) we get:

$$f_k(\varepsilon) = \frac{\beta_m}{g(\varepsilon_p)} \frac{N_m^2(r_0) J_0\left(\mu_k \frac{r_0}{R}\right)}{\int_0^R J_0\left(\mu \frac{r_0}{R}\right) r \, \mathrm{d}r} \frac{r_0}{e\phi'(r_0)} \times \tau_{\mathrm{at}} k(\theta(\varepsilon_p + e\phi(R) - \varepsilon) - \theta(\varepsilon_p - \varepsilon)). \quad (2.38)$$

The sum of the series (2.27) with $f_k(\varepsilon)$ in the form (2.38) is equal to

$$f_0(\varepsilon, r) = \frac{\beta_m}{g(\varepsilon_p) \varepsilon_p D_r e\phi'(r_0)} \int_r^R \frac{\mathrm{d}r'}{r'} \times \int_0^{r'} N_m^2(r'') \delta(\varepsilon - \varepsilon_p - e\phi(r'')) r'' \, \mathrm{d}r'' = \frac{\beta_m N_m^2(r_0) r_0(\varepsilon)}{g(\varepsilon_p) \varepsilon_p D_r e\phi'(r_0)} \left( \theta(r_0 - r) \ln \frac{R}{r_0} + [\theta(r - R) - \theta(r - r_0)] \ln \frac{R}{r} \right). \quad (2.39)$$

The series (2.27) is itself a Fourier–Bessel expansion of eq. (2.39), the right part, with $f_k(\varepsilon)$ according to (2.38). This result comes immediately from (2.2). There, in accordance with the examined boundary case, the diffusion and the drift in energy space have to be neglected. Then, the integration with boundary conditions (2.11), (2.12) immediately gives (2.39). Thus, the general solution (3.34) and the expression (3.39) enable us to calculate the electron distribution function in the decay plasma at $\varepsilon > e\phi(R)$ with a given initial energy spectrum of the source, $R_m(t)$, creating fast electrons. The expression (2.38) was obtained in the initial works [14, 15] by neglecting the difference between the total and the kinetic energy.

It has already been mentioned that, in the case when the processes of direct excitation (the reaction, inverse to (1.3)) can be neglected, the fast electron sources $R_m(w)$, (reactions (1.1), (1.2)) and $R_k(w)$, (reaction (1.3)) enter in (2.2) on equal base. For this reason, expressions (2.34) and (2.39) are also suitable to describe EDF in the energy region where the reaction (1.3) is important. It is necessary only to change $\varepsilon_p$ by $\varepsilon_1$ (excitation potential of the level $m$ in (1.3)).

Let us consider now the specificity of the EDF forming at $\varepsilon \simeq \varepsilon_1$, connected with the influence of the direct excitation processes. If we compare the efficiency of the diffusion departure and the direct excitation in the energy region $\varepsilon \sim \varepsilon_1$, we have to remember that the electrons with energy $\varepsilon_1 < \varepsilon < \varepsilon_1 + e\phi(R)$ can undergo direct excitation only in the region where their kinetic energy $w > \varepsilon_1$ (see Fig. 1). Therefore, the parameter, characterizing the ratio of the processes in question has to be written in the form (compare with $K_{\mathrm{in}}$ in (2.15)):

$$K^* = \nu_{0m}(\varepsilon_1 + T_e) \begin{cases} \tau_{\mathrm{at}}, & \varepsilon > \varepsilon_1 + e\phi(R) \\ (r^*)^2/\mu_1 D_r, & \varepsilon_1 < \varepsilon < \varepsilon_1 + e\phi(R). \end{cases} \quad (2.40)$$

Here, $r^*$ is determined by the condition $e\phi(r^*) = \varepsilon - \varepsilon_1$ (see Fig. 1). The inelastic collision frequency, $\nu_{0m}$, is taken for exactness at an energy equal to $\varepsilon_1 + T_e$. The formulas (2.34) and (2.39) are applicable when $K_{\mathrm{el}} \leqslant 1$ and the role of the inelastic collision is insignificant, e.g. $k_{\mathrm{in}} \ll 1$ or $k_{\mathrm{in}} \ll (\nu_e + \delta\nu_a)\tau_{\mathrm{at}} \varepsilon_1/4T$ (see (2.35)). The last inequity gives the ratio of the characteristic time spent by an electron for direct excitation to the time for which, due to elastic collisions, its energy decreases to values less than $\varepsilon_1$, e.g. it leaves the energy region, where it could accomplish a direct excitation.

In the examined purely nonlocal case for the source $R_k(w)$ (2.25), at a Maxwellian distribution of the electrons main group, we get [16]:

$$f_{0r} = \sqrt{\frac{2e}{m}} \frac{N_a(0) g_0}{D_r(\varepsilon_1) g_m} \left( \frac{m}{2\pi T_e} \right)^{3/2} \exp\left( -\frac{\varepsilon - \varepsilon_1}{T_e} \right) \times \int_r^R \frac{\mathrm{d}r'}{r'} \int_0^{r'} N_m(r'') \sigma_{0m}(\varepsilon - e\phi(r'')) r'' \, \mathrm{d}r''. \quad (2.41)$$

In Fig. 2, for comparison, one can find the result of nonlocal EDF calculation at different $r$ with account of the radial field (solid lines), following (2.41) and without it (dotted lines). The calculation was made by a linear approximation of the $\sigma_{0m}(w)$ energy dependence and $N_m(r) = constant$. The expression $e\phi(r) = 1.44 T_e^2 (r/R)$ was used for the radial potential profile. The accounting of the radial electric field leads to a shift of the maximum, connected with reaction (1.3), towards higher energies and also to a change in the EDF form, as seen in Fig. 2. This is due to the fact that the electrons from the tube peripheral regions give their contribution to the energy distribution with a shift by a value $e\phi(r)$ on the total energy scale.

An interesting limit case could be distinguished in the forming of the nonlocal EDF fast part, when $k_{\mathrm{el}} \leqslant 1$, but, at that, $k_{\mathrm{in}} \gg 1$ (see (2.15)). Similar conditions frequently occur since, usually, $\nu_{0m} > \delta\nu_a$. Then, the EDF beyond the excitation threshold $\varepsilon_1$ is determined by the local balance of excitation and quenching collisions. Thus, from (2.2), at a

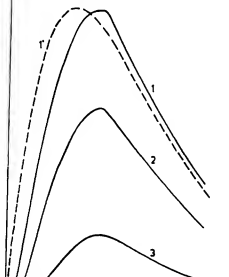


*Fig. 2.* Afterglow EEDF in the excitation threshold region in the nonlocal regime. 1–3 – calculation with account of the ambipolar field (2.41) for $r/R = 0$, 0.5 and 0.8; 1' – calculation for $r = 0$ under the assumption $\phi(r) = 0$.

Maxwellian distribution of the main group, we have [16],

$$f_{0r}(\varepsilon, r) = \frac{g_0}{g_m}\frac{N_m(r)N_e(0)}{N_a}\left(\frac{m}{2\pi T_e}\right)^{3/2}\exp\left(-\frac{\varepsilon-\varepsilon_1}{T_e}\right)$$
$$= \frac{g_0}{g_m}\frac{N_m(r)N_e(r)}{N_a}\left(\frac{m}{2\pi T_e}\right)^{3/2}\exp\left(-\frac{w-\varepsilon_1}{T_e}\right). \quad (2.42)$$

The EDF is nonlocal at $\varepsilon < \varepsilon_1$ and it is possible to obtain its decrease in this region in the same way as has been done deriving relation (2.34). From (2.42) can be seen that at $\varepsilon > \varepsilon_1 + e\phi(r)$ the EDF simply copies the distribution of the main group electrons.

2.3.2. *Local regime* ($K \gg 1$). It has already been pointed out that at $K \gg 1$, corresponding to $\lambda \gg \lambda_a$, the radial diffusion term in the kinetic equation (2.2) can be neglected. At that, it is possible to find EDF in a local approximation and to neglect also the difference between the total energy, $\varepsilon$, and the kinetic one, $w$ (see (2.1)).

The form of the fast electrons EDF, $f_{0r}$, depends on the relaxation mechanism of these electrons, determined by the ratio between the frequencies $\nu_{me}$ and $\nu_e + \delta\nu_a$, e.g. by the value of the parameter

$$a_e = \frac{\nu_{me}E_\varepsilon}{V_e} = \frac{\nu_{me}E_\varepsilon}{(\nu_e+\delta\nu_a)\varepsilon}. \quad (2.43)$$

As it follows from the evaluations (2.10), most typical is the situation, when $a_e < 1$. In this case the appearing fast electrons relax by electron–electron and by elastic electron–atom collisions, e.g. by processes with small energy losses. The integration of (2.2) at $T(\varepsilon) \ll \varepsilon_p$ and $a_e \ll 1$ gives immediately

$$f_{0r}(w < \varepsilon_1, r)$$
$$= \left\{\int_0^w \frac{dw'}{\sqrt{w'}D_e(w)}\left[C_1 + \beta_m N_m^2(r)\int_{w'}^\infty R_m(w'')\sqrt{w''}\,dw''\right]\right.$$
$$\left.\times \exp\left[\int_0^{w'}\frac{dw''}{T(w')}\right]\right\}\exp-\left[\int_0^w \frac{dw'}{T(w')}\right]. \quad (2.44)$$

The first term in (2.44) corresponds to the distribution of electrons, born in reaction (1.3), the second one to those born in (1.1), (1.2). The expression for $C_1$ depends on the ratio of efficiencies of direct excitation and elastic collisions in the energy region $w \geqslant \varepsilon_1$. In accordance with that mentioned above, it is determined by the parameter (compare with (2.21))

$$K' = 4a_1 = \frac{\nu_{0m}(\varepsilon_1+T_e)4T_e}{(\nu_e+\delta\nu_a)\varepsilon_1} = \frac{k_{in}}{k_{el}}\frac{4T_e}{\varepsilon_1}. \quad (2.45)$$

The parameter $K'$ values, calculated for the rare gases under the assumption $\nu_e < \delta\nu_a$ (weakly ionized plasma) are shown in Table I. In particular it follows from the table that in most of the cases at low temperatures ($T_e \leqslant 0.1$ eV), $K' \ll 1$ is realized, e.g. the role of direct excitation is insignificant. Then, for $C_1$ in (2.44) the expression:

$$C_1 = \beta_e N_m N_e \quad (2.46)$$

is correct. That corresponds to the results of works [14, 15].

In the opposite case, $K' \gg 1$, when EDF at $w > w_1$ is determined by the balance of exciting and quenching collisions and is expressed by (2.42) [16], $C_1$ can be found by the condition of sewing (2.42) and (2.44) at $w = \varepsilon_1$.

Table I. *Parameters $K_{in}^*$ and $K'$, characterizing the role of the low metastable level direct excitation in the EDF forming ($T$ – in eV, $R$ – in cm, $p$ – in Torr)*

| Atom | $K_{in}^* = \nu_{0m}(\varepsilon_1+T_e)\tau_{el}$ | $K' = [\nu_{0m}(\varepsilon_1+T_e)/\delta\nu_a]kT_e/\varepsilon_1$ |
|---|---|---|
| He | 1.62 | 19.5 |
| Ne | 0.0296 | 3.2 |
| Ar | 1.87 | 4.43 |
| Kr | 2.17 | 21.5 |
| Xe | 29.2 | 87.6 |

$\cdot\, p^2R^2\sqrt{T_e}$ and $\cdot\, T_e^{3/2}$

$$C_1 = \frac{g_0}{g_m}\frac{N_m(r)N_e(r)}{N_a}\left(\frac{m}{2\pi T_e}\right)^{3/2}$$
$$\times\left[\int_0^{\varepsilon}\frac{dw'}{\sqrt{w'}D_e(w')}\exp-\int_{w'}^w\frac{dw''}{T(w'')}\right]^{-1} \quad (2.47)$$

It is possible to simplify the expressions obtained for $f_{0r}$ in the energy range $w \gg T_e$, in which we are interested, taking into account that with an accuracy up to the correction $T_e/w \ll 1$,

$$\int_0^w \frac{dw'}{\sqrt{w'}D_e(w')}\exp\left(\int_{w'}^w\frac{dw''}{T(w'')}\right)$$
$$= \frac{1}{w^{3/2}(\nu_e+\delta\nu_a)} = F(w) \quad (2.48)$$

is satisfied.

Indeed, integrating the right side of (2.48) by parts we get:

$$\int_0^w \frac{dw'}{\sqrt{w'}D_e(w')}\exp\left(\int_{w'}^w\frac{dw''}{T(w'')}\right)$$
$$\approx F(w)\left[1-\frac{T(w)}{w}+\frac{T^2(w)}{w^2}+\right]$$
$$\approx F(w)\left[1-\frac{T(w)}{w}\right]^{-1} \approx F(w), \quad (2.49)$$

where $T(w) = D_e/V_e$ is the characteristic electron temperature.

For this reason, in the case $K' \ll 1$, having in mind (2.44), $f_{0r}$ can be written down in the approximate form:

$$f_{0r} = \frac{\sum_{i=m,\,l}\theta(\varepsilon_j-w)\beta_j N_m N_j\int_w^\infty R_j(w')\sqrt{w'}\,dw'}{w^{3/2}(\nu_e+\delta\nu_a)}, \quad (2.50)$$

where $\varepsilon_l = \varepsilon_1$, $\varepsilon_p$ is the minimal energy of an electron appearing in reaction (1.1). As seen from (2.17), (2.50) the complete EDF in the examined local case consists a Maxwellian (or near to it at $\nu_e \sim \delta\nu_a$) distribution in the low energy region and two steps at high energies, connected with reactions (1.1), (1.2) and (1.3). The physical meaning of these expressions is evident: the appearing fast electrons relax in the processes with small energy losses, creating a continuous electron spectra in the region $\varepsilon < \varepsilon_j$. In the case $K' \gg 1$ (see (2.45)), the second step, accounting for (2.42), $f_{0r}$ will take the form:

$$f_{0r} = \frac{g_0}{g_m}\frac{N_m(r)N_e(r)}{N_a}\left(\frac{m}{2\pi T_e}\right)^{3/2}\left\{\left[\frac{\nu_e(\varepsilon_1)+\delta\nu_a(\varepsilon_1)}{\nu_e(w)+\delta\nu_a(w)}\left(\frac{\varepsilon_1}{w}\right)^{3/2}\right]\right.$$
$$\left.\times\,\theta(\varepsilon_1-w)+\theta(w-\varepsilon_1)e^{-(w-\varepsilon_1)/T_e}\right\}. \quad (2.51)$$

Expressions of the type of (2.50) have been obtained in [14, 15]. In the work [16] solutions were given, similar to (2.51), yielded by neglecting the terms with $df/d\varepsilon$ in (2.2). In Fig. 3 are shown typical results of an experimental study in the helium afterglow plasma. They are illustrations to the relations derived here. The measurements have been carried out by the method of probe current modulation 70 μs after the end of the discharge. The duration of the discharge active stage was 10 μs with 650 μs repetition period for the pulses. The pulse current was 0.5 A. The parameter $K$ at $\varepsilon_p = 15$ eV was 0.75, 1.9 and 3.7 for pressures $p = 2.6$, 4.2 and 5.8 Torr, respectively. It can be seen that with increasing pressure, the EDF maxima, caused by the reactions (1.1)–(1.3), involving $He(2^3S_1)$ atoms, became more and more wide, due to the growing role of the elastic collisions in comparison with the diffusion. Already at $p = 5.8$ Torr they turn into a step, described by the expressions given above.

The number of fast electrons $N_{ef}$ is determined by the source intensity and the value $\nu_a + \delta\nu_a$, e.g. in the first row by the densities of normal atoms, excited atoms and electrons. For the source, conditioned by the chemiionization processes,

$$N_{ef} = \beta_m N_m^2/(\nu_e + \delta\nu_a). \tag{2.52}$$

At $\varepsilon_p > \delta\nu_a$, for $\beta_m \simeq 10^{-9}\,\mathrm{cm^3\,s^{-1}}$ and $\varepsilon_p \simeq (4.5 - 15)$ eV,

$$N_{ef} \simeq (10^{-4} - 10^{-5}) N_m^2/N_a. \tag{2.53}$$

For the weakly ionized plasma ($\nu_e < \delta\nu_a$), for typical values of $\nu_a \simeq 10^5 p$ ($p$ – gas pressure in Torr),

$$N_{ef} \simeq 10^{-14} N_m^2/p. \tag{2.54}$$

From the results obtained above and the conducted estimations follow that in the region $\varepsilon > T(\varepsilon)$, the chemiionization processes and the superelastic collisions can substantially enrich the distribution function by fast electrons. This effect manifests itself most clearly in the currentless plasma, when low electron temperatures are realized and the EDF fast part is determined completely by both types of processes. In the discharge plasma, where $T_e$ is high, the influence of the CI processes on the EDF can usually be neglected. However, at a relatively large metastable atom density, as in the cryogenic discharges, the effect of distribution function enrichment at the expense of these processes is quite substantial, too. We shall also point out that the CI role could be significant in not self sustained discharges, where, in contrast to the self sustained discharges, the metastable atoms densities are large, while the parameters $E/N_a$ (and therefore $T_e$, too) are small ($T_e \ll 1$ eV).

In the other boundary case, $a_c \gg 1$, the appearing fast electrons relax on stepwise processes. As a result the energy loss proceeds not quasi continuously but in a discrete way with a step equal to the threshold, $E_c$. Then, as can be seen from (2.2), (2.7), $f_{of}$ has the form of maxima (nearly equal height) around the points

$$\varepsilon = \varepsilon_j - nE_c \qquad (\varepsilon_j = \varepsilon_p, \varepsilon_1;\ n = 0, 1, 2, \ldots)$$

$$f_{of}(\varepsilon_j) = \frac{I_j R_j(\varepsilon)}{\sqrt{\varepsilon}\,\nu_{ms}(\varepsilon)};$$

$$f_{of}(\varepsilon) = \frac{\sqrt{\varepsilon + E_c}\,\nu_{ms}(\varepsilon + E_c)}{\sqrt{\varepsilon}\,\nu_{ms}(\varepsilon)}\, f_{of}(\varepsilon + E_c). \tag{2.55}$$

For a source, conditioned by the superelastic collisions, the relation (2.55) is correct at $a_1 \ll 1$ or at $a_1 \ll a_c$. From (2.11) follows that a quite hard condition, $N_m \gg 20 N_a$, should exist in order to accomplish this boundary case. It is quite difficult to create such conditions in a discharge plasma either in the active stage or in the afterglow period. The situation changes in the currentless photo-plasma, where a large resonance state density $N_m$ is created (up to a saturation with the normal atom density at laser excitation [17]) by an external selective photo excitation. Further, we consider the cases when the power of the external light is insufficient for the multi-photon ionization processes. In laboratory conditions the photo plasma is made usually in metal vapors, therefore the fast electron sources are superelastic collisions.

The case $a_c \gg 1$ is realized easily in non-stationary conditions at creation of photo plasma. In stationary conditions, with low radiation intensities, usually $N_m/N_e = (10 - 10^2)$ is settled [18] at $N_m \ll N_a$. Thus the intermediate case, $a_c \simeq 1$ is accomplished.

The solution of the kinetic equation, in the local regime for an arbitrary ratio between the frequencies $\nu_e + \delta\nu_a$ and $\nu_{mc}$, is given in [6].

The fact that the stepwise processes could be important in the forming of the fast electron DF is confirmed by the experiments, conducted in cesium photo plasma [18] under the conditions $N_a = 2 \cdot 10^{15}\,\mathrm{cm^{-3}}$, $N_e = 2 \cdot 10^{11}\,\mathrm{cm^{-3}}$, $N_m = 2 \cdot 10^{12}\,\mathrm{cm^{-3}}$ and $T_e = 2000$ K (see Fig. 4). As seen from the figure, a drop, connected with the stepwise processes influence is observed at $\varepsilon < \varepsilon_1 = 1.42$ eV.

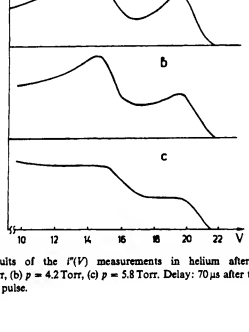


*Fig. 3.* Results of the $I''(V)$ measurements in helium afterglow. (a) $p = 2.6$ Torr, (b) $p = 4.2$ Torr, (c) $p = 5.8$ Torr. Delay: 70 μs after the end of the current pulse.

### 2.4. *Determination of different elementary processes characteristics by the plasma electron spectroscopy method*

In this part we will consider the possibility to acquire information about processes going on in currentless plasma, using the electron energy distribution function. Primary

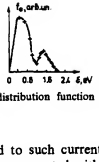


*Fig. 4.* Electron velocity distribution function in currentless Cs photo plasma [18].

attention will be paid to such currentless plasma such as afterglow plasma. It is connected with the simplicity of its creation and with the possibility for application of various experimental methods.

It turns out that the comparison of the experimental EEDF with the results of the corresponding theoretical calculation allows to determine the characteristics of various elementary processes taking place in afterglow plasma.

This circumstance is the background of the method of plasma electron spectroscopy (PIES). It is developed in several works [4, 14, 15, 19], which will be discussed further on.

It has already been mentioned that some of the most important processes, determining the EDF forming in the afterglow plasma are the reactions involving excited atoms. The distribution function itself is represented by the characteristics of these processes: $\beta_m$, $\beta_\varepsilon$, $R_m$ and $R_\varepsilon$.

From the examination conducted so far it follows that in the nonlocal regime, when the relaxation parameter (2.15) $K \ll$ , the fast part of the EDF has the form of maximums in the energy regions, where fast electrons have been born in reactions (1.1)–(1.3). The distribution drops exponentially beyond the limits of the corresponding energy spectra (see (2.39)). In this case the fast electrons move to the tube walls, failing to undergo energy relaxation in the volume, while the form of the EDF fast part is determined by the form of the reactions (1.1)–(1.3) electron spectra. If we integrate the kinetic equation (2.2) in the limits of existence of these spectra, then, due to the absence of the energy flux beyond this region ($K \ll 1$), the second term of the equation drops out. The next integration over $r$, using the boundary conditions for the fast electron number, $S_\varepsilon$,

$$\left.\frac{dS_\varepsilon}{dr}\right|_0 = 0; \quad S_\varepsilon(R) = 0, \tag{2.56}$$

gives immediately

$$S_\varepsilon^{(j)}( = \frac{\beta_j}{D_\varepsilon(w_j)} \int_r^R \frac{dr'}{r'} \int_0^{r'} N_m(r'')N_j(r'')r''\, dr''. \tag{2.57}$$

Here the indices $m$, $j$ refer to reactions (1.1), (1.2) and (1.3), respectively. It is presumed, that the direct excitation did not play a significant role.

We must point out that the integration of expression (2.3 over the energy immediately gives (2.57), as well.

As can be seen from (2.57), the determination of the coefficient $\beta_j$ requires: first, to determine the number of fast electrons $S_\varepsilon(0)$, from the distribution function absolute measurements, for example on the tube axis; second, to measure in absolute scale the excited atom, $N_m(r)$, and electron $N_j(r)$, density radial dependencies; third, to calculate the electron diffusion coefficient of the fast electrons, $D_\varepsilon(r)$.

It can be shown [16] that the formula derived in [19] for calculation of the fast electron number on the tube axis is the first term of the (2.57) expression expansion in a Fourier–Bessel series. Indeed, if, after the integration of (2.2) on $\varepsilon$, the substitution

$$S_\varepsilon^j(r) = \sum_{k=1}^{\infty} A_k J_0\left(\mu_k \frac{r}{R}\right),$$

is made and the consideration is confined by the series first term, we can get:

$$S_\varepsilon^{*(j)}(0) = \frac{\beta_j R^2}{\mu_1^2 D_\varepsilon(w_j)} \frac{\int_0^R J_0\left(\mu_1 \frac{r_0}{R}\right) N_m(r) N_j(r) r\, dr}{\int_0^R J_0^2\left(\mu_1 \frac{r_0}{R}\right) r\, dr}, \tag{2.58}$$

which coincides with expression (3) of work [19]. Here, $\mu_k$, in accordance with the boundary condition (2.56), are roots of the Bessel function $J_0(x)$. According to (2.57), the value $S_\varepsilon^{*(j)}(0)$ can vary from $0.85 S_\varepsilon^j(0)$ at $N_m(r)N_j(r) \sim J_0^2[\mu_1(r_0/R)]$, to $1.1 S_\varepsilon^j(0)$ at $N_m(r)N_j(r) = constant$, depending on the $N_m(r)$ and $N_j(r)$ radial profile.

Further, we shall turn to the application of the PIES method for investigation of superelastic collisions. It was presumed at deriving expression (2.57), that the processes inverse to (1.1)–(1.3) did not play a role in the fast electron balance. This is correct in a wide range of conditions for reactions inverse to (1.1), (1.2). However, the processes of direct excitation could be quite significant in afterglow plasma of low pressure. In compliance with the previous part these processes are not significant and the use of (2.57) is legal, if the conditions $K_m^* \ll 1$ or $K' \ll 1$ could be fulfilled. The values of the parameters $K_m^*$ and $K'$ for rare gas plasma are shown in Table I (the low metastable level is taken for exactness). The approximations of the cross-section for elastic electron–atom collisions, $\sigma_u$, were taken from [20], data for $\beta_\varepsilon$ – from [4, 14] and it was presumed that $v_e < \delta v_u$ (typical conditions for measurements of the superelastic collision constant).

The table shows that, in most of the cases, for $\beta_\varepsilon$ measurements by the PIES method in the nonlocal regime, it is possible to accomplish conditions when the direct excitation processes are insignificant. An appropriate pressure and a sufficient delay after the discharge pulse end are required, when $T_e$ is near to the ambient one. Thus, the rate coefficients of the elementary processes are determined in the described PIES method, using the immediate product of the corresponding reaction – the fast electrons.

We shall point out that two groups of problems can be solved by the PIES method. The solution of the first one, the rate coefficients determination, has been considered above. In this case it is necessary to measure the integral electron spectra – the fast electrons density $S_\varepsilon$ or $S_m$. At that, the requirements towards the energy resolution of the experimental device for EDF measurements are not high. The second group of problems is connected with acquiring detailed information about the processes (1.1)–(1.3). Examples are – efficiency of Penning and associative ionization, particle potential curves in the entrance and exit reactions channel, energy state of the formed molecular ion. For that it is necessary to investigate the structure of the $R_m(v)$ spectrum, formed by the appearing electrons. The integral information is insufficient here. It has already been shown that the nonlocal regime is most convenient for determi-

nati of the (1.1)–(1.3) reaction spectra. Then the role of the isions is negligible and the function's form is determ- mir by the form of the fast electron source (see (2.24)).

E cession (2.34), obtained in the previous part (the Gre function of the kinetic equation (2.2)), can be reg d as a theoretical broadening function of the reac- tio .1)–(1.3) initial electron spectrum. It enables us to cal e the broadening of these spectra, due to broadening inte ions and radial electric field in each particular case. Besi s, each spectra is, generally speaking, a solution of the inte l equation. Its right part is the experimental EDF and s left part is a convolution of the spectrum with exp ion (2.34).

I lear that a better way to determine the $R_m$ and $R_*$ is to t onditions where $f_{0r}$ repeats the $R_m$ and $R_*$ form with hig curacy (see (2.24)) and the spectra distortion, given by ression (2.34), is minimal, instead of solving the res ve incorrect problem (by working out the integral equ n).

T broadening of the initial spectra due to the collisions is g n by the expression $\sim \exp(\sqrt{(4T/w_j K)} \cdot (\varepsilon - \varepsilon_j)/T)$. Thi oadening can be made indefinitely small by selecting the periental conditions in which $K \ll 4T_e/\varepsilon_j \ll 1$. The phy l meaning of this fact is obvious. The variable of the ED n these conditions is the total energy and the radial elec field will be the single factor distorting the energy spe . The corresponding broadening function, which co lso be named theoretical instrumental function (IF) of PIES method, is given by expression (2.39). It is ob from (2.39) that the IF of the radial field $I_{\phi'} \cdot f_0(\varepsilon, r)$ exi t a finite energy interval, from $\varepsilon = w_0$ to $\varepsilon = w_0$ + e ). The width of the $I_\phi$ base is equal to $e\phi(R)$, the val f which is determined by $T_e$, while the $I_\phi(\varepsilon, r)$ form to a g extent depends on the metastable radial distribution, $N_m$ The dependencies $I_\phi(\varepsilon, r)$ at $N_m(r) = N_m(0)J_0(\mu_m r/R)$ wi $_m = 0$ (curves 1, 2, 3) and $\mu_m = 2.4$ (curves 1', 2', 3') are sh in Fig. 5. It can be seen that the $I_\phi(\varepsilon, r)$ half width, de ined as the FWHM of the instrumental function, de s substantially on $r$. It grows up from the center to s the peripheries. The IF half width decreases sub- sta y at the transition from a rectangular profile of $N_r$ o a Bessel one with $\mu_m = 2.4$ (see curves 1–3 and 1'– specially in the tube centre regions, other conditions bel qual. For this reason the experiments for determi- na of the spectra of reactions, producing fast electrons us e PIES method by EDF measurements in the after- gl ould be done in the axis. Besides, it is necessary to cr onditions, when $K \ll 4T_e/w_p$. In addition, the meta- sta rofile should be as narrow as possible.

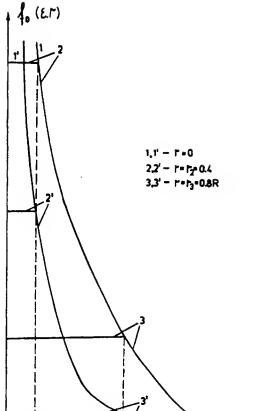


*Fig. 5.* Electron velocity distribution function. See text.

## 3. rimental methods of investigation

It hown in the previous paragraph that the investiga- tio the electron spectra and the rate constants of reac- tio .1)–(1.3) have to be conducted in the afterglow pl whose parameters satisfy the condition $K \ll 1$. In or obtain the quantitative characteristics of reactions (1. 3) it is necessary to measure with adequate time re m: the EDF fast part, the electron temperature and de as well as the radial distribution of the exited atoms de

l as examine consecutively the methods applied for investigation, paying special attention to the EDF measurement.

### 3.1. *Measurement of the electron energy distribution function*

The analyzer of the electron energy for non distorted measurement of the EDF has to fulfill the requirement $\lambda \gg d$, where $\lambda$ is the electron free path length and $d$ is the analyzer characteristic size. The implementation of the condition $K \ll 1$ and the high density of the excited atoms ($\simeq 10^{10}$–$10^{12}$ cm$^{-3}$) require a pressure of the examined gas in the plasma volume between 0.1 and 5 Torr. As a result, for the maximal possible value of $d$ we get the estimation $d \simeq 0.1$ cm. This limitation makes impossible the application in our condition of traditional electron analyzer used for example in the Penning electron spectroscopy. At the same time it is obvious that a single Langmuir probe can serve in the capability of such analyzer. For measurements of the electron velocity distribution function it will operate in the pulse mode. Stemming from all that, the investigation of the reactions (1.1)–(1.3) in this work are carried out by an electrical probe. A probe method for the EDF measurements in a plasma with periodically varying parameters, based on probe current commutation is used [21].

As it is well known [2], the scheme of the Penning electron spectroscopy experimental setup consists of four main parts: 1 – source of excited particles; 2 – collision cell for interaction of the excited particles; 3 – analyzer of the electron energy; 4 – registration unit.

The first and the second scheme parts are united in the PIES method. Their role is played by the plasma volume, while the electric probe works as an energy analyzer. That simplifies substantially the experimental setup.

probe methods for EDF investigations are based on
uvestayn relation [22]. It connects the distribution
n and the second derivative of the electron probe

$$f(\quad = \frac{m^2}{2\pi e^3 S}\frac{d^2 I_e}{dV^2}, \qquad (3.1)$$

S is the probe area, $V$ is the probe potential with
to the plasma potential, $I_e$ is the electron probe

methods for EDF determination used in the practice
mainly in the manner by which $d^2I/dV^2$ is obtained.
work, for a double differentiating of the probe
its modulation has been used [22]. An alternative
with a small amplitude (differentiating signal) is
ced into the probe circuit and some of the probe
t harmonics are recorded. In our investigations
$\Delta V$, of the type:

$$\Delta \quad 2V_1 \cos \omega_1 t \qquad (3.2)$$

$$\Delta \quad \sqrt{2}\, V_1(1 + \sin \Omega t) \sin \omega_2 t \qquad (3.3)$$

ed as differentiating signals.
is shown in [23] that the amplitudes of the probe
harmonics, $I_{2\omega_1}$, on frequency, $2\omega_1$ (in the first case),
harmonics on frequency, $\Omega$ (in the second case), are
ed with the second derivative of the probe current
spect to the probe potential $I''(V) = d^2I/dV^2$ by the
n:

$$I_2 = V_1^2 \int_0^\infty I''(V') A_{1,2}(V, V')\, dV' \equiv V_1^2 (I'' * A_{1,2}), \qquad (3.4)$$

$A_1$ and $A_2$ are the normalized instrumental functions
of device for EDF measurements. A more detailed
tion of the used probe methods and measurement
is given in [4]. The probe circuit current sensitivity
experimental setup was $5 \cdot 10^{-11}$ A on the detection
cy $2\omega$ (for modulating signal $\Delta V_1$). The minimal fast
density, which should be detected at a probe of
$4.5 \cdot 10^{-3}$ cm, length 2 cm, $2V_1 = 0.15$ V, is $10^5$ cm$^{-3}$.
cal form of the distribution function fast part,
ed experimentally in the afterglow is presented in Fig.
The measurements have been carried out in neon at
ure of 0.9 Torr, a current in the pulse of 0.8 A and a
fter the current pulse end of 120 μs. It is seen from
ure that the distribution function has a complicated,
notonous character in the energy range 8–20 eV.
eculiarities can be explained by the appearance of
trons in reactions (1.1)–(1.3). Thus, the maximum at
gy of 16.6 eV arises at the expense of the superelastic

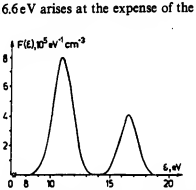


Fi ectron energy distribution function in neon afterglow plasma.

collisions of slow electrons with excited neon atoms in the states $2p^53s$. The maximum at the energy 11 eV is due to the binary interactions of the excited neon atoms in the same states.

### 3.2. *Measurements of the electron temperature, electron density and the excited atoms density*

In this work the electron temperature was determined from the measured curve of the probe current second derivative $I''$, by the relation

$$T = 11\,600\ \Delta V/\Delta \ln I''(V), \qquad (3.5)$$

where $T_e$ is the temperature in K, $\Delta \ln I''(V)$ is the variation of the second derivative logarithm on the interval of probe potential variation, $\Delta V$, in volts. In the afterglow plasma, at not too low density of electrons, a Maxwellian distribution is established. It is a consequence of the intensive inter-electron interactions, due to the low energy of the electron aggregation. This determines the correctness of expression (3.5). The existence of a linear ln $I''$ dependence in an interval with a sufficient length (about $3–4kT_e$) serves as a guarantee for a correct determination of $T_e$. At that, the systematic error in $T_e$ value did not exceed 10%. The experimentalists come up against a number of difficulties at measurements of the electron density, $N_e$, in decay plasma. These difficulties are a result of the afterglow specificity–low electron temperature, inaccurate determination of the plasma potential, $V_p$, distortion of the probe current near $V_p$. For this reason, $N_e$ determination either by probe current measurements at $V = V_p$ or by integration of the area beneath the $f(\varepsilon)$ curve did not yield reliable results. A preference was given to the $N_e$ measurement by the plasma conductivity. Two variants of the method were used: an additional pulse is applied on the discharge tube electrodes in a chosen moment of the afterglow. The conductivity is measured during the time of pulse action in the first version. (It is the so-called method of the second pulse [24].)

The conductivity, and, therefore, the plasma density is measured in the discharge active phase with a following calculation of the $N_e(t)$ evolution in the second one. The accuracy of $N_e$ determination is about 30% by this method. There are several ways to measure the excited atom density in a plasma [25] nowadays. The spectral lines intensity, emitted by the afterglow plasma is low. That is why the most convenient method here is the two tubes absorption method. It enables us to find the density of atoms in low energy states. The errors in the determination of the excited atoms density have values of about 20% in this method.

After this brief inspection of the experimental methods, applied in the investigations, it is expedient to compare, once again, the resources of the conventional Penning electron spectroscopy and the PIES. As far as the information of the studied elementary processes in the Penning electron spectroscopy and the PIES method is derived by the analyses of the electron spectra, yielded by the corresponding reactions, these two methods are near by their possibilities. However, there are substantial differences between them due to the fact that the investigations by the PIES method are conducted in a plasma, while the Penning electron spectroscopy uses atomic beams encounter. In this respect the plasma electron spectroscopy has evident advantages at the study of the ionization processes involving two

me ble atoms, all the more if these atoms are not in
me ole but in radiative states. Due to the above men-
tio dvantages up to now the electron spectra of the che-
mi zation reactions involving two excited atoms were
stu d by the PIES method only. The opportunity to apply
op l methods for measurements of the excited atoms
de y allows to carry out (unlike to the Penning electron
sp o-copy) absolute measurements with a high accuracy.
As as the energy resolution is concerned, at present the
Pe g electron spectroscopy surpass in this parameter
Pl v 5–10 times. We shall point out that the application
of Penning electron spectroscopy allows to obtain the
cr tion dependence on the colliding partners energy
an o the angle distribution of the emerging electrons.
Th S method enables to determine the processes rate
co t for different atoms temperatures of the interacting
pa s. As it is known, the reactions rate constants give
in ation about the reaction's cross-sections, averaged
ov e velocities of the colliding particles and over the
el scattering angles. At present, a considerable infor-
m for the ionization processes, involving excited atoms
is s l by the Penning electron spectroscopy method. The
co nding results and also the detailed description of
th hod itself is given in reviews and books, for example
[2 For this reason further we shall present and discuss
th lts obtained by the Penning electron spectroscopy
an o by the mass-spectroscopic and optical methods,
cl elated to the subject of this review.

## 4. igation of the interaction between the rare gases d atoms

### 4.1 ermination of the rate constant of the chemiionization pr s (*reactions* (1.1), (1.2))

In resent work investigations of the ionization pro-
ce volving noble gases atoms in identical or different
ex tates have been carried out. As is seen from relation
(2. eculiarities connected with one or several simulta-
ne actions are observed on the distribution function.
Th pend on the densities $N_m^{(i)}$, $N_m^{(k)}$ of different excited
atc nd the corresponding rate constant $\beta_m^{(i,k)}$ values. The
sel of the binary reactions, involving excited atoms in
dil states is conducted by the PIES method, using their
ele spectra directly (in the case when they are
se, l) or using the intensity variation of the electron
sp at variation of the different excited states relative
de .

easurements were carried out under the following
co s: a periodic DC pulse discharge of the rare gases
he eon, argon, krypton, xenon and mercury, as well as
m of helium with krypton, xenon, $CO_2$ and $N_2$ was
fir ylindrical glass tubes (tube diameters – 30–40 mm)
wi d electrodes. The active phase durations were 10–
90 e repetition frequencies 0.5–5 kHz, the current
va 01–2 A. The gas pressure was varied in the range
0.1 r. Mobile and immobile probes with diameters
0.( 4 mm and lengths 10–20 mm have been introduced
in es.

### A. m

In lium afterglow six reactions are possible in which
th table atoms $He(2^1S)$ and $He(2^3S)$ as well as the metastable molecule $He_2(2^3\Sigma)$ could take part. The density of the $He_2(2^3\Sigma)$ molecules, existing in the afterglow mainly at the expense of conversion and recombination, become substantial at pressures higher than several Torr. Processes with their participation have not been examined in this work. A typical experimental result of EDF measurements in helium is shown in Fig. 7 [27] (pressure, 0.2 Torr, pulse current; 0.2 A, delay after the pulse switch off: 50 μs, amplitude of the modulating signal: 1 V from peak to peak). The maximum at the energy 14.4 eV appears, due to reaction $He(2^3S)$–$He(2^3S)$; the maximum at the energy 15.6 eV is due to the reaction $He(2^3S)$–$(2^1S)$; the maximum at energy of 16.2 eV is due to the reaction $He(2^1S)$–$(2^1S)$. As seen from the figure, we did not succeed in resolving the second and the third maxima on curve 1. This curve is widened by the instrumental function of the device, which hampers the determination of the rate constants of reactions involving $2^1S$–$2^1S$ metastable atoms. A processing of the yield EEDF was made by the Tikhonov regularization method [28], since eq. (3.4) is the first kind Fredholm integral equation with the experimental device instrumental function $A_2$ as a kernel in order to find the real EEDF from the measured one. The result of the processing [27] is also shown in Fig. 7 (curve 2). As far as the electron spectra of the different reactions overlap, results of EDF measurements at different $2^3S/2^1S$ atoms density ratio were used to resolve them (points). Thus, it is possible to observe only the maximum at 14.4 eV or two maxima (14.4 eV, 15.4 eV), or all three maximums. The electron yield spectra were used for determination of the reactions rate constants. The fact that the constant $\beta_m(2^3S, 2^3S)$ is well known was taken into account in order to decrease the systematic errors in the measurements of the constants $\beta_m(2^3S, 2^3S)$ and $\beta_m(2^1S, 2^1S)$. Its value, averaged upon the results of a great number of measurements is $\beta_m(2^3S, 2^3S) = (0.9 \pm 0.1)10^{-9}\,\mathrm{cm^3\,s^{-1}}$ [29, 30]. At the conditions in which the curve 1, Fig. 7 was obtained, the density of He $2^3S$ and He $2^1S$ atoms on the tube axis were $4.1 \cdot 10^{11}\,\mathrm{cm^{-3}}$ and $8 \cdot 10^{10}\,\mathrm{cm^{-3}}$, respectively.

The rate constants $\beta_m$, calculated from the experimental results by formula (2.57) and also the rate constants for close collision interaction, $K_m$, of the small atoms, are presented in Table II. The calculation of the close collision rate constant was made, using the relation [31]:

$$K_m = \alpha\gamma 2^{-1/6}\pi^{1/2}6\Gamma(5/3)C_6^{1/3}(kT_g)^{1/6}\mu^{-1/6}. \tag{4.1}$$

Here, $\alpha = 1$ for atoms of different kind, $\alpha = 1/2$ for similar atoms; $\gamma$ is a term, accounting for the spin conservation (4/9 for the $2^3S$–$2^3S$ couple and 1 for the other two couples); $\Gamma$ is the gamma function; $C_6$ is the Van der Vaals interaction

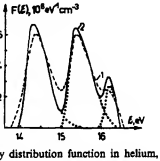


*Fig. 7.* Electron energy distribution function in helium, 1 – experimental results; 2 – result of the data processing by regularization method.

*Reaction rate constants, $\beta_m$, for various reactions constants for close collision interaction, $K_m$ as well e cross-sections, $\sigma_\beta$ and $\sigma_k$*

| on | $\beta_m$ $.10^{-9}\,cm^3\,s^{-1}$ | $K_m$ | $\sigma_\beta$ $.10^{-15}\,cm^2$ | $\sigma_{k_2}$ |
|---|---|---|---|---|
| 1 | )–He($2^1S$) | 0.9 ± 0.1 [42] | 0.92 | 5 ± 0.5 | 5.1 |
| 2 | )–He($2^1S$) | 4.0 ± 0.5 | 4.92 | 22.5 ± 3.0 | 27.6 |
| 3 | )–He($2^1S$) | 4.1 ± 0.9 | 3.36 | 23.0 ± 5.0 | 18.9 |
| 4 | )–Ne($^3P_2$) | 0.38 ± 0.04 | 0.86 | 4.8 ± 0.5 | 10.8 |
| 5 | )–Ne($^3P_2$) | 1.3 ± 0.4 | 1.59 | 16 ± 5 | 20.0 |
| 6 | )–Ar($^3P_2$) | 1.2 ± 0.2 | 0.81 | 22 ± 4 | 14.4 |
| 7 | )–Kr($^3P_2$) | 1.1 ± 0.2 | 0.52 | 29 ± 5 | 13.5 |
| 8 | )–Xe($^3P_2$) | 0.19 ± 0.03 | 0.48 | 6.2 ± 0.9 | 15.4 |

co
the
sta

$\mu$ is the reduced mass of the colliding atoms; $T_k$ is temperature, in our case equal to 300 K. The con- were taken from [32].

V
cor
sur
ass
cre
coi
in
ha
chi
co
sec
rat

'll point out that in Table II are presented the rate values with indicated accidental errors of mea- s and without distinguishing the channels of e and Penning ionization. They characterize the ate of fast electrons in the examined reactions and ith the rate constants for excited atoms quenching es, where different kinds of atoms take part. They e multiplied by a factor of two, when the quen- e in symmetrical collisions of excited atoms is 1. In the same table are given the effective cross- lues, determined as a ratio of the corresponding nt to the average relative atoms velocity,

$$\sigma_\beta = \left(\frac{8kT_k}{\pi\mu}\right)^{1/2}. \qquad (4.2)$$

he
Th
m

seen from the table, the measured rate values in quite close to the calculated close collision rates. vs a high auto-ionization efficiency of the quasi- appearing at the collision of the excited atoms.

re
qu
tri
[2.
figu
di
rea
ha

d be mentioned that under certain conditions the with participation of metastable atoms could be ficant in the forming of the electron energy dis- ot only in the currentless plasma. For example in g a glow discharge with a specific electrode con- in helium, for the first time the maxima on the n function have been observed, induced by the (1.1)–(1.3) and the corresponding rate constants calculated.

B.

*nd argon*

Th
sta
de
le

onstants of reactions between excited atoms in the $2p^53s\,^3P_2$, $^3P_1$, $^1P_0$ and Ar $3p^54s\,^3P_2$ have been l by the method described above [34, 35]. The and $^3P_0$ are metastable, while the level $^3P_1$ is

*Term parameters of the initial ($R_{i\varepsilon}$, $D_i$) and final ($R_{f\varepsilon}$, $D_f$) states; width $\Delta\varepsilon$ iative and Penning ionization spectra overlapping region at $E_i = 0.026\,eV$*

| C | oms | $R_{i\varepsilon}$, $a_0$ | $D_i$, eV | $R_{f\varepsilon}$, $a_0$ | $D_f$, eV | $\Delta\varepsilon$, eV at $E_i = 0.026$ eV |
|---|---|---|---|---|---|---|
| H | $^2S$) | 6.5 [45] | 0.6 [45] | 2 [45] | 2.5 [45] | 0.22 |
| N | $^3P_2$) | 5.9 [31] | 0.75 [31] | 3.2 [49] | 1.17 [49] | 0.06 |
| A | $^1P_2$) | 7.4 [49] | 0.52 [48] | 4.8 [31] | 1.23 [31] | 0.02 |
| K | $^3P_2$) | 7.8 [48] | 0.49 [48] | 5.4 [31] | 1.15 [31] | 0.02 |
| X | $^3P_2$) | 8.3 [48] | 0.45 [48] | 6.3 [31] | 1 [31] | 0.01 |

Pl

ta 50

In principle 10 binary reactions, involving atoms in the states $^3P_2$, $^3P_1$, $^3P_0$ and $^1P_1$ could proceed. However, due to the small energy gap between the levels (several hundredths eV), it is not possible to resolve the spectra of these reactions. For this reason it is necessary to carry out the measurements at different ratios of the different excited atoms densities and to solve the equation system afterwards. Besides, it turns out that all the 10 constants could not be determined from the derived system, since a part of these reactions should give a negligible contribution to the total fast electron density (substantially less than the accidental error of measurements). Therefore, the equation system will be unstable. That is why a preliminary assessment of the expected rate-constant values for the respective reactions is necessary. It was done using the relation (4.1). The constants $C_6$ for the neon and argon atoms (further for the krypton and xenon atoms, too) were calculated by the Slatter–Kirkwood formula [31]; a value of 1 was accepted for the multiplier $\gamma$ since it is not known whether the spin conservation rule is always abided by at the decay of the quasi-molecule [2].

The observed shape of the distribution function fast part in the neon afterglow plasma was presented above in Fig. 6. The maximum on the distribution function at energy 11 eV was used to find the fast electron density $S_m^{ia}$ and the constants $\beta_m^{ia}$. An equation system was worked out from the results of the measurements (more than 10 regimes). It was solved by the least square method. At that the three constants $\beta_m^{(2,2)}$, $\beta_m^{(2,1)}$ and $\beta_m^{(2,0)}$ are taken into account. The results obtained for the first two constants are shown in Table II. For the third one only the estimation $\beta_m^{(2,0)} < 5 \cdot 10^{10}\,cm^3\,s^{-1}$ turns out to be possible. If we for the constants not accounted for in the calculation accept the close collision rate values, this would not change the value of $\beta_m^{(2,2)}$ with more than 2% and the value of $\beta_m^{(2,1)}$ with more than 10%. This is an indication of the conducted calculation reliability. Since the density of atoms in the level $3p^54s\,^3P_2$ in the argon afterglow is between 70 and 95% of all the excited atom densities from the studied configuration, only the rate constant $\beta_m^{(2,2)}$ was determined (see Table III).

The following constant values: $\beta_m^{(2,2)} = (0.37 \pm 0.1)10^{-9}\,cm^3\,s^{-1}$ for neon and $\beta_m^{(2,2)} = (1.3 \pm 0.4)10^{-9}\,cm^3\,s^{-1}$ for argon are given in the works [36, 37], made by the same method. They agree well with the data in Table II.

### C. *Krypton and xenon*

The requirement for prevalence of the fast electrons free diffusion over their energy relaxation leads to a specific condi-

$\beta_m$ measurements for krypton and xenon, using ameter 3.5 cm, turn out to be correct at pressures r and discharge currents $i \leqslant 40$ mA. The total of the levels $^3P_1$, $^3P_0$ and $^1P_1$ does not exceeds e $^3P_2$ population in these cases [38–40]. The ant numbers are given in Table II. In the work experimental $\beta_m^{(2,2)}$ value in krypton was $0^{-9}$ cm$^3$ s$^{-1}$ (the methods of measurements are The same authors [42] obtained for xenon $6 \pm 1)10^{-10}$ cm$^3$ s$^{-1}$. In [38–40] at the measure- the xenon metastable atoms density the corre- transition probability value $A_{IR} = 2 \cdot 10^6$ s$^{-1}$ was However, if for $A_{IR}$ more recent data, $A_{IR} = 0.72 \cdot$ s used [44], then the corresponding constant has reased $(2/0.72)^2$ times and considered equal to $10^{-10}$ cm$^3$ s$^{-1}$, as it is shown in the table.

*on spectra of the chemiionization*

ady mentioned that the most detailed information processes (1.1)–(1.3) can be obtained by investi- electron spectra of the indicated reactions. With ie electron velocity distribution function (EVDF) ded by the smallest possible modulating signal. eak to peak amplitude was used in helium, while vere sufficient in krypton and xenon, due to appli- a storage registration system. Then, the electron re found by solving of the inverse problem. The ie integral equation were the functions $\phi$, $A_{1,2}$ or olution. A maximum of the EVDF, appearing ion (1.3) was used for absolute calibration of the le. This method of calibration ensured 0.1 eV t the measurements in helium, 0.02 eV in krypton V in xenon. The measured distribution and the ed electron spectra of the chemiionization pro- lving two $^3P_2$ metastable atoms in krypton and shown in Figs 8 and 9. To the best of our know- ther experimental investigation of the CI electron sulting from binary collisions of two metastable s so far. A computer simulation of the ionization e($2^3S$)–He($2^3S$) spectra was done in the theoreti- 15]. However, there is an essential question of the ectroscopy that has not been discussed in [45]. It he spectra overlapping of Penning (PI) and (AI) ionization and is crucial for the electron by practical application. This question was n detail in [46]. The point is that at the spectra

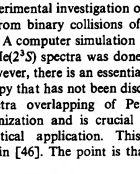


Fi- imental electron velocity distribution function in krypton (1) an cted electron spectra (2). Pressure – 67 Pa, pulse current – 10 elay after the current pulse $t_{del} = 200$ μs.

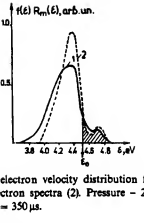


*Fig. 9.* Experimental electron velocity distribution function in xenon (1) and reconstructed electron spectra (2). Pressure – 27 Pa, pulse current – 40 mA, time delay $t_{del} = 350$ μs.

overlapping calculation difficulties arise, connected with the accounting for the quasistationary states. They are formed at the electron transition in the effective potential of the reaction exit channel. At that, depending on the experimental conditions, two formulations of the problem make sense [47]: classical, in which the centrifugal barrier is considered completely impermeable, and quantum, where the centrifugal barrier is considered completely permeable. In [46] was shown that the maximal width $\Delta\varepsilon$ of the overlapping region between the AI and PI spectra is

$$\Delta\varepsilon = 0.9\left(\frac{R_{1e} D_1^{1/6}}{R_{fe} D_f^{1/4}}\right)^4 E_0^{4/5}. \tag{4.3}$$

Here, $R_{1e}$, $R_{fe}$ are the equilibrium distances of the terms of the initial and final states; $D_1$, $D_f$ are their depths in eV; $E_0$ is the energy of the colliding particles in eV. The corresponding data [46] for symmetric collisions of the rare gas excited atoms are given in Table III. At that, the similarity between the rare gas metastable atoms and the alcalyne metal atoms was used in a number of cases.

The value of $\Delta\varepsilon$, small in comparison with the total spectral width (about 1 eV) gives a reason to assume that the part $Q$ quantities of the molecular ion yield in the total ion yield in the classical and quantum approaches are close to each other. It is possible, in this case, to neglect the influence of the quasi-stationary states, appearing due to the centrifugal barrier, on the efficiency of the molecular ion creation.

The additional overlap of the AI and PI spectra can be connected with the velocity distribution of the colliding particles. The analyses of the reaction He($2^3S$)–He($2^3S$) electron spectra [46], averaged on the Maxwellian distribution of atoms at $T_a = 300$ K, shows that the overlapping value accounting for the additional widening (about $kT_a$) agrees well with the estimation, made by formula (4.3).

Using the computed spectra it was derived that $Q = 10\%$ in the quantum calculation, while the classical calculation gives $Q = 14\%$. Therefore, if we have an experimental electron spectrum, a reliable estimation of $Q$ could be obtained by dividing the spectra into two parts at $\varepsilon_0 = \varepsilon_\infty + kT_a$, where $\varepsilon_\infty = 2E_1 - E_i$. The electrons, appearing in AI have energies $\varepsilon > \varepsilon_0$, while the electrons born in PI correspond to energies $\varepsilon \leqslant \varepsilon_0$. The yield of molecular ions determined in this way, is shown in Table IV.

Such a seemingly natural division of the spectra, is in contradiction with the results of work [45], where the $Q$-value for the reaction He($2^3S$)–He($2^3S$) was also calculated. According to other [45] data, $Q \geqslant 80\%$ in the thermal

*Fundamental characteristics of the ionization reactions, involving excited oms*

| oms | $\varepsilon_{ai}$, eV | $Q$, % | AI spectra width, eV | vibr. exc., eV | $D_i$ experim. values, eV |
|---|---|---|---|---|---|
| $2^3S$) | 15.05 | 7 ± 4 | ≃0.5 | >2 | 0.9 ± 0.2 |
| $2^1S$) | 15.05 | 16 ± 6 | ≃0.5 | >2 | 0.6 ± 0.2 |
| $^3P_2$) | 5.85 | 13 ± 6 | 0.5 ± 0.1 | >0.6 | 0.6 ± 0.1 |
| $^3P_2$) | 4.49 | 12 ± 4 | 0.4 ± 0.1 | >0.6 | 0.4 ± 0.1 |

ion. That should testify for strongly overlapping I spectra in the classical calculation and for an ty to use the total experimental electron spectra ination of $Q$. However, the testing shows [46], ake was made in [45] at the calculation of $Q$. The ie molecular ions for reaction $He(2^3S)$–$He(^3S)$, able IV [46], agrees well with the work [1], where obtained in merging beams, $Q = (4.6 \pm 0.6)\%$, he calculation results [46]. The molecular ions chemiionization reactions of the couples $He(2^1S_0)$, $Kr(^3P_2)$–$Kr(^3P_2)$ and $Xe(^3P_2)$–$Xe(^3P_2)$ ned for the first time. Similar experiments were t in neon, but the insufficient scheme sensitivity in lows to find only an estimation, e.g. for the reac- $_2$)–$Ne(^3P_2)$ the molecular ions yield $Q < 25\%$.

pay attention to the recent work [50] in which ion reactions in binary collisions of the $2^3S$ and metastable atoms have been investigated by the ectroscopy method in beam experiments. The pectra of the corresponding reactions were ith high energy resolution (36 and 70 meV). The he thoroughly completed theoretical calculations ization cross-section, the electron spectra and the ion relative yield were compared with the experi- a. The $Q$ values of helium, given in Table IV, the results of work [50] within the experimental s. The study [51], conducted in the afterglow of igh frequency discharge by mass-spectroscopic o gives small yields of molecular ions, $Q = 7\%$ in $) = 5\%$ in argon.

bination of the experimental data obtained by ethod permits us to maintain that mainly atomic rmed in the collision of two rare gases excited molecular ion yield is $Q < 25\%$). That is appar- o the difference of the equilibrium internuclear f the initial and final state terms in these reac-

esting peculiarity of the spectra obtained in d xenon (Figs 8 and 9) is the existence of the ximum, corresponding to the classical turning he quasimolecule potential curve. This special feature at 300 K is typical for the heavy rare gases. It was not observed in He [46].

The circumstance that the AI electron spectra width is substantially less than the dissociation energy of the corresponding molecular ions $D_f$ (see Tables III and IV) shows that at slow collisions of excited helium, krypton and xenon atoms, the appearing molecular ions are in high excited vibrational states. This conclusion is correct also for the other rare gas atom couples [46]. It is connected with a considerable difference in the equilibrium distances for the terms of the initial and final states. With this circumstance the small value of $Q$ has already been explained.

If we presume that the equilibrium distances on the quasimolecule potential curves correspond to the regions of weak changes of the respective molecular ions potential curves, then the dissociation energy, $D_i$, of the quasimolecule could be found from the electron spectra. This value is determined by the energy width of the Penning ionization electron spectra on 44% height level of the peak [26]. It is given in Table IV. A satisfactory agreement can be seen between the obtained $D_i$ values and the Table V data. As it is well known, two possible states, $^2P^*_{1/2}$ and $^2P^*_{3/2}$ correspond to the configuration $s^2p^5$ of the rare gas ion. The term $^2P^*_{3/2}$ is situated 0.67 eV below the term $^2P^*_{1/2}$ in krypton and 1.19 eV in xenon [52]. The energies of the electrons born in reactions (1.1) and (1.2), depending on the state of the forming ion, should differ in the same value. The existence of such a gap principally gives a possibility to distinguish between similar electron groups, since it is large in comparison with the FWHM of the instrumental function, accounting for collisions and for the modulating signal finite amplitude. The examination of the $R_m(\varepsilon)$ spectra show that the atomic ions in the $^2P^*_{1/2}$ state and the corresponding molecular ions are formed in not more than 8% of the total ion quantity in Kr and not more than 6% in Xe.

*elative efficiencies for creation of heavy rare gases $P_{1/2}$ in the interaction $He(2^{1,3}S) + R$*

| io | Rare gas Ar | Kr | Xe | References |
|---|---|---|---|---|
| | 1.92 | 1.90 | 2.24 | [56] |
| | 1.94 | 1.80 | 2.03 | [57] |
| | 2.04 | 1.60 | 1.45 | [56] |
| | 2.00 | 1.80 | 1.34 | [57] |

## 5. Penning ionization of normal atoms and molecules by the helium metastable atoms

It is evident that the PIES method described above could immediately be applied for investigation of the Penning ionization processes between the excited and normal atoms and molecules. A substantial interest from the viewpoint of the theory and the practical applications represents the ionization of the heavy rare gases – argon, krypton and xenon atoms as well as the molecular gases – carbon oxide and nitrogen, by the metastable helium atoms.

### 5.1. *Ionization of the heavy rare gases atoms*

Investigations of the interaction reactions of $He(2^3S_1, {}^1S_0)$ with Ar, Kr and Xe were conducted in many works, whose results are summarized in [29]. The averaging of the results

] shows that only the rate constant for ioniza-
ɔton and xenon atoms by the triplet helium
tom is found with a comparatively small error
he averaged data of the other rate constants
esponding values with 50–80% errors. The rate
tios $\beta_{m1}/\beta_{m3}$, concerning the ionization of all
Ar, Kr and Xe by the helium ($2^1S_0$) and ($2^3S_1$)
toms were determined with similar substantial
his reason, it seems expedient to conduct mea-
f the ratio $\beta_{m1}/\beta_{m3}$ by the new method of PIES,
e from the shortcomings inherent to the beam
fficulties with the measurements of the excited
'y) as well as to the methods, based on record-
ited atoms density variation in time or in space
: of other competitive processes for the metasta-
destruction). The examined reactions could
ugh the channels (1.1)–(1.2). The application of
scopy and electron spectroscopy methods in
s us to determine the relative yield of the molec-
uclear ions at the interactions $He(2^{1,3}S) + R$ ($R$
gas atom) [29, 53]. The relative contribution of
onization in the total cross-section of the pro-
(1.2) has been found, respectively, and its value
eed 10–15%. So, at the reactions $He(2^{1,3}S) + R$
ing ionization is going on.
sis of the Penning ionization spectra shows
as, a result of the reactions ($R$ = Xe, Kr),

$$R \xrightarrow{K_{3,3/2}} \begin{cases} He + R^+(^2P_{3/2}) + e(\varepsilon_{p1}), & (5.1) \\ He + R^+(^2P_{1/2}) + e(\varepsilon_{p2}), & (5.2) \end{cases} \quad K_{1,1/2}$$

$$R \xrightarrow{K_{3,3/2}} \begin{cases} He + R^+(^2P_{3/2}) + e(\varepsilon_{p3}), & (5.3) \\ He + R^+(^2P_{1/2}) + e(\varepsilon_{p4}), & (5.4) \end{cases} \quad K_{1,1/2}$$

be formed in two states, $^2P_{3/2}$ and $^2P_{1/2}$ as it is
of interaction between two excited rare gases
Section 4.2). Besides, the term $^2P_{1/2}$ of argon is
eV above the term $^2P_{3/2}$. The corresponding
ton and xenon has already been given.
ner works [26, 53, 56, 57] it has also been found
energy spectra width of the reaction
$R$) and the shift of its maximum from the
ave small values ($\leqslant 0.1$ eV). The angular dis-
the forming electrons was studied in a limited
scattering angles $\theta = 20–90°$ [47, 48]. In partic-
90° the relative efficiencies for creation of ions
have the values given in Table V.
y, using the available information, the PIES
applied for more reliable measurements of the
ization rate constant ratio, $\beta_{m1}/\beta_{m3}$, and for
n of the averaged over the scattering angles
te constant ratio with a creation of ions $R^+$ in
$^2P_{3/2}$ and $^2P_{1/2}$ (there are no such data in the
ments [58] have been carried out in the after-
of a pulse discharge in a glass tube with a
, at He pressures 0.3–0.8 Torr. The admixtures
rare gases were in the range of $10^{-5}$–$10^{-3}$ Torr,
pulse current values 60–100 mA, pulse duration 10–20 μs, repetition frequency 1 kHz, time delay at the measurements 60–100 μs. At that the electron density varied in the interval $10^{10}$–$10^{11}$ cm$^{-3}$. In order to account correctly for the contribution of the ion current second derivative in the experimental EEDF measurements were conducted of the probe current second derivative under conditions similar to the examined ones but in pure helium, where the maxima caused by the reactions (5.1)–(5.4) are absent. The corresponding curve allows to determine the ion component value at measurements in He + $R$ mixtures.

5.1.1. *Helium–xenon mixture.* Typical result of EEDF measurements under conditions when the triplet and the singled metastable helium atoms densities are comparable is shown in Fig. 10. In this case, it was possible to observe all four maxima dependent on the reactions (5.1)–(5.4) in the energy region 6–9 eV. It is seen that the observed peaks are partially overlapped. For separation of the curves related to each of the reactions in particular, the obtained recordings were handled by the following procedure: in compliance with that already mentioned above, the small width of $R_m(\varepsilon)$ (it's width as well as the widening, connected with the radial field is substantially less than the widening value due to interactions in the volume and the finite width of the setup instrumental function) enables to put down the dependence $R_m(\varepsilon)$ in a delta-function form and then to account for the widening connected with the finite width of the experimental device instrumental function and the interactions in the volume. The experimental curve was approximated with the function thus obtained by the least square method. Figure 10 presents every maximum (points), found in this way. Their summation (dotted line) is close to the experimental data (solid line). As a result, the ratio of the efficiencies for creation of two ion states $Xe^+$ in the interaction $He(2^{3,1}S_0)$ + Xe was found:

$$\beta_{m3}^{(3/2)}/\beta_{m3}^{(1/2)} = 2.4 \pm 0.2; \quad \beta_{m1}^{(3/2)}/\beta_{m1}^{(1/2)} = 1.3 \pm 0.3.$$

It should be pointed out that the PIES method gives value averaged on the scattering angles. This value coincides with the analogous data, shown in Table IV for $\theta = 90°$ in the uncertainty range. $\beta_{m1}/\beta_{m3} = 2.7 \pm 0.5$ was also determined by averaging of the different measurements data. We shall point out that the error of this value is substantially

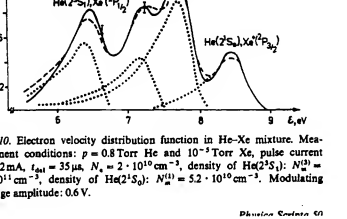


*Fig. 10.* Electron velocity distribution function in He–Xe mixture. Measurement conditions: $p = 0.8$ Torr He and $10^{-3}$ Torr Xe, pulse current $i = 42$ mA, $t_{del} = 35$ μs, $N_e = 2 \cdot 10^{10}$ cm$^{-3}$, density of $He(2^3S_1)$: $N_m^{(1)} = 2 \cdot 10^{11}$ cm$^{-3}$, density of $He(2^1S_0)$: $N_m^{(1)} = 5.2 \cdot 10^{10}$ cm$^{-3}$. Modulating voltage amplitude: 0.6 V.

e error of the same $\beta_{m1}/\beta_{m3}$ value derived by e results obtained in various works.

this ratio and using the value of $\beta_{m3} = (1.53$ $^0\,cm^3\,s^{-1}$ (known with a good accuracy [3]), ue for 300 K can be determined as follows: $1)10^{-10}\,cm^3\,s^{-1}$.

*um–krypton mixture.* The experimental curve of rement in He–Kr plasma is shown in Fig. 11. ergy gap between the $Kr^+$ ion states $^2P_{3/2}$ and r than that one in Xe, the maxima coming from s (5.1) and (5.4) are completely overlapped in the He + Xe mixture. In order to compare the each of the processes (5.1)–(5.4), the experimen- re treated in this way: initially, as in the xenon . the partially overlapped maxima were separat- 11, where the results of such a procedure are ols are here as in Fig. 10). Further, the depen- e ratios of the fast electron numbers in the he third maxima, or in the second and the first s drawn as a function of the different metastable ies ratio. This enables us to find

$= 2.4 \pm 0.4$; $\beta_{m1}^{(3/2)}/\beta_{m1}^{(1/2)} = 1.4 \pm 0.4$.

nstant ratio $\beta_{m1}/\beta_{m3}$ the value $\beta_{m1}/\beta_{m3} = 2.9$ derived and, using the well known value of $\pm 1.2)10^{-11}\,cm^3\,s^{-1}$ [3], the $\beta_{m1}$ value at 300 K nined:

$0.7)10^{-10}\,cm^3\,s^{-1}$.

*um–argon mixture.* The energy gap between the and $^2P_{1/2}$ of the argon ion is small ($\simeq 0.18$ eV) iently the PIES method does not allow to naxima on the EEDF, corresponding to the for- e $Ar^+$ in these two states. For this reason only $.1 \pm 0.3$ constant ratio was found for the He–Ar

*on of the carbon oxide molecule*

of the helium metastable atoms with the CO thermal energies the Penning ionization reac-

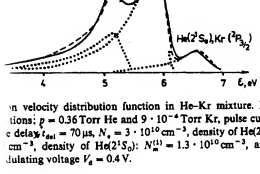


n velocity distribution function in He–Kr mixture. Mea- tions: $p = 0.36$ Torr He and $9 \cdot 10^{-4}$ Torr Kr, pulse current e delay $t_{del} = 70\,\mu s$, $N_e = 3 \cdot 10^{10}\,cm^{-3}$, density of $He(2^3S_1)$: $cm^{-3}$, density of $He(2^1S_0)$: $N_m^{(1)} = 1.3 \cdot 10^{10}\,cm^{-3}$, ampli- dulating voltage $V_a = 0.4$ V.

tion is the only one observed ionization process.

$$He(2^3S_1) + CO \rightarrow He + CO^+(X^2\Sigma) + e(5.8\,eV), \quad (5.5)$$

$$He(2^1S_0) + CO \rightarrow He + CO^+(X^2\Sigma) + e(6.5\,eV). \quad (5.6)$$

The rate constant $K_{m3}$ for quenching of the $He(2^3S_1)$ atoms in collisions with CO is $K_{m3} = (16 \pm 3)10^{-11}\,cm^3\,s^{-1}$ at $T_a = 300$ K (averaged on the nine works which we know). The value derived by averaging over the works [59–63] results seems to be more precise. It was obtained by the most reliable techniques – the flowing afterglow and the flash photolysis. In this case, $K_{m3} = (10.0 \pm 0.6)10^{-11}\,cm^3\,s^{-1}$. The quenching constant $K_{m1}$ of the atoms $He(2^1S_0)$ is measured in two works [59, 64]. The divergence between them is two times, but the ratio of the constants for quenching of the states $2^3S$ and $2^1S$ is equal ($3.2 \pm 0.3$ and $3.3 \pm 0.6$). From this value the rate constant for quenching of the state $2^1S$ can be obtained:

$K_{m1} = (32 \pm 0.6)10^{-11}\,cm^3\,s^{-1}$.

The reactions (5.5) and (5.6) cross-section energy dependences were found in the work [65]. These dependences are translated into absolute units by normalizing against the quenching rates from work [59], which for CO practically coincide with the average values shown above. The absolute cross-sections (without normalizing by a quenching rate), for fixed energies (30, 60 and 140 meV, respectively) are measured in works [66–68]. The difference between the data of these works and the results of [65] is from 30% up to 3 times for the $2^3S$ state and from 40% up to 2 times for the $2^1S$ state. Such a divergence is a consequence of the large systematic error of the beam method, appearing in the device calibration procedure.

At thermal collisions (besides the reactions (5.5) and (5.6)) are the processes possible:

$$He(2^3S_1) + CO \rightarrow He + C + O, \quad (5.7)$$

$$He(2^1S_0) + CO \rightarrow He + C + O. \quad (5.8)$$

The excessive energy, 8.7 eV in the first case and 9.5 eV in the second, can be lost for excitation of atoms. The rate constant of the reaction (5.7), leading to a formation of atoms C* with excitation energies 7.5–7.9 eV is measured in works [69, 70]. The total probability of CO dissociation with excitation of these levels turns to be small. In compliance with the more precise data [70], it is equal to 2%. According to the opinion of the authors of [70], the remaining 98% are entitled to Penning ionization.

It is just the value ($\simeq 1$), of the reaction (5.5) branching factor $\eta_{m3}$, that allows to normalize the cross-section, obtained in [65] against the rate constant (5.5) for quenching of $He(2^3S_1)$ atoms. The same has been done for the process (5.6), although there is no information about the branching factor $\eta_{m1}$ in this case.

It should be noted that, besides the C* levels examined in [69, 70], in reaction (5.7) is possible, by the energy conservation law, the population of the lower metastable levels of C and O, as well. The possibility for simultaneous excitation of the lower levels of C and O, for example the state $C\,^5S_2^0$ and the state $O\,^1S_0$, with 8.4 eV summary energy could be presumed, too. For this reason the problem of the reaction (5.7) rate constant value, and, hence the reaction (5.6) rate constant value is not completely solved. All the more this could

for the processes involving $He(2^1S)$ atoms, since 5.8) more C* and O* levels, including those near tance one can be excited from the viewpoint of ervation than in reaction (5.7).

irect measurement of the processes (5.5) and (5.6) nts was conducted for the first time, using the od. The investigations were carried out in a CO gas mixture at a pressure of 0.5 Torr (the impurity density does not exceed $5 \cdot 10^{-4}$%, to the spectral and chemical analyses data). A blowing through of the examined gas mixture in order to exclude the cataphoresyses and to e debris of the plasma chemical reactions in the \ pulse periodic discharge (duration of the active µs, period – 500 µs) was fired in a tube with an ter 2.3 cm. The EEDF measurements were con- 0–150 µs after the current pulse end (the time vas 5 µs). A typical EDF in the energy regions hemiionization reactions take place is shown in

acteristic maxima correspond to the reactions

$$CO \rightarrow He + CO^+(X^2\Sigma) + e(5.8\,eV), \qquad (5.9)$$

$$CO \rightarrow He + CO^+(X^2\Sigma) + e(6.5\,eV). \qquad (5.10)$$

ima at 14.4 and 15.4 eV appear as a result of, ussed, reactions involving two triplet and triplet helium metastable atoms. The rate constants of ons are well known and the EEDF in this region ) control the accuracy of the fast electrons and atoms density measurements in specific experi- ditions. At the separation of reactions (5.9) and ibutions, it was accounted in accordance with heir spectral widths could be neglected in com- h the widening due to the interaction processes rumental function of the recording system (0.2 V he following rate constant values were obtained: = 0.1)$10^{-10}$ cm$^3$ s$^{-1}$ for reaction (5.9) and $\beta_{m1}^{(X)}$ = $)^{-10}$ cm$^3$ s$^{-1}$ for reaction (5.10).

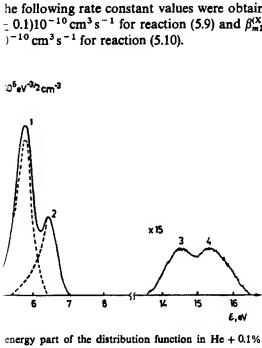


energy part of the distribution function in He + 0.1% CO ire 0.5 Torr, pulse current 10 mA, $t_{del}$ = 40 µs, density of $^{1}$) = $1.4 \cdot 10^{11}$ cm$^{-3}$, density of $He(2^1S_0)$: $N_m^{(1)} = 4.4 \cdot$ maxima correspond to the reactions: 1 – to reaction (5.9), 2 to reaction ($He(2^3S_1)$, $He(2^3S_1)$), 4 – to reaction ($He(2^3S_1)$,

The large energy spectral width (~2 V) [72] of the reaction:

$$He(X^{3,1}S) + CO \rightarrow CO^+(A^2\Pi) + He + e(2.5\text{–}4\,eV),$$

and the fast growth of the ion current second derivative, at probe potentials below 4 V, prevents accurate determination of the respective constants. The value $\beta_{m3}^{(A)} = (0.15 \pm 0.06)10^{-10}$ cm$^3$ s$^{-1}$ was obtained for the reaction involving $He(2^3S_1)$. The process

$$He(2^{3,1}S) + CO \rightarrow CO^+(B^2\Sigma) + He + e(1,\ 0.2\,eV)$$

has not been revealed, since there is a large number of Maxwellian electrons in the region where the electrons of these reactions will appear.

Using data from works [70, 72–74] for the relative yield of $CO^+$ ions in the states $X^2\Sigma_g^+$, $A^2\Pi_u$, $B^2\Sigma_u^+$, at reactions of the type (5.5) and (5.6), the total rate constants for Penning ionization are determined: for reaction (5.5), $\beta_{m3} = (9 \pm 2)10^{-11}$ cm$^3$ s$^{-1}$, and for reaction (5.6), $\beta_{m1} = (2.4 \pm 0.6)10^{-10}$ cm$^3$ s$^{-1}$. Respectively for $\eta_{m3}$ and $\eta_{m1}$ the following values are derived. $\eta_{m3} = 0.9^{+0.1}_{-0.2}$, $\eta_{m1} = 0.8 \pm 0.2$ and $\eta_{m3}/\eta_{m1} = 0.85 \pm 0.15$.

From these data it follows that the main channel for quenching of metastable helium atoms by CO molecules is the Penning ionization. For the $He(2^3S_1)$ atoms, that is in compliance with the results of papers [69, 70]. Moreover, it agrees with the data of work [75], showing that the probability for Penning ionization in collisions with $He(2^3S_1)$ exceeds 0.6 for all examined molecules, while for the two-atomic molecule it exceeds 0.7. For collisions with $He(2^1S)$ such results were not available before.

The data presented so far show that the absolute values of the Penning ionization rate constants are determined in the PIES method using the simplest calibration procedures, which introduce minimum errors. As a result the errors of the obtained results could be reduced to 20–30%, which is near to the errors of the contemporary methods for measurements of the rates for the metastable atoms quenching. The derived data can be used afterwards for a calibration of the energy dependence of the cross section for Penning ionization (or, in the common case, for chemiionization). This appears more justified than the calibration using the quenching constants since in this case the assumption that the branching factors in the ionization are equal to 1 is not necessary. Besides, from the comparison of the ionization and quenching rate constants, the $\eta_m$ values are yielded with 25–40% errors. The methods for $\eta_m$ determination used in the previous works [75, 76] do not have smaller, but in many cases bigger, errors (up to 100% [75]), at that practically they give only the relative values, while a calibration using "bench-marks" processes with well known rate constants, or $\eta_m$ values, are needed in order to obtain the absolute values.

### 5.3. *Ionization of the nitrogen molecule*

Because the $N_2$ molecules have a structure similar to that of the CO molecules, their ionization by the metastable helium atoms has a lot in common with the former case.

Let us remind that it is necessary to conduct the investigation of the Penning ionization by the PIES method in a mixture with a small content (~0.1%) of the molecular gas because with the molecular density growth the life time of

le atoms decreases and the relation between the
he initial electron spectra becomes too compli-
axation parameter could be close to unity). The
calibrated He–$N_2$ mixtures did not allow to
experiments in a regime of blowing through the
control the $N_2$ density due to the "hardening"
his reason only the rate constants ratios, which
end on the nitrogen pressure in the examined
e determined by the PIES method. At the same
ative character of the measurements increases
y of the results. Figure 13, [77], shows typical
EEDF measurements under the conditions:
sure 0.4 Torr, nitrogen pressure $3 \cdot 10^{-4}$ Torr,
e 8 mA, delay time 75 μs, discharge repetition
8 kHz. The densities of helium metastables in
S and $2^3S$ were, respectively, $3.1 \cdot 10^{10}$ cm$^{-3}$
$^{10}$ cm$^{-3}$. In this mixture, as in the He–CO
following reactions are going on:

$$_2 \rightarrow He + N_2^+(X^2\Sigma) + e(4.2\,eV), \quad (5.11)$$

$$N_2 \rightarrow He + N_2^+(X^2\Sigma) + e(5\,eV), \quad (5.12)$$

$$N_2 \rightarrow He + N_2^+(A^2\Pi) + e(3.1\,eV), \quad (5.13)$$

$$N_2 \rightarrow He + N_2^+(A^2\Pi) + e(3.9\,eV), \quad (5.14)$$

$$_2 \rightarrow He + N_2^+(B^2\Sigma) + e(0.9\,eV), \quad (5.15)$$

$$N_2 \rightarrow He + N_2^+(B^2\Sigma) + e(1.8\,eV). \quad (5.16)$$

on (5.15) can hardly be detected by the PIES
e this energy region is influenced by the energy
Maxwellian part. The reaction (5.16) reveals
peculiarity on the background of a rapidly
n current. The reaction (5.14) spectra is compa-
, due to the contribution of different vibrational
ions. The energy disposition and the branching
e different $N_2^+$ ion levels in the recorded spectra
the range of errors with the data of works [74,
reactions (5.11)–(5.16) have been studied before
od of Penning electron spectroscopy mainly
l as by measurements of the He($2^3S_1$) density

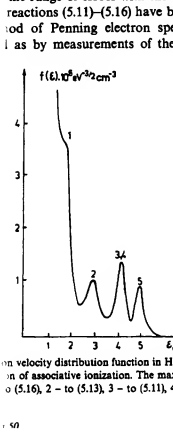


on velocity distribution function in He with small $N_2$ admix-
on of associative ionization. The maxima correspond to the
o (5.16), 2 – to (5.13), 3 – to (5.11), 4 – to (5.14) and 5 – to

decay in the flowing afterglow [59]. The advantages and the shortcomings of these methods have already been discussed.

The value of the quenching rate constant for the triplet atoms is well known. By averaging of a large quantity of works it is $K_{m3} = (7.1 \pm 0.1)10^{-11}$ cm$^3$ s$^{-1}$ [29]. As far as the respective rate constant for He($2^1S$) is concerned, up to our knowledge there is a single work in which this value is determined with a substantial error: $K_{m1} = (17 \pm 5)10^{-11}$ cm$^3$ s$^{-1}$ [59]. According to [70], the basic channel for quenching of the helium metastable atoms by the $N_2$ molecules is the Penning ionization (that agrees with the CO molecule data obtained before). Therefore, the measurements made by the PIES method at known branching factor of the reactions (5.11)–(5.16) [74, 78, 79], enable to derive the constant ratio $\beta_{m1}/\beta_{m3} = 2.1 \pm 0.1$ with a satisfactory accuracy and to decrease the error of the value $K_{m1}$, shown in [59]. At that it becomes

$$K_{m1} = (15 \pm 3)10^{-11}\,\text{cm}^3\,\text{s}^{-1}.$$

It should be pointed out that, in principle, it is possible to examine the Penning reaction between the metastable atoms and the molecules in an excited electron state by the PIES method under similar conditions, for example:

$$He(2^{3,1}S) + N_2(A^3\Sigma) \rightarrow He + N_2^+ + e. \quad (5.17)$$

There are no similar data in the literature. In accordance with [80], the relative part of the electron excited molecules in a plasma of helium mixture with a small nitrogen addenda could reach several percent of the normal molecules density. The electron spectrum of the reaction like (5.17) was detected on the EEDF recordings in the energy region 7–11 eV. However, measurements in a regime of blowing through the mixture, combined with optical measurements of the $N_2(A^3\Sigma)$ molecule density are necessary in order to obtain quantitative data.

## 6. Quenching of the excited rare gases and mercury atoms by the electrons

This part of the work is dedicated to the examination of reaction (1.3) in the rare gases and mercury afterglow plasma at the electron temperature range 300–3000 K by the method described above. We shall point out its merits regarding the superelastic collision study. First, it is a direct method, since the rate constant of the considered process, $\beta_e(T_e)$, is determined immediately by the forming particles – the fast electrons. On the second place, using the heating of the electron gas by an additional pulse [24], it is possible to determine the $\beta_e(T_e)$ temperature dependence. On this ground we can make a judgment about the near threshold behavior of the excitation and deexcitation cross-sections. By definition, the process (1.3) rate constant is connected with the quenching collision cross-section $\sigma_2(\varepsilon)$ by the relation $\beta_e(T_e) = \langle \sigma_2(\varepsilon) \cdot v(\varepsilon) \rangle$. Here, $v(\varepsilon)$ is the velocity of an electron with energy $\varepsilon$. The averaging is made over a Maxwellian electron distribution with a temperature $T_e$. The excitation cross-section $\sigma_1$ is connected with $\sigma_2$ by the detailed balance principle [29]:

$$\sigma_2(\varepsilon) \cdot \varepsilon \cdot g_m = \sigma_1(\varepsilon_1 + \varepsilon) \cdot (\varepsilon_1 + \varepsilon) \cdot g_a.$$

e to the theory [81], the $\sigma_1$ dependence on the
rgy near to the excitation threshold is of a
type. However, the existence of energy levels,
ig to a creation of negative ions could change
ence and lead to a non-monotony in the $\sigma_1(\varepsilon)$
2]. The appearance of resonances complicates
cal calculations of $\sigma_1(\varepsilon)$ in the near threshold
n. For the rare gas atoms, as far as we know,
rks [83, 84] are completed in helium and neon.
erable quantity of information is stored by the
s of electron beam scattering on atoms in normal
ble states (see for example [85, 86]). However, in
works the uncertainties in the electron beam
).5–0.7 eV. Therefore their results are not useful
$\sigma_1(\varepsilon)$ behavior in the near threshold region that
sted in. The intensive development of the beam
he last years decreases the energy spread in the
tron beams substantially [87–91]. Thus, in [87]
50 meV and even 4.88–9.7 meV in [88, 89].
he devices used in the experimental works
not allow to carry out the excitation cross-
lute measurements. Few are the works like [91],
bsolute values of the differential cross-section for
f Kr $4p^5 5s$ states were obtained by a beam with
pread 33–35 meV, but for three scattering angles

siderations should highlight the actuality of the
imental determination at low electron tem-

find the absolute value of the rate constant $\beta_e(T_e)$
ion

$$e \rightarrow He(1^1S_0) + e \tag{6.1}$$

perature dependence, a maximum at the energy
of the EEDF was used [30]. The data for $\beta_e$,
ar in the literature [33, 92–97], reveal substan-
icies in the constant absolute value as well as in
emperature dependence. Let us pay attention to
nstant $\beta_e$ temperature dependence. The most
from the experimental works is [96]. The elec-
excitation function in helium, $\sigma_1(\varepsilon)$, was studied
of secondary electrons in this work. The initial
curve, corresponding to the excitation of the
tate $2^3S_1$ was used by many authors to find
$(T_e)$. The results of these calculations depend
on the method by which the paper's [96]
l curves are approximated. Some authors [33,
d $\sigma_1(\varepsilon) \sim (\varepsilon - \varepsilon_1)$ for energies $(\varepsilon - \varepsilon_1)$ below
s of eV and obtained $\sigma_2(\varepsilon) = const.$ and $\beta_e \sim$
uthors, for example [97], considered $\sigma_1(\varepsilon) \sim (\varepsilon$
d obtained $\sigma_2 \sim \varepsilon^{-1/2}$, $\beta_e = const.$ In our
experimental data of [96] did not give a possi-
ermine firmly the constant $\beta_e = \beta_e(T_e)$ depen-
e most frequently existing temperatures in the
$\leqslant 2000$ K, since the energy spread of the inci-
beam was 0.1 eV. Apparently, it is also difficult
this dependence by examining the $2^3S$ level
the afterglow, as, for example, it has been done
is case several plasma parameters ($N_e$, $N_m$, $T_e$)

should be measured simultaneously, with a high accuracy, in order to obtain reliable results.

The accuracy of the rate constant temperature dependence determination can be increased substantially in this way: as seen from the relation (2.5), the $\beta_e$ value is proportional to $S_e$ at fixed $N_e$ and $N_m$ numbers. Therefore, if we could vary the electron temperature to a certain degree in a given afterglow stage and measure $S_e$ at constant $N_e$ and $N_m$, the $\beta_e(T_e)$ dependence can be derived. A second pulse, delayed to the main one, was applied to the discharge tube electrodes in a selected afterglow moment [24] for such $T_e$ variation. This pulse creates a weak electric field which increases $T_e$ without changing $N_e$ and $N_m$.

Figure 14 shows the results of $S_e$ measurements under the following conditions: the helium pressure is 0.8 Torr, the current of the main pulse is 1.2 A, the second pulse delay is 350 μs. The current and the electrical field intensity in the second pulse varied from 5–35 mA and from 6–34 mV/cm. The constancy of the metastable atoms density at variation of the second pulse current was controlled, using the area of the EEDF maximum at energy 14.4 eV, which was proportional to $N_m^2$. This density remained constant within 5% accuracy. As seen from the picture, $S_e$ and, consequently, $\beta_e$ are constant within 10% of the value in the range of examined temperatures (550–1100 K).

The theoretical calculations [84, 98] and the results of the experimental work [92] also show an $\beta_e$ independence on temperature at $T_e \leqslant 1000$ K. The constant absolute value was determined by formula (2.5): $\beta_e = (3.1 \pm 0.6)10^{-9}\,cm^3\,s^{-1}$. This result is quite near the data of works [92] – $(4.2 \pm 0.6)10^{-9}\,cm^3\,s^{-1}$, [84] – $(2.9 \pm 0.1)10^{-9}\,cm^3\,s^{-1}$ and [96] – $(4.5 \pm 1)10^{-9}\,cm^3\,s^{-1}$. It coincides with the averaged value $(2.8 \pm 1)10^{-9}\,cm^3\,s^{-1}$, reported in [29].

### 6.2. *Neon and argon*

The maxima on the EVDF at energies of 16.6 eV and 11.5 eV respectively were used [34, 35], to investigate the reactions

$$Ne(2p^5 3s\,^3P_2) + e \rightarrow Ne(2p^6\,^1S_0) + e, \tag{6.2}$$

$$Ar(3p^5 4s\,^3P_2) + e \rightarrow Ar(3p^6\,^1S_0) + e. \tag{6.3}$$

As four reactions, involving lower excited states $^1P_1$, $^3P_{1,2,3}$, are possible in the Ne and Ar afterglow, let us introduce designations $\beta_e^{(k)}$, where the index $k = 0, 1, 2, 3$ relates to atoms in the states $^3P_0$, $^3P_1$, $^3P_2$, $^1P_1$. To our knowledge, there were no data from immediate determination of these constants for electron energies $\varepsilon < 1$ eV until the works [34–37].

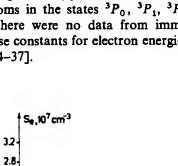


*Fig. 14.* $S_e$ dependence on $T_e$ in helium.

ergy gap between the sub-levels of the exam-
tion was 0.05–0.13 eV, while the modulating
dc was $\simeq 1$ V, the value of $S_e^{(2)} = S_e^{(k)}$ deter-
√DF was a total for all the four possible reac-
re, the constant $\beta_e^{(2)}$, yielded by using $S_e^{(2)}$
ffective constant.
of the data processing of measurements in
n in Fig. 15.
o the theoretical predictions [83, 99] the rate
superelastic collisions involving atoms in the
$^3P_1$, $^3P_2$ and $^1P_1$ are comparable. Besides, the
$^{(2)} \leqslant 0.25$; $N_m^{(0)}/N_m^{(2)} \leqslant 0.05$; $N_m^{(1)}/N_m^{(2)} \leqslant 0.01$
in our experiment. For this reason, it was
the obtained effective constant $\beta_e^{(2)}$ is the rate
f (6.2) and (6.3). The $\beta_e^{(2)}$ value did not depend
rature in the range $T_e = 470$–$1600$ K within
It is equal to: $\beta_e^{(2)} = (2.0 \pm 0.3)10^{-10}\,\mathrm{cm^3\,s^{-1}}$.
e rate value is constant within ±20% limits in
= 800–1500 K. It is equal to: $\beta_e^{(2)} = (4.0$
$\mathrm{m^3\,s^{-1}}$.
, for an average electron energy of 0.06 eV,
$\beta_e^{(2)} = (2.7 \pm 0.5)10^{-10}\,\mathrm{cm^3\,s^{-1}}$ in neon and
.5)$10^{-10}\,\mathrm{cm^3\,s^{-1}}$ in argon.
nergy resolution in the investigations of the
s excitation by electron beam experiments was
8]. Even these results do not allow to calcu-
dependence of neon and argon in a wide elec-
ure range and to compare the calculated
e ones presented above. The point is that the
section curve for a summary excitation of
$P_0$ metastable states is given in [88] and since
p between these states is 0.09 eV in neon and
on, that confines the possible $\beta_e(T_e)$ calcu-
lectron temperatures $T_e \leqslant 600$ K in neon and
argon. The lower temperature limit is deter-
beam energy spread. It is 300–400 K. That is
t the consideration of the $^3P_2$ level excitation
urve character in the threshold region. It
ur results that this cross-section is close to the
$^{2)} \sim \sqrt{\varepsilon - \varepsilon_1}$. It should be mentioned that the
or the cross-section, obtained from the $\beta_e^{(2)}$
has a integral character and is not sensitive
cture of this dependence.
re shown the cross-section $\sigma_1^{(2)}(\varepsilon) \sim \sqrt{\varepsilon - \varepsilon_1}$,
g the measured rate constant $\beta_e^{(2)}$, and the
taken from work [88] and calibrated in an
. The calibration was fulfilled, using the rate
s which we obtained at $T_e = 600$ K in neon
in argon.

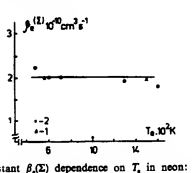


stant $\beta_e(\Sigma)$ dependence on $T_e$ in neon: 1. $p = 120$ Pa,
$n^{-3}$, $S_e = 7 \cdot 10^2\,\mathrm{cm^{-3}}$, $N_e = 3.5 \cdot 10^{11}\,\mathrm{cm^{-3}}$. 2.
$= 3.5 \cdot 10^{11}\,\mathrm{cm^{-3}}$, $S_e = 10^6\,\mathrm{cm^{-3}}$, $N_e = 1.7 \cdot 10^{11}\,\mathrm{cm^{-3}}$.

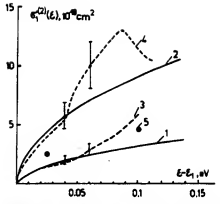


*Fig. 16.* Energy dependence of the cross-section for excitation of the $^3P_2$ level in the threshold region: 1, 2 – results of the works [32] and [33] respectively for neon and argon; 3, 4 – results of the beam experiments [61] for neon and argon; points are ion calculation results, taken from [56].

### 6.3. *Krypton and xenon*

Two circumstances were accounted at the conducting of measurements in heavy rare gases. First, as it follows from Table I, the role of the fast electron impact excitation of the normal atoms into the $^3P_2$ and $^3P_1$ states increases in krypton and xenon. That provides a decrease of the fast electron number $S_e^{(2)}$ in the EVDF maximum in which we are interested (9.9 eV in Kr, 8.3 eV in Xe) at electron temperatures $T_e \geqslant 600$ K, and complicates the relation between $S_e^{(2)}$ and $\beta_e^{(2)}$. Second, the energy gap between the $^3P_2$ and $^3P_0$ metastable levels increases in comparison with the lighter rare gases and is 0.65 eV in Kr and 1.14 eV in Xe, which enables to plot the $\beta_e^{(2)}(T_e)$ relative temperature dependence in the range $500 \leqslant T_e \leqslant 2000$ K. For this reason the following procedure was accepted: the rate constants for quenching the $^3P_2$ metastable states by slow electrons were determined, using the described above PIES method in the decay plasma at temperatures of 600 K. The other excited states densities turned out to be negligibly small. These values are: $\beta_e^{(2)} = (3.4 \pm 0.5) \cdot 10^{-10}\,\mathrm{cm^3\,s^{-1}}$ for krypton and $\beta_e^{(2)} = (6.9 \pm 0.7) \cdot 10^{-10}\,\mathrm{cm^3\,s^{-1}}$ for xenon. After that, the dependence $\beta_e^{(2)}(T_e)$, plotted in arbitrary units according to the results of [88], was calibrated at a temperature of 600 K, using the values given above. The curves obtained in this way are presented in Fig. 17. Therefore, the knowledge of the $\beta_e^{(2)}$ rate constant enables us to plot the $\sigma_1(\varepsilon)$ dependence of work [88] in an absolute scale. The corresponding curve of xenon is shown in Fig. 18. The determined rate constants of quenching of the metastable atoms by slow electrons are presented in Table VI.

### 6.4. *Mercury*

The investigation of the quenching in the mercury afterglow shows that the rate constant value for electron impact deex-

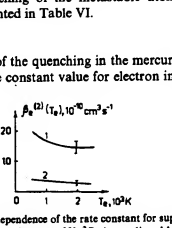


*Fig. 17.* Temperature dependence of the rate constant for superelastic collisions between electrons and atoms of Xe $^3P_2$ (curve 1) and krypton Kr $^3P_2$ (curve 2).

*ults of determination of the rate constants for he metastable atoms by slow electrons in rare*

| $\beta_e$, $10^{-10}$ cm$^3$ s$^{-1}$ | $\beta_e$ dependence on $T_e$ | Range of $T_e$ variation, K |
|---|---|---|
| $31 \pm 6$ | const. | 550–1100 |
| $2.0 \pm 0.3$ | const. | 470–1600 |
| $4.0 \pm 0.8$ | const. | 800–1500 |
| $3.4 \pm 0.5$ | see Fig. 17 | 600 |
| $6.9 \pm 0.7$ | see Fig. 17 | 600 |

$^3P_2$ metastable atoms is substantially higher sponding rate constants in the rare gases. At he constant turns to be: $\beta_e = (2.9 \pm 1.2) \cdot$ That is connected with the fast rise of the or excitation of the $^3P_2$ level close to the een from the Fig. 19. For calibration of this d in [100], the rate constant presented above he cross-section value at the $\varepsilon = 5.6$ eV $2 \cdot 10^{-16}$ cm$^2$. It is somewhat lower than the cross-section, measured in [101], ,2) and the calculated value, $3 \cdot 10^{-16}$ cm$^2$

**the processes creating fast electrons upon the meters**

esented so far show that the processes (1.1)– a significant role in the decay of the excited he creation of electrons, atomic and molecu- the plasma is a system, whose parameters are ected, the examined reactions influence other for example the recombination, the stepwise forming of the electron temperature, etc. ifferent experimental conditions the role of the hich fast electrons appear is different, so in ecific consideration of these phenomena and on the plasma parameters is necessary. A sis of the reactions (1.1)–(1.3) possible influ-

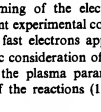


n cross-section of the $^3P_2$ level in xenon.


n cross-section of the $^3P_2$ level in mercury.

ence upon the plasma parameters is given in review [6]. Here we shall consider briefly some of the problems which, in our opinion, are of most interest.

### 7.1. *Character of the electron diffusion, the ambipolar electrical field and the near wall potential jump with an account of the processes creating fast electrons*

The problems considered in this part have been discussed in detail in many works (see for example [9]), without taking into account the fast electron sources.

Let us analyze the diffusion of the charged particles in the low temperature plasma at conditions, when fast electrons are born in CI reactions (1.1), (1.2) and in superelastic collisions (1.3). We shall choose as an object for investigation a weakly ionized currentless plasma, where the role of these processes is most significant. Two regions could be distinguished in radial direction (a cylindric geometry volume is considered): quasi neutrality region and near wall region, where the charges are divided and a potential difference, $\Phi_b$, appear. It balances the currents of ions and electrons and sustains the plasma quasi neutrality in the volume.

The ion and electron fluxes are given by the expressions:

$$\mathbf{J}_i = N_i \mathbf{u}_i = -D_i \nabla N_i + b_i \mathbf{E}_a N,$$

$$\mathbf{J}_e = N_{es} \mathbf{u}_{es} + N_{ef} \mathbf{u}_{ef} = -D_{es} \nabla N_{es} - b_{es} N_{es} \mathbf{E}_a - D_{ef} \nabla N_{ef} - b_{ef} N_{ef} \mathbf{E}_a. \quad (7.1)$$

Here, $\mathbf{u}$ is the drift velocity, $N$ is the density, $D$ and $b$ are the coefficients of diffusion and mobility, $\mathbf{E}_a$ is the ambipolar electric field. The index i refers to the ions, e refers to the electrons, es corresponds to the main group of electrons, ef refers to the fast electrons. Considering the ion distribution as a Maxwellian one, we will get:

$$b_i = \frac{2e}{M\langle \nu_{in} \rangle}; \quad D_i = \frac{2T_i}{M\langle \nu_{in} \rangle}; \quad \frac{D_i}{b_i} = \frac{T_i}{e}. \quad (7.2)$$

Here, $\langle\ \rangle$ denotes averaging over the EDF, $\nu_{in}$ is the resonance charge exchange frequency of the ions on the atoms.

The flux of electrons at a known EEDF is:

$$J_e = \frac{4\pi}{3} = \int_0^\infty v^3 f_1(\mathbf{v} \cdot \mathbf{r})\, dv \quad (7.3)$$

where

$$f_1 = -\frac{eE}{m\nu_a} \frac{\partial f_0}{\partial v} - \frac{v}{\nu_a} \frac{\partial f_0}{\partial r} \quad (7.4)$$

is the orientated part of the EDF. For a Maxwellian distribution of the main electron group

$$b_{es} = \frac{e}{m\langle \nu_a \rangle_s}; \quad D_{es} = \frac{T_e}{m\langle \nu_a \rangle_s}; \quad \frac{D_{es}}{b_{es}} = \frac{T_e}{e}. \quad (7.5)$$

For the fast electrons:

$$b_{ef} = \frac{e}{m\langle \nu_a \rangle_f}; \quad D_{ef} = \frac{\bar{\varepsilon}_f}{m\langle \nu_a \rangle_f}; \quad \frac{D_{ef}}{b_{ef}} = \frac{\bar{\varepsilon}_f}{e}, \quad (7.6)$$

where $\bar{\varepsilon}_f$ is the fast electrons average energy. The averaging in (7.5) and (7.6) is made on different EDF: $f_{0s}$ and $f_{0f}$. It is not difficult to obtain more rigorous expressions for $D_{ef}$, $b_{ef}$ and $\varepsilon_f$, using the known $f_{0f}$ form.

$_e \gg D_i$; $b_e \gg b_i$, from (7.1) for the ambipolar
e get:

$$= -\frac{D_{es}\nabla N_{es} + D_{ef}\nabla N_{ef}}{N_{es}b_{es} + N_{ef}b_{ef}}. \tag{7.7}$$

n from (7.7), it is created by the radial gra-
nd $N_{ef}$. For the ratio $E_{ef}/E_{es}$ we obtain the

$$(T_e N_{es}). \tag{7.8}$$

r example in He, where $\delta\nu_a \simeq 7 \cdot 10^5 p$:

$$\frac{\varepsilon_p}{T_e} \simeq \frac{10^{-15} N_m \varepsilon_p}{N_e p T_e}. \tag{7.10}$$

n in the final expressions: $N_m$, $N_e$ in $cm^{-3}$; $p$
in eV.
nd (7.8) the boundary cases follow:
$N_{ef}\varepsilon_f$ – the average energy of the electron gas
$T_e$. Then, $E_{ef} \ll E_{es}$, $N_{es} = N_i$ and

$$= \frac{T_e}{e}\frac{\nabla N_{es}}{N_{es}} \tag{7.11}$$

wn field of ambipolar diffusion for a Maxwel-
e existence of fast electrons do not influence
At that, the ambipolar potential difference is

$$\sqrt{\frac{T_i}{T_e}}). \tag{7.12}$$

ider the near wall potential jump in this case.
nd, as usual, from the equality of the electron
n the wall. The flux of ions to the wall at their
tion is:

$$= D_a N_i(0) J_1(2.4)/\Lambda,$$
$$_R$$
$$). \tag{7.13}$$

n flux to the wall, $\Gamma_e = \Gamma_{es} + \Gamma_{ef}$, is expressed
.3), substituting the lower integration limit
le $f_1(v, r)$ has to be calculated at $r = R$. The
the main electron group flow to the wall for
rms are obtained in [103], with an account
n departure and the inelastic processes influ-
ular, at a Maxwell distribution of $f_{es}$ near the
9, 103]:

$$N_{es}(0) \exp\left(-\frac{e\phi(R)}{T_e}\right), \tag{7.14}$$

l potential $\phi(R) = \Phi_a + \Phi_b$, while $\Phi_a$ is given
2).
gh pressure and (or) large $N_i$), the appearing
undergo energy relaxation in the volume
ng the wall. Their flux to the wall is small and
alculated as for a Maxwellian DF, equalizing

$\Gamma_i$ (7.13) and $\Gamma_{es}$ (7.14). It is

$$\Phi_{hm} = \frac{T_e}{e} \ln\left(\sqrt{M}/\sqrt{m}\,6\sqrt{\pi}\,J_1(2.4)\right). \tag{7.15}$$

At $K \ll 1$, the fast electrons, born in CI reactions and quenching collisions, influence the near wall potential jump value [11, 103, 104]. If $e\Phi_b < \varepsilon_p, \varepsilon_1$, then the fast electrons move to the walls in a free diffusion regime. As a result, $f_{ef}$ is described by the formula (2.23), (2.38), e.g. it is a narrow peak in the energy region of their origin. Then, from (7.3) or immediately from the kinetic equation for the flux of fast electrons to the wall we get:

$$\Gamma_{ef} = \bar{I}_m + \bar{I}_e = \frac{2}{R^2}\int_0^R (\beta_m N_m^2(r) + \beta_e N_m(r) N_e(r))r\,dr. \tag{7.16}$$

Introducing [105], the diffusion parameter $P = \Gamma_{ef}/\Gamma_i$ ($\Gamma_{ef}$ and $\Gamma_i$ are given by (7.16) and (7.13), respectively) and equalizing the electron, $\Gamma_e = \Gamma_{ef} + \Gamma_{es}$, and the ion flux to the wall we obtain:

$$\Phi_b = \Phi_{hm} \cdot \left(-\frac{T_e}{e}\right) \ln(1 - P). \tag{7.17}$$

It should be pointed out that (7.17) is correct at $\Phi_b < \varepsilon_p, \varepsilon_1$. That is equivalent to the condition $P < 1$.

From (7.17) is seen that in the common case, the near wall potential jump value is determined not only by the Maxwellian electrons (main group), but also by the fast electrons. It increases in comparison with the value $\Phi_{hm}$, calculated at the assumption of Maxwellian distribution when $P$ increases. The relation (7.17) becomes incorrect at $P \to 1$, $\Phi_b \to \varepsilon_p, \varepsilon_1$. In order to maintain the quasineutrality, part of the fast electrons flow, equal to $\Gamma_{ef} - \Gamma_i$, is trapped in the volume. In this case the near wall jump is equal to the energy by which the fast electrons appear $\Phi_b \simeq \varepsilon_p, \varepsilon_1$ and the EEDF consists of a continuous electron spectrum, instead of a sharp peak as it is at $K \gg 1$.

The appearing fast electrons at $e\phi(R) > \varepsilon_p, \varepsilon_1$ are trapped in the volume and the EDF could be found by solving eq. (2.2) with boundary conditions (2.21). The EDF at $\varepsilon < e\phi(R)$ does not depend on $r$ [7] and for a determination of $f_{of}(w)$ the kinetic equation (2.2) should by integrated from $r$ to $r_1(w)$. As a result, the first term in (2.2) becomes zero and the kinetic equation will have a form, formally coinciding with the local case form by an exchange of the kinetic to the total energy and the coefficients $D_i(w)$, $V_i(w)$, $\nu_{mc}(w)$, $R_i(w)$ to the coefficients $\bar{D}_i(\varepsilon)$, $\bar{V}_i(\varepsilon)$, $\bar{\nu}_{mc}(\varepsilon)$, $\bar{\nu}_{1m}(\varepsilon)$, $\bar{R}_i(\varepsilon)$, using the relation (2.22).

$$\begin{Bmatrix} \bar{D}_i(\varepsilon) \\ \bar{V}_i(\varepsilon) \\ \bar{I}_j \bar{R}_j(\varepsilon) \end{Bmatrix} = \frac{2}{R^2}\int_0^{r_1(\varepsilon)} \begin{Bmatrix} D_i(\varepsilon - e\phi(r)) \\ V_i(\varepsilon - e\phi(r)) \\ I_j R_j(\varepsilon - e\phi(r)) \end{Bmatrix} \times \sqrt{(\varepsilon - e\phi(r))} \cdot r\,dr, \tag{7.18}$$

$$\bar{\nu}(w) = \frac{2}{R^2}\int_0^{r_k(\varepsilon)} \nu_k(\varepsilon - e\phi(r))\sqrt{(\varepsilon - e\phi(r))} \cdot r\,dr,$$

where the indices $j = m, c$; $k = mc, 1m$, while $r_k$ is determined from the condition $w - \varepsilon_k = e\phi(r_k)$, $\varepsilon_k = E_c, \varepsilon_1$. It should be pointed out that at $\varepsilon > T_e$, $r_1(w) = R$. From (7.18) we get:

$$\overline{I_j R_j} = \frac{I_j(r_0(\varepsilon))r_0(\varepsilon)}{e\phi'(r_0)\sqrt{\varepsilon_j}}(\theta(\varepsilon - \varepsilon_j) + \theta(\varepsilon_j + e\phi(R) - \varepsilon)) \tag{7.19}$$

pe form of the source $R_j$ energy dependence

n of the equation obtained in this way could be a manner similar to the local case which was bove in Section 2.3.

e shall pay attention to the currentless plasma, mperature $T_e$ usually is low, therefore the pro- emiioinization and superelastic collisions influ- ubstantially the distribution function fast part. ider the typical conditions when the main group (Maxwellian electrons) determine the ambipolar plasma and the ambipolar difference of potential $T_e/e$ (see relation (7.12)). At that, the large wall potential $e\phi(R) \geqslant \varepsilon_p, \varepsilon_1 \gg T_e$, equal to the $_h$, is given entirely by the near-wall jump, $\Phi_h$. $\Phi_h \simeq e\phi(R)$. Similar conditions are accomplished of anomalous potential jump which we discuss r example is the experiments on controlling the rt. In case $\varepsilon_1, \varepsilon_p \gg e\Phi_h$, the difference between w e neglected in (7.18), (7.19) and the kinetic equa- trapped electrons will coincide completely with se equation (discussed in Section 2.3.2). The ction is that the sources intensity, $I_j$, does not :

$$f_j(r) \cdot r \, dr. \tag{7.20}$$

) either the formula (2.43) or the limit expres- (2.54) with a substitution of $\tilde{I}_j$ for $I_j$ will be $_{ef}$. At $a_e < 1$ the fast electrons EDF represents a ne region $\varepsilon < e\phi(R)$. The same situation was e local case. The regime is nonlocal so an he $f_{0f}$ radial dependence will be a distinctive the local regime. The distribution functions of ial points will coincide in their fast parts.

iments conducted in the afterglow plasma com- rm these conclusions. As an example, the results easurements in xenon afterglow plasma at pres- 2 Torr, $N_e = 3 \cdot 10^9\,\mathrm{cm}^{-3}$, $N_m = 6 \cdot 10^{10}\,\mathrm{cm}^{-3}$, nd $e\phi(R) \simeq 4.3$ eV are presented in Fig. 20. It is EEDF radial dependence is practically absent. listinctive feature of the nonlocal regime at s the growth of the number of fast electrons in with the case $e\phi(R) \ll \varepsilon_p$. Indeed, at $e\phi(R) \ll \varepsilon_p$, ed by relation (2.23) and $N_{ef} \simeq \beta_m N_m^2 \tau_{df}$. At the $\sqrt{}_{ef} \simeq \beta_m N_m^2 (\nu_e + \delta\nu_e)$ at $e\phi(R) \geqslant \varepsilon_p$. All this is by Fig. 20. The EEDF at $e\phi(R) \ll \varepsilon_p$ is also dashed line there. Thus, for the electron dis- nction calculation in the regime when anom- ial jumps appear, the expressions are correct, btained with a substitution of $\Gamma_{ef} - \Gamma_i$ for $\tilde{I}_j$ in $e\Phi_h$, and $\Gamma_i$ for $\tilde{I}_j$ in (2.23) at $\varepsilon > e\Phi_h$. It should be mentioned that two cases could be realized in the process of plasma decay at $K \ll 1$: first, $P < 1$ and $e\Phi_h \ll \varepsilon_p, \varepsilon_1$ in the initial time period; second, $P \geqslant 1$, $e\Phi_h \simeq \varepsilon_p, \varepsilon_1$ in the successive periods, when the electrons cool to low temperatures. The appearance and the evolution of this interesting phenomenon was observed in the rare gases afterglow plasma [104]. For example, the results of the EEDF fast part measurements in xenon at conditions: $p = 0.2$ Torr, $i = 5$ mA are shown in Fig. 21. A transition from a free diffusion regime ($P < 1$) to a regime with an anomalous large potential jump ($P > 1$) occurs in the course of time in the afterglow. Simultaneously with the time growth, a creation of a continuous electron spectrum in the energy region $\varepsilon \leqslant 4.5$ eV is clearly observed. That corresponds to the analysis conducted so far. Figure 22 shows the results of the potential, $\Phi_h$, measurements for the same experimental conditions as well as the results of the $\Phi_h$ value calculation by relations (7.15) and (7.17). It is seen that accounting for the fast electrons leads to an agreement between theory and experiment.

B. $T_e N_{ea} \ll \varepsilon_f \tilde{N}_{ef}$. This case is not examined in detail, but it is important for the practice because such conditions can materialize in cryogenic afterglow plasma. It follows from (7.7), (7.8), that in this case $E_{as} < E_{af}$ and

$$\mathbf{E} = -D_{ef} \frac{\nabla N_{ef}}{N_{ef}} \simeq \frac{\tilde{\varepsilon}_f}{e} \frac{\nabla N_{ef}}{N_{ef}}. \tag{7.21}$$

It is seen that the ambipolar field is determined entirely by the fast electrons and sharply increases in comparison with the field, calculated under the assumption of a Maxwellian EEDF and without accounting for chemiionization reactions. At that, evidently, its $T_e$ dependence is absent. The

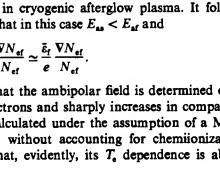


*Fig. 21.* Electron velocity distribution function in xenon decay plasma at different moments of the afterglow period.

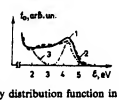


n velocity distribution function in xenon afterglow plasma e tube axis (1), and on 9 cm distance from the axis (2), $(r/$ ) $\simeq \varepsilon_p$. Curve 3 is for the tube axis at $e\phi(R) \ll \varepsilon_p$.

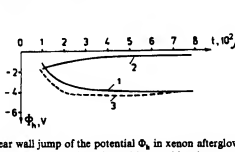


*Fig. 22.* Near wall jump of the potential $\Phi_h$ in xenon afterglow plasma; 1 – experimental result, 2 – calculation without taking into account the fast electrons appearance and arising of anomalous potential jump, 3 – calculation accounting for these effects.

sion coefficient,

$$D_i \simeq D_i \tilde{e}_i / T_a, \tag{7.22}$$

can lead to an abrupt decrease of the time for sion to the wall. Respectively, an account of ances can change the ratio between the losses of the charged particles and their ie wall. It can lead to an acceleration of the Under similar conditions for the fast elec- with a trapping of part of their flow in the ys accomplished.

ons show that this case can be realized in the f helium cryogenic afterglow, where at ypical conditions are: $N_e = (5 \cdot 10^8$ $N_m = (10^{12} - 10^{13})\,\mathrm{cm}^{-3}$, $T_e = (10 - 100)$ K r, these effects were not taken into account in ı works (see for example in [105]). Direct of EEDF, $T_e$ and $\Phi_h$ are necessary for more is of these interesting problems, but as far as data are not available in the literature.

### *of the energy distribution function and the ie currentless plasma*

es could implement in the non-local regime lasma as it was shown above in Section 7.1. ch is equivalent to $e\phi(R) < \varepsilon_p$, the appearing ove to the walls in a free diffusion regime. As s a maximum on the EEDF fast part due to 1–3). If $\Gamma_{el} > \Gamma_i$, an anomalous large near- jump, $e\phi(R) \simeq \varepsilon_p$, appears. Part of the fast energy $\varepsilon < e\phi(R)$ is trapped in the volume ous electron spectra appears on the EEDF. is observed during the plasma decay process, ssary conditions are fulfilled (see Fig. 21). matic investigations in the regimes with ire complicated by the fact that these regimes w range of conditions and are not always hat, it is not possible to regulate the value of ".

ons could also be created artificially [106], given regulated blocking potential on the e from conducting materials. We shall con- anism of the EDF forming in this regime

se that the bigger part of the discharge gap is metallic cylinder with a radius $R$ and length lose to the inner tube wall. If we apply nder and the reference electrode a negative $w_0/e$, blocking the electrons and thus artifi- the $\Phi_i$ value, then practically the whole in the plasma will be concentrated in the of the volume charge. The ambipolar field with an accuracy up to the term $\sim b_i/b_e \ll$ r wall potential jump value will increase up tead of several $T_e/e$ in the case when such a applied). This conclusion is also confirmed potential measurements made by moving

hand, since the electron flux on the wall $> \varepsilon_p/e$) a longitudinal field $E_z$ should appear he movement of electrons in this field compensates the ion flux to the metallic wall, e.g.

$$2b_e \int_0^R NE_z 2\pi r\, dr = -D_a (\nabla N)_{r=R} 2\pi RH. \tag{7.23}$$

From this expression it is possible to get an estimation for $E_z$,

$$E_z \sim \frac{D_i(1 + T_e/T_i)}{b_e} \frac{H}{R} \frac{(\nabla_r N)_{r=R}}{N}$$

$$\sim \frac{D_i}{D_a} \frac{H}{R} E_r \ll E_r \sim \frac{T_e}{eR}. \tag{7.24}$$

For this reason the longitudinal field, $E_z$, could not be taken into account further at the analyses of the EEDF forming in a regime with a trapping potential (TPR). This circumstance was confirmed by the direct experiments, when a voltage pulse was applied in different afterglow moments on the tube electrodes. The corresponding longitudinal field of the pulse was adjusted to be equal to $E_z$ in TPR. At that, in agreement with (7.24), the plasma parameters ($N_e$, $T_e$) in the regimes under investigation practically did not change. The surface area of the reference electrode in TPR should not be so small because the electron current on it has to compensate the ion flux to the metal wall.

In the case of EEDF nonlocal forming ($K \ll 1$), using a negative potential, applied to the wall, it is possible to make a transition from regimes with maximums in the EEDF fast part (2.23), (2.38), to a "step" type distribution, described approximately by relations (2.43), (2.49), with sources averaged according (7.20). The fast electron number increases $\sim[(2\nu_i + \delta\nu_a)\tau_{dif}]^{-1}$ times, what could really be 1–2 order of magnitude.

By changing of the blocking potential value, $\Delta V$, one can control the value of the EDF "step", since it turns out that one or other part of the fast electrons, born in the energy region of $R_m(v)$ and $R_a(v)$ existence, is blocked in the volume. Thus, it is possible to regulate the slow and fast electron ratio in a wide range by the proposed method.

As it was already pointed out, the EDF enrichment at $w \gg T_e$ could lead to several interesting effects: rising of the electron temperature, $T_e$, connected with this an acceleration of the plasma deionization and corresponding decreasing of $N_e$, growth of the number of excitations from the metastable states. Further will be presented an experimental study of the influence of EDF controlled fast part upon these parameters of the decaying plasma. A periodic discharge was fired in a tube with a total length of 43 cm. A thin Ni cylinder with radius $R = 1.8$ cm and a length of $H = 9$ cm was fitted on the tube wall. The tube construction allows: to burn the discharge between different couple of electrodes; to apply a negative potential on the wall and to carry out probe and optical diagnostic of the decaying plasma.

Typical results of EDF fast part controlling experiments are shown in Fig. 23. A negative pulse with a voltage $\Delta V$ is applied on the wall electrode 60 μs after the end of the discharge pulse. The EDF is recorded in this afterglow moment. The electron temperature, determined from the EDF slow part, $T_e = 1100$ K, as well as the electron density, yielded by the method of additional pulse with different probe couples and averaged upon the radius, $N_e = 3.7 \cdot 10^{10}\,\mathrm{cm}^{-3}$, did practically not change in the conditions when $\Delta V$ is switched on.

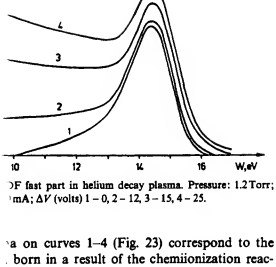


)F fast part in helium decay plasma. Pressure: 1.2 Torr; mA; $\Delta V$ (volts) 1 – 0, 2 – 12, 3 – 15, 4 – 25.

a on curves 1–4 (Fig. 23) correspond to the born in a result of the chemiionization reac- ing He ($2^3S_1$) metastable atoms. With increas- more and more of the fast electrons turn to be quantity in the EDF high energy part sub- eases. In addition, the absence of radial depen- EDF step part is confirmed experimentally, ame time at $\Delta V = 0$ the value of the maxima is it follows from the consideration in Section

*tion of elastic electron–atom and on collisions by the PIES method*

fast electrons at local forming has the "step" (2.50) Section 2.3.2). From expression (2.50) is ias a simple relation with the values of the n–atom, $\nu_a(\varepsilon)$, and electron–electron, $\nu_e(\varepsilon)$, colli- es. In principle, they could be determined by DF measurements. However, the measure- F in local regimes are complicated by the lim- ie probe method at high pressures. If the )–(1.3) serve as fast electron sources, the EDF e at such pressures ($pR > 10$ Torr · cm) is com- all (see (2.52)–(2.54)).

ocal case ($K < 1$), at a regime with continuous ra (anomalous potential jump), (see Section xperiments of the electron energy distribution ction 7.2), the EEDF also has a "step" form:

$$\bar{\nu}_e + \delta\nu_a), \tag{7.25}$$

$_f - \Gamma_i$ in the regime when the anomalous ) appears (see (7.13), (7.16)). The averaging on g expression (7.20).

ioned above that the regime with continuous ra exists in a limited range of conditions and s be observed. Besides, the $\Gamma_{ef}$ and $\Gamma_i$ values d only from the solution of the self-consistent lem. The uncertainty at $\Gamma_{ef} - \Gamma_i$ calculation, n this, allows to determine the $\nu_a(\varepsilon)$ and $\delta\nu_a(\varepsilon)$ ence only in relative units.

nts of the EEDF, conducted in a regime of tential jump [107], were used for determi- frequency, $\nu_a$, of helium in arbitrary units. In 3] was proposed to use the regime with a control of the electron energy distribution (see Section 7.2) for absolute measurements of the frequencies $\nu_a(\varepsilon)$ and $\nu_e(\varepsilon)$. The experiments were conducted in helium and xenon afterglow plasma. A pulse discharge with a duration $\sim 10\,\mu$s and repetition rate $\sim 1$ kHz was burnt in a similar glass tube (radius $R = 1.8$ cm) with a conducting cylinder closely fitted to the wall. Sources of fast electrons in this case were reactions (1.1)–(1.3) in which the metastable atoms He($2^3S_1$), ($\varepsilon_a \approx 14.4$ eV, $\varepsilon_1 = 19.8$ eV) and Xe($^3P_2$), ($\varepsilon_a \approx 4.5$ eV, $\varepsilon_1 = 8.3$ eV) take part. The negative voltage pulse was applied 10–20 $\mu$s before the measurement phase on the metallic cylinder inside the tube.

In order to test the possibilities of the proposed method experiments were conducted for determination of the elastic electron–atom collision frequency, $\nu_a$, in helium at conditions when $\nu_a \ll \delta\nu_e$ for energy $\varepsilon \sim \varepsilon_a$.

On Fig. 24 are shown the EDF forms, yield in one of these regimes in He afterglow (the blocking potential $\Delta V = 0$ and 25 V, delay time – 150 $\mu$s after the end of the discharge pulse). The maxima on the curves are formed by fast electrons, born in reaction (1.1). The error in the EEDF absolute value determination did not exceed 10% and was controlled by measurements of the reaction rate constant $\beta_m$, using the PIES method.

As seen from Fig. 24, the number of fast electrons sharply increases in the blocked regime while the EDF has the form of a step. The result of EDF calculation, according to relation (7.25) with a $\nu_a$ frequency taken from [109, 20], is shown there by a dotted line. The tiny maximum, appearing on the step, widened at the expense of the instrumental function, is connected with the fast electrons diffusion departure through the metallic cylinder ends. Since the number of these electrons is not large and is in compliance with the corresponding estimations, it isn't necessary to take into account this departure in the calculation. Thus the measured and the calculated EEDF coincide with a good accuracy. That testifies for a coincidence between the experimentally determined $\nu_a$ value and the literature data, and indicates for an absence of substantial systematic errors of the measurements.

The beam methods and the drift tube experiments are widely used in measurements of cross-sections for elastic scattering of electrons on atoms [109]. Such cross-sections are yielded with enough accuracy in most gases. However, quite amazing is the situation with electron–electron collisions, whose role in the plasma kinetic is well known. In spite of that, due to the inapplicability of the traditional experimental methods, as far as we know, direct measurements of the $\nu_e(w)$ absolute value was not carried out so far.

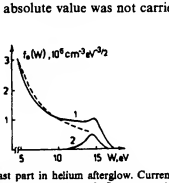


*Fig. 24.* The EVDF fast part in helium afterglow. Current pulse 100 mA; pressure 0.7 Torr; $N_a(0) = 2.66 \cdot 10^{11}$ cm$^{-3}$, $\bar{N}_e = 1.4 \cdot 10^{10}$ cm$^{-3}$; Curve 1 – $\Delta V = 25$ V, $T_e = 1680$ K; Curve 2 – $\Delta V = 0$ V, $T_e = 930$ K. Dotted line – calculation using [105].

the possibility of the $\nu_a(w)$ direct experimen-
n by the EDF in afterglow, turns out to be
ue.

ation of the $\nu_a(\varepsilon)$ dependence we choose
ditions when $\nu_e \gg \delta\nu_e$ in the energy region
rimental curve and the experimental condi-
] are shown, as an example, in Fig. 25. In
are measured with calculated EDF the

$$\ln \Lambda, \tag{7.26}$$

$(K)/\bar{N}_a(cm^{-3}))^{1/3}\varepsilon(eV)$,

$\bar{N}_e$ was determined by the plasma conduc-
mined stage of the afterglow.
ependence of $\nu_e \sim 1/v^3$ in the energy range
confirmed by the form of the distribution
*stant* under the condition $\nu_e \gg \delta\nu_e$ (see Fig.
on afterglow. The value $\gamma = 2.0 \pm 0.4$ was
e multiplier $\gamma$ in [108].

*pon the temperature of the Maxwellian*

hat as electron temperature $T_e$ we accept the
the main group electrons, which should be
energy balance equation. It is evident that at
t coincides with the average energy of the

s (1.1)–(1.3) have effects upon the electron
two ways. On the first place the interaction
rons with the main group electrons leads to
)n the second place the presence of the fast
to a change in the energy losses by diffusion
ain group electrons.
ler these problems in detail.

*he main group electrons by the fast electrons*

) case the fast electrons, arising in reactions
lissipate their energy in several ways: (a) in
h slow electrons; (b) by collisions with gas
ecombination at the tube walls and in the

between (a), (b) and (c) leads to a situation in
ive energy, introduced by the fast electrons
into the electron system can assume any
o to $\varepsilon$. These problems have been studied at
[14]. Using it we shall derive the necessary

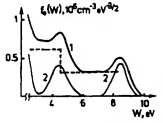


fast part in krypton afterglow. Current pulse: 160 mA;
$\nu_m(0) = 5.6 \cdot 10^{11}\,cm^{-3}$, $\bar{N}_e = 3.9 \cdot 10^{10}\,cm^{-3}$; Curve 1
200 K; Curve 2 – $\Delta V = 0$ V, $T_e = 1000$ K. Dotted line –
05, 106].

At $K \gg 1$ the effective energy $E_{eff}$ introduced by the fast electrons with initial energy $\varepsilon'$ to the slow electrons is:

$$E_{eff}(\varepsilon') = \sum_0^{\varepsilon} \frac{\nu_a(\varepsilon)\,d\varepsilon}{[\nu_e(\varepsilon) + \delta\nu_e(\varepsilon) + \nu_{mc}(\varepsilon)E_c/\varepsilon]} \tag{7.27}$$

and the term in the energy balance equation accounting for the heating of the main group of electrons has the form

$$H_\delta = 2E_{eff}(\varepsilon_j)I_j/3N_e. \tag{7.28}$$

As seen from (7.28), $E_{eff} = \varepsilon'$ if $\nu_e \gg \delta\nu_e(\varepsilon) + \nu_{mc}(\varepsilon)E_c/\varepsilon$. In the opposite case, $E_{eff} \ll \varepsilon'$.

When $K \ll 1$ and $P < 1$:

$$E_{eff}(\varepsilon') = \nu_e(\varepsilon)\tau_{df}(\varepsilon')\varepsilon'. \tag{7.29}$$

Since, in this case $\nu_e\tau_{df} \ll 1$, practically the total fast electron energy is carried away to the tube walls. The relevant heating is expressed by formula (7.28) with $E_{eff}(\varepsilon')$ in the form of (7.29).

At $K \gg 1$, $P > 1$, as it is noted above, part of the flow $\Gamma_{af} - \Gamma_i$ turns out to be trapped in the volume. Its effective energy $E_{af}$ is determined by formula (7.27). The corresponding heating term in the energy balance equation is expressed by (7.28) with an exchange of $I_j$ for $\Gamma_{af} - \Gamma_i$.

The other part of the fast electron flow, which is equal to $\Gamma_i$, goes to the wall in a free diffusion mode. The corresponding heating is analogous to that discussed at $K \ll 1$ and $P < 1$. Usually, it could be neglected in comparison with the heating by the trapped electrons.

B. *Variation of the electron temperature at the expense of diffusion cooling*

These losses are a sum of the energy, carried away by the electrons to the walls and the work spent to overcome the potential gap, $\phi(R)$, between the tube axis and the wall [9].

The problem of the diffusion cooling has been considered most completely in the work [103], where it is shown that the corresponding term in the energy balance equation has the form:

$$\begin{aligned} &K \gg 1, && H_{d1} = 2(2T_e + e\phi(R))/(3\tau_{ad}),\\ &K \ll 1,\ P < 1, && H_{d2} = 2(2T_e + e\phi(R))(1-P)/(3\tau_{ad}),\\ &K \ll 1,\ P \geqslant 1, && H_{d3} = 0. \end{aligned} \tag{7.30}$$

A common expression for $\phi(R)$ is yielded in paper [103], taking into account the possible change of the wall potential in comparison with the Maxwellian distribution, resulting from the departure of the main group electrons to the wall, the presence of fast electrons arising in reactions (1.1)–(1.3) and the stepwise processes.

If it is possible to neglect the stepwise processes and if the main group of electrons has a Maxwellian distribution in the volume including the near wall region, then $\Phi_b$ is expressed by the relation (7.17), while $\Phi_a$ is expressed by (7.12).

The diffusion cooling is influenced by the chemiionization reactions and the superelastic collisions in two ways. First of all the main group electrons flow to the wall is less than the ion flow by the value of the fast electrons flow. This is accounted in (7.30) by the multiplier $(1 - P)$. Besides that, with the rise of the diffusion parameter $P$ the $\Phi_b$ value grows (up to $\varepsilon_e/e$ at $P = 1$). As can be seen from (7.17) and (7.30) when $P$ increases, the diffusion cooling effect decreases

wall potential growth) and at $P \to 1$, $H_d \to 0$. means that at $P \to 1$ the near wall jump s such a value $(\varepsilon_p/e)$ that practically all of the ons turn to be trapped in the volume. In this lectrons ensure the equalizing of the ion and o the wall as well as the losses for sustaining mbipolar field and the near wall potential he fast electrons get their energy from the (as it follows from (7.30), too) the diffusion e main group of electrons is switched off in ons. Naturally, during the transition from = 1 case, a gradual decrease of $H_d$ is taking

ion of the diffusion cooling relative part in ance of the electron gas (see [70]) shows that , calculated at the assumption of a Maxwell function in the conditions range cm), is comparable or exceeds the energy astic electron–atom collisions, e.g. this term is n electron gas cooling. Owing to this at the $T_e$ similar conditions (for a typical $R \sim 1$ cm that o gas pressures $p \leqslant 1$–3 Torr), the incorrect could lead to serious mistakes in the $T_e$ deter- seen from (7.30), when the diffusion parameter decreases (down to zero at $P \to 1$). For this ding on the value of this parameter, it is pos- nine the temperature relaxation in the after- ffusion cooling at small $P$, while at large $P$ – losses, and the rate of the $T_e$ decrease substan- From these considerations it follows that the arameter $P$ should be controlled carefully at ion.

balance equation of the main group electrons ionized plasma has the form:

$$'_e - H_{in} - H_d, \qquad (7.31)$$

are the losses of electron energy in elastic and ctions, $H_\delta$ (7.28) describes the heating of the ectrons by the fast electrons, $H_d$ is the diffu- s follows from the examination made above, 31) has substantially different form at the dif- ter value $P < 1$ and $P > 1$. In these cases the 3) have different effects upon the temperature e the continuous electron spectra in the after- o not usually appear soon after the end of the e, a transition from $P \ll 1$ to $P \geqslant 1$ is possible ) relaxation. We conducted experiments in the of rare gases and made the corresponding cal- $'_e(t)$. For example the measurements and the sults in a regime with $P < 1$ are shown in Fig. resents results for which the diffusion param- changes from $P \ll 1$ to $P \geqslant 1$ in the course of cay. A good agreement between theory and n be seen. Substantial discrepancies appear if reactions creating fast electrons are not n the calculations.

*upon the charged and excited particles densities*

plasma, the rate of the impact-radiation ion- ly small due to the low $T_e$. The chemiioniza-

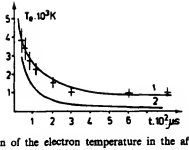


*Fig. 26.* Relaxation of the electron temperature in the afterglow plasma. Xenon, $p = 0.1$ Torr, $i = 10$ mA. Crosses – experiments, solid line – calculations, 1 – taking into account reactions (1)–(3), 2 – without accounting for these reactions.

tion processes are the single effective mechanism of ionization. In case of absence of CI processes, the plasma is decaying with a characteristic time, $\tau_{da}$, of ambipolar diffusion in a diffusion mode of $\tau_r = (\alpha N_e)^{-1}$ of recombination in a volume charge particle losses. Thus, after removing the excitation source, the electron density monotonously falls down with a characteristic time $\tau_{N_e} = (\tau_{da}^{-1} + \tau_r^{-1})^{-1}$ in the common case. In the presence of a comparatively high density, $N_m$, of the long living excited atoms (particularly metastables), the CI processes with these atoms lead to a situation when beginning in a certain moment, the rate of the $N_m(t)$ decrease substantially changes and is determined by the lifetime $\tau_{met}$. At $N_m(t) > N_e(t)$, sometimes a paradoxical situation is realized, when the charge particle density increases in the decaying plasma.

When the charge particles extinction is controlled by recombination, similar effects have been observed even in [110]. In the diffusion mode analogous effects are observed under conditions, when a free diffusion mode did not take place for the fast electrons and an anomalous potential jump appear as considered above [11]. That stated so far is illustrated by Fig. 28, where possible cases in the time behavior of $N_e(t)$ in the afterglow plasma are qualitatively presented.

It should be pointed out that conditions, when the processes of chemiionization influence the electron density and temperature temporal curves are typical for the afterglow of a weakly ionized plasma in noble gases and their mixtures up to pressures of several tens of Torr.

More interesting, and unexpected at first sight, is the population of the excited states by the chemiionization processes. Actually, if we presume that in the decay plasma the EEDF is Maxwellian with a temperature abruptly falling to

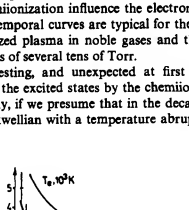


*Fig. 27.* Relaxation of the electron temperature in the afterglow plasma. Krypton, $p = 1$ Torr, $i = 80$ mA, crosses – experiments, solid line – calculations, 1 – taking into account reactions (1)–(3), 2 – without accounting for these reactions, with an account of the elastic electron–atom collisions only.


e behavior of the charge particles density time variation
sma. 1 – a decay without accounting for the chemiioni-
–4 – decay curves at different ratio between the rates of
ocesses, recombination and diffusion.

ature in time, then at $T_e \leqslant 0.5$ eV the conclu-
bination population of the excited states is
ever, as it was already shown, owing to the
n processes and to the superelastic collisions
electrons in the EEDF fast part turns out to
s of magnitude higher than that of a Maxwel-
n with the slow-electron temperature $T_e$. The
t electron number is relatively slow. For this
distribution function should play a consider-
electron impact excitation from the metasta-
wise excitation), even at low $T_e \leqslant 0.5$ eV. Such
r the helium afterglow plasma was indicated
111]. In work [112] expressions for the step-
calculation were derived and also the relative
s process and the recombination in the popu-
ited levels were considered.
on case the probability of the stepwise exci-
resence of fast electrons can be given by a
is

$$W_{mn}^{(t)} \tag{7.32}$$

d $W_{mn}^{(t)}$ are the rates of excitation in a unit
level $n$ from the level $m$. They are expressed
wn formula

$$\langle \varepsilon \rangle_{0n}(\varepsilon)\sqrt{\varepsilon}\, d\varepsilon, \tag{7.33}$$

e excitation cross section, $\Delta E_{mn}$ is the energy
= s, f.
tive calculations the particular expressions
d in Section 2 and the data of $\sigma_{mn}(\varepsilon)$, for
ork [69], should be substituted in (7.33).
I pay attention to the following important
$T_e$, when $W_{mn}^{(s)} \ll W_{mn}^{(f)}$ the stepwise excitation
y the fast electrons, appearing in reactions
is case the efficiency of excitation depend on
fast electrons and the values of the param-
$K \gg 1$ and arbitrary $P$, and also at $K \gg 1$
$W_{mn}^{(f)}$ value in the relaxation process is deter-
havior of $N_m^2(t)$ and decreases at decreasing
and $P \geqslant 1$ (regime with anomalous jump of
$W_{mn}^{(f)}$ is determined by the value $N_m(\beta_m N_m^2)$
, depending on the conditions ($N_m$; $N_e$, $T_e$),
r decrease as well. For this reason the $W_{mn}^{(f)}$

behavior could exhibit a nonmonotonous character. Therefore, the maxima observed on the temporal curves of the spectral lines intensity in the afterglow [8] plasma, could not be from a recombination origin. The relative participation of the stepwise excitation and the population of the excited levels at the expense of the impact-radiative and dissociative recombination in the afterglow plasma of noble gases were analyzed in the work [112]. It was shown there that a thorough control is necessary for a possible population, due to stepwise processes in the weakly ionized plasma of middle pressures, at conditions when the recombination population of the levels is determined by the impact-radiative recombination. At low pressures, when the main channel of the molecular ion $N_4^+$ formation is not the conversion of atomic into molecular ions but the chemiionization processes, the stepwise excitation competes successfully with the more effective recombination population by the dissociative recombination.

In particular, at conditions considered so far, the appearance of the potential jump, when $N_e$ grows up due to the CI processes, changes also the character of the inequilibrium excited atomic levels distribution from a recombination to an ionization type.

## 8. Summary

At present, a vast amount of information has been derived for the ionization and quenching processes involving excited atoms, owing to the application of different experimental methods. The chemiionization processes in which participate two excited particles, especially in the radiative states, are quite interesting for theoretical analyses and practical applications. In this field more works could be expected in the nearest future, including the use of laser excitation and deexcitation of the separate levels.

In order to obtain most complete and detailed results about the examined processes, it is indispensable to search for a complex application of different methods: mass-spectrometry, Penning electron spectroscopy and PIES. This will enable us to use the advantages of each of them and to mutually compensate the shortcomings.

It is necessary to enlarge the amount of derived information by increasing the sensitivity and the resolution of the experimental devices. As far as the PIES method is concerned, a detection of the electron spectra in plasma with energy resolution 30–50 meV and sensitivity $10^4\,cm^{-3}$ will be possible in the nearest future. The resources of the PIES method could be increased by its application in the flowing afterglow plasma and also used for a study of the chemiionization processes in cryogenic plasma.

## References

1. Neynaber, R. H., Proc. 11th Int. Conf. on the Phys. of Electr. and At. Col., Inv. Pap. and Progr. Rep., Kyoto, 1979, p. 287.
2. Leonas, V. B. and Kalinin, A. P., Usp. Fiz. Nauk **121**, 561 (1977).
3. Smirnov, B. M., Usp. Fiz. Nauk. **133**, 569 (1981); Sov. Phys. Usp. **24**, 251 (1981).
4. Kolokolov, N. B., in: "Chemistry of the Plasma" (Edited by B. M. Smirnov) (Energoatomizdat, Moskva 1985), vol. 12, p. 56. (In Russian.)

v. A. N. and Jansons, M. L., "Elementary Processes in
:ali Metals" (M. Energoatomizdat 1988).
N. B. and Kudrjavtcev, A. A., in: "Plasma Chemistry"
M. Smirnov) (Energoatonizdat. Moskva 1989), vol. 15,
ssian.)
D. and Golubovskii, Yu. B., Zh. Tekh. Fiz. **47**, 1839

. M., Vorob'ev, V. C. and Jakubov, I. T., "Kinetics of
ium Low-Temperature Plasma" (Nauka, Moscow
ssian.)
., Zhilinskii, A. P. and Saharov, I. E., "Fundamentals of
ics" (Atomizdat, Moskva 1977). (In Russian.)
., Yu. B., Kagan, Yu. M. and Lyagushchenko, R. I., Zh.
Fiz. **57**, 2222 (1969).
I. and Kolokolov, N. B., Zh. Tekh. Fiz. **50**, 564 (1980);
ech. Phys. **25**, 338 (19 ).
N. B., Kudrjavtcev, A. A. and Romanenko, V. A., Proc.
'onf. on Gas Disc. Phys. (Kiev 1986). Abstracts, part II,

N. B., Kudrjavtcev, A. A. and Romanenko, V. A., Zh.
, 1737 (1986).
B., Kagan, Yu. M., Kolokolov, N. B. and Lyagush-
., Zh. Tekh. Fiz. **44**, 333, 339 (1974); Sov. Phys.-Tech.
, 215 (1974).
B., Kolokolov, N. B., Lyagushchenko, R. I. and Prama-
i. Tekh. Fiz. **47**, 2102 (1977); Sov. Phys.-Tech. Phys. **22**,

N. V., Kolokolov, N. B., Kudrjavtcev, A. A. and
, V. A., Zh. Tekh. Fiz. **58**, 469 (1988); Sov. Phys.-Tech.
' (1988).
M. and Cardinal, P. G., Phys. Rev. **A23**, 804 (1981).
'. D. and Kravchenko, A. I., Zh. Tech. Fiz. **45**, 1342
Phys.-Tech. Phys. **20**, 848 (1975).
N. B., Lyagushchenko, R. I. and Pramatarov, P. M., Zh.
', 2108 (1977); Sov. Phys.-Tech. Phys. **22**, 1225 (1977).
Rutcher, A., Ann. Phys. **22**, 166 (1969).
B., Kolokolov, N. B. and Milenin, V. M., Zh. Tekh. Fiz.
2); Sov. Phys.-Tech. Phys. **17**, 1359 (1973).
M., Perel', V. I., Usp. Fiz. Nauk **81**, 409 (1963); Sov.
, 767 (1964).
B., Kagan, Yu. M., Kolokolov, N. B. and Lyagush-
., Zh. Tekh. Fiz. **45**, 579 (1975); Sov. Phys.-Tech. Phys.
).
G. N., Lyagushchenko, R. I. and Startcev, G. P., Opt.
, 306 (1971).
"Spectroscopy of the Gas Discharge Plasma" (Nauka,
70), p. 63. (In Russian.)
C. E. and Kabanov, C. P., "Plasma Chemistry" (Edited
irnov) (Energoatonizdat, Moskva 1976), vol. 3, p. 189.

M. *et al.*, Zh. Tekh. Fiz. **53**, 913 (1983); Sov. Phys.-Tech.
(1983).
. I. and Arsenin, V. Ya., "Methods for Solving of Ill-
ms" (Nauka, Moskva 1974), p. 224. (In Russian.)
M., "Excited Atoms" (Energoatomizdat, Moskva 1974),
ssian.)
N. B. and Pramatarov, P. M., Zh. Tekh. Fiz. **48**, 2108
'hys.-Tech. Phys. **23**, 176 (1978).
M., "Ions and Excited Atoms in Plasma" (Atomizdat,
), p. 352. (In Russian.)
. and Smirnov, B. M., "Handbook in Atom and Molec-
(Atomizdat, Moskva 1980), p. 240.
N., Opt. Spektrosk. **31**, 181 (1871).
L. and Kolokolov, N. B., Zh. Tekh. Fiz. **48**, 1832 (1978);
ch. Phys. **23**, 1044 (1978).
'u., Demidov, V. I. and Kolokolov, N. B., Izv. Vyssh.
d., USSR, ser. Fiz. **8**, 117 (1982).
. and Popov, Tc. K., Phys. Lett. **A66**, 210 (1978).
. and Popov, Tc. K., Phys. Lett. **A70**, 416 (1979).
'. B. and Toronov, O. G., Opt. Spektr. **55**, 434 (1983).
N. B. and Toronov, O. G., Proc. of 19th All-Union
ır. (Tomsk 1983). Abstracts, part I, p. 285.
'. B. and Toronov, O. G., Proc. 6th All-Union Conf. on
sma Phys. (Leningrad 1983). Abstracts, part I, p. 23.

41. Blagoev, A. B., Mishonov, T. M. and Popov, Tc. K., Proc. 15th Int. Conf. Phen. Ion. Gas., contr. paper (Minsk 1981), p. 381.
42. Blagoev, A. B., Mishonov, T. M. and Popov, Tc. K., Phys. Lett. **A99**, 221 (1983).
43. Aymar, M. and Coulombe, M., At. Data Nucl. Data Tables **21**, 537 (1978).
44. Wiese, W. L. and Martin, G. A., "Transition Probabilities" (Gov. Print. Office, Washington 1980). NSRDS-NBS, vol. 68, part II, p. 359.
45. Garrison, B. J., Miller, W. H. and Shaefer, H. F., J. Chem. Phys. **59**, 3193 (1973).
46. Devdariani, A. Z. *et al.*, Zh. Eksp. Teor. Fiz. **84**, 1646 (1983).
47. Miller, W. H., J. Chem. Phys. **52**, 3563 (1970).
48. Dickinson, H. O. and Rudge, M. R. H., J. Phys. **B3**, 1448 (1970).
49. Cohen, J. S. and Schneider, B., J. Chem. Phys. **61**, 3230 (1974).
50. Miller, W. H. *et al.*, Z. Phys. **D21**, 89 (1991).
51. Borisov, V. B., Egorov, V. S. and Ashurbekov, N. A., Proc. 6th All-Union Conf. on Low Temp. Plasma Phys., L. (1983). Abstracts, p. 20.
52. Frish, S. E., "Optical Spectra of Atoms" (M, L. Fizmatizdat 1963).
53. Hotop, P. and Niehaus, A., Zs. Phys. Bd **228**, h1, 68 (1969).
54. Coleman, M. L., Hammond, R. and Durbin, J. W., Chem. Phys. Lett. **19**, 271 (1973).
55. Chermak, F., J. Electron Spectr. Rel. Phenom. **9**, 419 (1976).
56. Le Nadan, A. *et al.*, J. de Physique **43**, 1607 (1982).
57. Brion, C. B. and McDowell, C. A., J. Electron Spectr. Rel. Phenom. **1**, 113 (1972).
58. Nikitin, A. G., Ph.D. Thesis, S. Pb Univers. (Sankt Petersburg 1992).
59. Schmeltekopf, A. L. and Fehsenfeld, F. C., J. Chem. Phys. **53**, 3173 (1970).
60. Bolden, R. C. *et al.*, J. Phys. **B3**, 61 (1970).
61. Lee, F. W. and Collins, C. B., Chem. Phys. **65**, 5189 (1976).
62. Ueno, T. *et al.*, Chem. Phys. Lett. **45**, 261 (1980).
63. Koizumi, H. *et al.*, J. Chem. Phys. **85**, 1931 (1986).
64. Ionikh, Yu. Z., Penkin, N. P. and Yakovitskii, S. P., Opt. Spektrr. **66**, 1286 (1989).
65. Parr, T. P., Parr, D. M. and Martin, R. M., J. Chem. Phys. **76**, 316 (1982).
66. Sholette, W. R. and Muschlits, B. B., J. Chem. Phys. **36**, 3368 (1962).
67. West, W. P. *et al.*, J. Chem. Phys. **63**, 1237 (1975).
68. Jerram, P. A. and Smith, A. C. H., J. Phys. **B18**, 1747 (1985).
69. Hurt, W. B. and Grable, W. C., J. Chem. Phys. **57**, 734 (1972).
70. Chang, R. S. F., Setser, D. W. and Taylor, G. H., Chem. Phys. Lett. **25**, 201 (1978).
71. Ionikh, Yu. Z. *et al.*, Opt. Spektr. **71**, 941 (1991).
72. Harada, Y., Ohno, K. and Mitoh, H., J. Chem. Phys. **79**, 3251 (1983).
73. Hotop, P. and Niehaus, A., Int. J. Mass. Spectr. Ion Phys. No. 5, 415 (1970).
74. Yee, D. S. C. *et al.*, J. Electr. Spectr. Rel. Phen. **7**, 93 (1975).
75. Jones, M. T. *et al.*, J. Chem. Phys. **89**, 4501 (1985).
76. Golde, N. F., Ho, Y. S. and Ogura, H., J. Chem. Phys. **76**, 3535 (1982).
77. Hromov, N. A., Ph.D. Thesis, S. Pb. Univers. (Sankt Petersburg 1991).
78. Hotop, H., Kolb, E. and Lorenzen, J., J. Electron Spectrosc. **16**, 213 (1979).
79. Ohno, K., Mutch, H. and Harada, Y., J. Am. Chem. Soc. **105**, 4555 (1983).
80. Ivanov, E. E., Ionikh, Yu. Z. and Penkin, H. P., Him. Vis. Energ. **18**, 159 (1984).
81. Landau, L. D. and Lifshitc, E. M., "Quantum Mechanics" (Fizmatgiz, Moskva 1963), p. 702.
82. Schulz, G. J., Rev. Mod. Phys. **45**, 378 (1973).
83. Vainshtein, L. A. and Minaeva, L. A., Zh. Prikl. Spektrosk. **9**, 60 (1968).
84. Nesbet, R. K., Phys. Rev. **A12**, 444 (1975).
85. Schaper, M. and Scheibner, G., Beitr. Plasma Phys. **9**, 45 (1969).
86. Korotkov, A. I., Mitryuchin, L. K. and Prilezhaeva, N. A., Proc. 8th All-Union Conf. Electr. Atom Coll. Phys. (Leningrad 1981). Abstracts, p. 199. (Preprint LIYaF.)
87. Pichanik, F. M. J. and Simpson, J. A., Phys. Rev. **168**, 64 (1968).
88. Brunt, J. N. H., King, G. C. and Read, F. H., J. Phys. B, Atom Mol. Phys. **9**, 2195 (1976).
89. Brunt, J. N. H., King, G. C. and Read, F. H., J. Phys. B, Atom Mol. Phys. **10**, 3781 (1977).

N. *et al.*, Zh. Eksp. Teor. Fiz. **81**, 842 (1981).
J. Phys. B, Atom. Mol. Phys. **15**, 4259 (1982).
fonchicourt, P. and Cheret, M., Phys. Rev. **A13**, 1140
. Deloche, R. and Monchicourt, P., J. Phys. **34**, 301
ell, K. L. and Kingston, A. B., Proc. Phys. Soc. **91**, 288
d Fox, R. E., Phys. Rev. **106**, 1179 (1957).
Grigorashchenko, O. N. and Mjshkis, D. A., Zh. Eksp.
23 (1971).
. N., Startcev, G. P. and Frish, M. S., Opt. Spekrosk.
).
A., Sobel'man, I. I. and Yukov, E. A., "Cross-Sections
n of Atoms and Molecules by Electrons" (Nauka,
. p. 144. (In Russian.)
, Zubek, M. and King, G. C., J. Phys. **B18**, 185 (1985).
hys. Rev. **181**, 257 (1969).
B. L. and Smith, S. J., Rev. Mod. Phys. **40**, 238 (1968).
. and Kolokolov, N. B., Zh. Tekh. Fiz. **50**, 564 (1980).
103. Kolokolov, N. B., Kudrjavtcev, A. A. and Toronov, O. G., Zh. Tekh. Fiz. **55**, 1920 (1985).
104. Demidov, V. I., Kolokolov, N. B. and Toronov, O. G., Fizika Plasmi **12**, 702 (1986).
105. Samovarov, V. N. and Fugol', I. Ya., Zh. Eksp. Teor. Fiz. **75**, 877 (1978).
106. Kolokolov, N. B., Kudrjavtcev, A. A. and Romanenko, V. A., Zh. Tekh. Fiz. **58**, 2098 (1988).
107. Demidov, V. I. and Kolokolov, N. B., Izv. Vyssh. Uchebn. Zaved. USSR, ser. Fiz. **58**, 7 (1987); Sov. Phys. Journ. **30**, 97 (1987).
108. Kolokolov, N. B., Kudrjavtcev, A. A. and Romanenko, V. A., Fizika Plasmi, **15**, 481 (1989); Sov. J. Plasma Phys. **15**, 280 (1989).
109. Huxley, L. and Krompton, R., "Diffusion and Drift of Electrons in Gases" (John Wiley, New York, London 1977).
110. Rogers, W. A. and Biondi, M. A., Phys. Rev. **134**, 1215 (1964).
111. Kagan, Yu. M., Kolokolov, N. B. and Pramatarov, P. M., Opt. Spekrosk. **42**, 252 (1977); Sov. Opt. Spectrosc. **42**, 143 (1977).
112. Kolokolov, N. B., Kudrjavtcev, A. A. and Romanenko, V. A., Opt. Spekrosk. **59**, 1196 (1985).